Weather-driven power transmission in a highly renewable European electricity network

– models, strategies, and optimisation

Rolando A Rodriguez

Submitted as a PhD dissertation
at the Department of Mathematics,
Aarhus University, 2014

Contents

Summary

We attempt to describe the characteristics of a future European electricity system with a high share of wind and solar photovoltaic capacities. The output of these variable renewable energy sources (VRES) is highly dependent on weather patterns. Relying on 8 years of data with a high spatial and temporal resolution, we estimate the potential generation in 30 European countries. We find that, even with a VRES penetration of 100%, an average country would waste around 24% of its energy due to generation coming at times when it cannot be used, leading to the need for dispatchable backup power to cover the deficit.

By allowing countries to share their excess generation, this amount can be brought down to 15%, though this implies a very large transmission capacity. We use a constrained power flow model to find out how much can a limited transmission capacity reduce the need for additional backup. Our results show that a total transmission capacity roughly five times larger than the present one allows for most of the reduction of backup energy. Transmission alone does not lower maximum backup power, meaning that countries cannot remove their installed dispatchable generation capacity. We design export schemes that allow countries to share their backup capabilities, so that overall backup capacities can be reduced.

The sharing of VRES and backup power implies a large amount of power flows in the system. Using graph theory and a flow tracing algorithm, we are able to determine the share of the power imported to a country that comes from a specific other one. This allows us to see which countries are trade partners due to the correlation between their resources and their placement in the network, as well as the pathway that these exports take to reach their destination. The stake that a country has on the network can then be quantified.

A large transmission network can not simply be justified purely on its ability to reduce backup capacities; It remains to be seen if the cost of the backup reduction is larger than the cost of the transmission network. Using cost estimates from the literature, we find that co-operation between countries (in the form of sharing of backup capacities) provides the lowest levelised cost of electricity (LCOE) for VRES penetrations between 50% and 130%. The cost-optimal system is found to be one with a VRES penetration of 50%, consisting primarily of wind power. In order to preserve the strength that the weather-driven approach gives to our results, we perform a sensitivity analysis to see the effects of variations in our assumptions in the optimal system. We find that the cost of wind capacity and backup energy are the defining attributes for the characteristics of the optimal system.

In an effort to reduce the LCOE of a fully renewable system, we explore heterogeneous distributions of VRES capacities. A distribution proportional to the countries' capacity factors makes better use of resources in Europe, meaning that fewer wind turbines and solar panels need be placed. We use optimal portfolio theory to assess the risk and return that different distributions of VRES capacities can offer, and discover that highly heterogeneous distributions imply much higher transmission capacities. A genetic algorithm offers other distributions with significantly lower LCOE.

Résumé

I denne afhandling søger vi at karakterisere et fremtidigt europæisk elsystem med en høj andel af vind- og solkapacitet, sidstnævnte i form af solceller. Udbyttet af disse midler til variabel energiproduktion (VRES) er stærkt afhængigt af vejrmønstre. På baggrund af otte års data med høj rumlig og tidslig opløsning estimerer vi den potentielle produktion i 30 europæiske lande. Vi konkluderer, at selv med en VRES-andel på 100% ville et gennemsnitligt land miste omkring 24% af dets energi, som følge af at produktionen foregår på tidspunkter, hvor energien ikke kan benyttes, hvilket leder til et behov for kontrollerbar reserveenergi til at dække underskuddet.

Ved at muliggøre deling af overskydende produktion mellem lande kan den tabte mængde nedsættes til 15%, selvom dette dog forudsætter en meget stor eltransmissionskapacitet. Vi anvender en model for begrænset eltransmission til at undersøge, hvor meget en indskrænket transmission kan reducere behovet for reserveenergi. Transmission i sig selv sænker ikke den maksimale reservekraft, hvilket betyder, at lande ikke kan nedjustere eller afskaffe deres nuværende reservekapacitet for kontrollerbar produktion. Vi designer scenarier for eksport, der tillader lande at dele deres reserveevne, sådan at den samlede reservekapacitet kan reduceres.

Deling af VRES og reservekraft indebærer en stor mængde strømbevægelser i systemet. Ved brug af graf-teori og en algoritme for bevægelsessporing er det muligt for os at udlede, hvor stor en andel af et lands importerede strøm, der kommer fra et givent andet land. Herigennem kan vi identificere landes handelspartnere ud fra korrelationen mellem deres ressourcer og deres placering i netværket samt afdække den rute, disse eksporter gennemløber for at nå deres destination. Et lands andel i netværket kan derefter kvantificeres.

Et omfattende transmissionssystem kan ikke retfærdiggøres alene ud fra dets evne til at reducere reservekapacitet; det er tillige nødvendigt at afgøre, om reduktionen i omkostninger ved nedskalering af reservekapaciteten er større end de øgede omkostninger som følge af transmissionsnetværket. Med udgangspunkt i omkostningsberegninger fra litteraturen udleder vi, at kooperation mellem lande (forstået som deling af reservekapacitet) giver de laveste samlede levetidsomkostninger for elektricitet (LCOE) ved en VRES-andel mellem 50% og 130%. Det konkluderes, at det omkostningsoptimale system findes ved en VRES-andel på 50%, bestående overvejende af vindenergi. En sensitivitetsanalyse bliver endvidere brugt til at afdække effekten af variationer i antagelserne. Vi konkluderer, at omkostninger vedrørende vindkapacitet og reserveenergi udgør de definerende egenskaber af det optimale system.

I et forsøg på at reducere LCOE for et system baseret udelukkende på vedvarende energi udforsker vi heterogene distributioner af VRES-kapacitet. En distribution proportionel til landenes kapacitetsfaktorer udnytter Europas ressourcer bedre, hvilket betyder, at antallet af vindmøller og solceller, det vil være nødvendigt at opstille, kan reduceres. Vi anvender optimal portfolio teori til at vurdere risici og afkast for en række forskellige VRES-kapaciteter og konstaterer, at meget heterogene spredninger medfører langt højere transmissionskapaciteter. En genetisk algoritme fremkommer med andre spredninger, der har signifikant lavere LCOE.

Preface

This thesis is a compilation of five peer-reviewed publications or submitted manuscripts, presented as part of an overarching research thread in highly renewable energy systems. Each of these publications is attached to a chapter, which also summarises it and places it in a context with relation to the others. In thematic order they are

Transmission needs across a fully renewable European power system [1], by Rodriguez RA, Becker S, Andresen G, Heide D, and Greiner M. Published in Renewable Energy;

Selfish vs. cooperative exports across a fully renewable pan-European transmission network [2], by Rodriguez RA, Dahl M, and Greiner M. Submitted to Energy, Sustainability and Society;

Tracing the flow of energy in a highly renewable Europe [3], by Rodriguez RA, Thomsen A, Andresen G, and Greiner M. To be submitted. Prepared in coordination with the Master's thesis work of Anders B. Thomsen;

Cost-optimal design of a simplified, highly renewable pan-European electricity system [4], by Rodriguez RA, Becker S, and Greiner M. Submitted to Energy;

and **Optimal heterogeneity of a highly renewable pan-European electricity system** [5], by Rodriguez RA, Sairanen B, and Greiner M. To be submitted. Prepared in coordinated with the Master's thesis work of Benjamin Sairanen.

The numbering of figures, equations, tables, and sections obeys the following rule: Elements in the accompanying text follow a single-digit scheme for the whole text (e.g. Figure 8), while elements that are part of a manuscript are numbered according to the manuscript (e.g. Section 4.2, which refers to the second section of the fourth manuscript). A general understanding of the thesis can be gained simply by reading the accompanying text, while deeper explanations of the methods and results are found in the original articles included. Other relevant peer-reviewed articles, which are not part of this thesis, are

Transmission grid extensions during the build-up of a fully renewable pan-European electricity supply [6], by Becker S, Rodriguez RA, Andresen G, and Greiner M. Published in Energy.

The potential for arbitrage of wind and solar surplus power in Denmark [7], by Andresen G, Rodriguez RA, Becker S, and Greiner M. Published in Energy.

In addition to these, some relevant conference papers are

Fundamental properties of and transition to a fully renewable pan-European power system by Andresen G, Rasmussen M, Rodriguez RA, Becker S, and Greiner M. Presented at the 2nd European Energy Conference 2012, Maastrich, Netherlands.

Transmission Needs In A Fully Renewable Pan-European Electricity System by Rodriguez RA, Andresen G, Becker S, and Greiner M. Presented at the International 100% Renewable Energy Conference and Exhibition (IRENEC 2012), Istanbul, Turkey.

Weather-Driven Modeling of Future Renewable Power Systems by Andresen G, Søndergaard A, Rodriguez RA, Becker S, and Greiner M. Presented at the 8th Conference on Sustainable Development of Energy, Water and Environment Systems 2013, Dubrovnik, Croatia.

What can transmission do for a fully renewable Europe? by Becker S, Rodriguez RA, Andresen G, Greiner M, and Schramm S. Presented at the 8th Conference on Sustainable Development of Energy, Water and Environment Systems 2013, Dubrovnik, Croatia.

Optimal placement of electrolysers in a German power-to-gas infrastructure by Robinius M, Rodriguez RA, Kumara B, Andresen G, ter Stein F, Schieben S, and Stolten D. Presented at the World Hydrogen Energy Conference 2014 (WHEC 2014), Gwangju, South Korea.

Some of the code used in preparation of this thesis and the related articles is publicly available. Contact rar(at)rar.pm for more information.

Acknowledgements

Thanks go, first and foremost, to Prof. Martin Greiner. This work could not have been possible without his inspiration, motivation, and helpful guidance. Thank you for helping me find my way in the thick mists of research.

Thanks to Gorm B. Andresen and Sarah Becker, for the many fruitful conversations and invaluable advice, and to Timo Zeyer, Tue V. Jensen, and Anders A. Søndergaard, for the challenging discussions and helping hands.

Thanks to Benjamin Sairanen, Anders B. Thomsen, Magnus Dahl, and Bo Tranberg, for keeping me on my toes and for their company and cheap labour.

Thanks to Uffe V. Poulsen and Morten G. Rasmussen, for so many hints with the tougher problems.

Thanks to my family, of friends and relatives, who pushed and cheered from many parts of the world. And especially thanks to Karen T. Sigaard, for support and motivation when it was most needed.

Introduction

Energy systems around the world have witnessed a transformation over the past decade. The environmental and health-related concerns associated with conventional sources and nuclear power, together with the expected decrease of availability of naturally occurring fossil fuels, have pushed the development of renewable energy technologies. Renewable sources differ radically from conventional sources, not only in their sustainability, but in the way they can be integrated into our energy systems. Some renewable sources, such as hydroelectric dams, biomass, and geothermal power, can be controlled and dispatched when needed. However, the availability of variable renewable energy sources (VRES), such as wind power and solar photovoltaics, depends directly on natural weather patterns. Whereas the former tend to be site-specific and are, at least in Europe, already close to being exploited to their maximum potential (in the case of hydroelectric or geothermal) or have a limited estimated potential (in the case of biomass) [8], the latter seem to have a promising future as key elements in the electrical system. Feasibility studies have shown how – and to what extent – energy demands can be covered by renewables, in Europe [8–11] and worldwide [12–19].

Wind power systems have become a nearly mature technology, becoming cost-competitive with traditional sources [20]. Solar photovoltaics have not arrived at that stage, but their easy scalability has sparked an explosive growth in deployment [9], potentially leading to much reduced costs over the next 10 to 15 years [21]. The increased presence of variable sources in our energy systems presents users, operators, and planners with new challenges and opportunities. From a system-stability perspective, grid connected VRES can introduce more variations than the electricity system was designed for, triggering the need for technological advancements. In a larger time scale, operators have been forced to cope with increased fluctuations and uncertainties in electrical generation, which must be precisely matched to electricity demand at every instant. In order to deal with these issues, the electricity system must be transformed to a more flexible system, with fast-acting backup power capacities, stronger connections to neighbouring grids, and a more fluid market [10, 13].

Excess generation caused by VRES also presents new opportunities. Flexible demands and smart grids can help operators accommodate excess production and make up for deficits, while allowing consumers a more direct management of their electricity usage. Low prices at times of abundance also open up the possibility for the

interaction between the electricity system and other energy sectors, such as heating and transportation via heat pumps, electric vehicles, or electrolysers.

Weather-driven modelling

The field of Energy Systems Analysis (ESA) explores these and other issues. Though a wide definition of ESA could include anything from an environmental impact assessment to the energy balance in a region. Even with this limitation, ESA can become very complex, encompassing many factors in high detail. To help planners and policy makers make sense of trends and limits in energy systems, an inordinate amount of modelling tools have been developed, each catering to a specific modelling need or point of view. A comprehensive comparison of such models can be found in [22].

Some disadvantages follow from relying excessively on these tools. The internal algorithms of the tool can be obscured by the complexity of the model. In treating the tool as a black box, a user could wrongfully make conclusions that do not follow from the results. Furthermore, in not being able to control the algorithms, the user is limited in the scope of what they can do with the tool. In many of these tools, the general trend is to move towards a wider modelling scheme, considering as many elements in the energy system as possible. However, when dealing with VRES, the added complexity of many factors can obscure the dynamics behind essential elements of the system: the weather patterns that dominate VRES generation.

We call our modelling approach "weather-driven", meaning that it is these dominating patterns that we are most interested in, rather than the details of the system or the specific technical, economical, or political issues that surround them. In avoiding a detailed technical description of the system, and instead focusing on the natural weather patterns, weather-driven modelling can deliver stronger results, independent of technologies or system operation. We talk of weather-driven modelling as a general approach rather than a concrete tool. The modelling itself is done in the simplest terms possible and is operated via a mathematical optimisation to recreate physical phenomena.

The simplicity of this approach determines its own limitations. The results we find will not change with improvements to technology or economic changes, but this means that they are also less specific in terms of technology or economy. Without introducing economical considerations, we can talk about natural limits and correlations, but not of optimal technologies or pricing.

The modelling approach relies on large amounts of weather data with high temporal and spatial resolution. The data was first used for these purposes in [23], and has since been expanded upon in [24–28]. It consists of an hourly, 8-year long time series (2000- 2007) with a spatial resolution of around 40 km $\times$ 40 km. From historical weather measurements, the Institut für Solare Energieversorgungstechnik (ISET), now part of the Fraunhofer Society, derived national wind and solar potential generation time series [29]. Though a specific installed capacity was assumed, the results can be extended to different capacity layouts and penetrations with only minimal loss in accuracy [30]. In the end, it is not the actual scale of a time series which

interests us, but rather its correlation to those at other locations. ISET also gathered corresponding electric load data from publicly available sources, extrapolated where needed, and detrended the results to their 2000 values.

Nodal modelling

The building block of our modelling approach, the node, is defined by these time series. This node can represent a geographical area varying in size from a city to a continent, though in most cases we will talk about a country. A node is characterised by a potential wind generation time series $W_n(t)$, a potential photovoltaic generation time series $S_n(t)$, and an electric demand time series $L_n(t)$. We refer to these as $potential$ generation time series because the actual generation depends on the capacity installed in a given location and the capacity factors ν_n^W and ν_n^S of the location.

Initially, to avoid talking about these capacity factors, we can normalise both generation time series so that

$$\langle W_n \rangle = \langle S_n \rangle = \langle L_n \rangle \,, \tag{1}$$

where the angled brackets represent the time average of the time series. We can then define the generation from VRES $G_n(t)$ at the node, which consists of a mix of wind and solar generation,

$$G_n(t) = \gamma_n(\alpha_n \cdot W_n(t) + (1 - \alpha_n) \cdot S_n(t)) \,. \tag{2}$$

The two factors γ_n and α_n represent, respectively, the mean generation of renewables in proportion to the load and the mix of wind in the generation. By varying these two factors, we can model any given combination of wind and solar generation in the node. A node with $\gamma_n = 0.5$ and $\alpha = 1.0$ is one in which the installed capacity of wind, whichever it may be, produces 50% of what the load consumes in average. This does not mean that 50% of the load is covered by wind, as generation may come at times when the load does not need it. Even for $\gamma_n = 1$, where VRES generates in average as much as the load consumes, there will almost always be an instantaneous mismatch

$$\Delta_n(\gamma_n, \alpha_n; t) = G_n(\gamma_n, \alpha_n; t) - L_n(t) \,. \tag{3}$$

At times when $\Delta_n(t) > 0$, more electricity is generated than what is needed. When $\Delta_n(t) < 0$, generation from VRES is not enough to cover the demand. In most of the analysis in [1–3], we talk about a fully-renewable European system, so that $\gamma_n = 1$ for all n. Only in [4, 5] do we explore $\gamma_n \neq 1.0$.

In electrical systems, consumption and generation must be instantaneously matched at every second, else the stability of the system could be compromised. The system must therefore either provide backup power (B_n) from conventional sources (or dispatchable renewables) or curtail (C_n) excess VRES generation:

$$B_n(t) = \begin{cases} |\Delta_n(t)| & \text{if } \Delta_n(t) \leq 0, \\ 0 & \text{otherwise} \end{cases} \,, \tag{4}$$

$$C_n(t) = \begin{cases} |\Delta_n(t)| & \text{if } \Delta_n(t) \geq 0, \\ 0 & \text{otherwise} \end{cases} . \tag{5}$$

When no constraints on B_n or C_n are considered, the residual mismatch Φ_n should always be zero,

$$\begin{aligned} \Phi_n(\gamma_n, \alpha_n; t) &= \Delta_n(\gamma_n, \alpha_n; t) + B_n(t)) - C_n(t) \\ \Phi_n(\gamma_n, \alpha_n; t) &= (G_n(\gamma_n, \alpha_n; t) + B_n(t)) - (L_n(t) + C_n(t)) \end{aligned} \tag{6}$$

In systems with a significant presence of renewables, we would like to minimise the amount of energy we need to provide from conventional sources. We introduce one of the key metrics in this analysis, the backup energy E_n^B, which is defined as

$$E_n^B = \frac{\sum_{t=0}^{\mathcal{T}} B_n(t) \cdot 1\text{h}}{\sum_{t=0}^{\mathcal{T}} L_n(t) \cdot 1\text{h}} = \frac{\langle B_n \rangle}{\langle L_n \rangle} , \tag{7}$$

where $\mathcal{T}$ is the number of hours. The normalisation by the mean load allows us to directly relate power into energy, so that a value of $E_n^B = 0.5$ means that the backup energy that must be provided equals 50% of the total demand. A similar measure can be made for excess energy,

$$E_n^C = \frac{\langle C_n \rangle}{\langle L_n \rangle} . \tag{8}$$

We are not only interested in knowing the total amount of energy expended by backup, we also want to know in what way it was delivered, as times with high backup power demands help determine the total backup power capacity that is required. We do not want to simply go with the maximum value of $B_n(t)$, as the events that determine this maximum are rare [30], leading to an overestimation of the backup capacity required. For this reason, we look at the probability distribution of $B_n(t)$. Figure 1 shows a histogram of distribution of $B_n(t)$ of a random node with $\gamma_n = \alpha_n = 1$. The maximum values are determined by a few hours, while a capacity large enough for 99% of the time is around half as large. We define the backup capacity required $\mathcal{K}_n^B$ as that for which

$$q_n = \int_0^{\mathcal{K}_n^B} p_n(B_n) \, \mathrm{d}B_n , \tag{9}$$

where $q_n = 0.99$ and $p_n(B_n)$ is the time-sampled distribution of backup power.

From only the natural weather patterns that dominate the generation from VRES in a region, and this simple mathematical model, we have found key quantities that describe the electrical system in a node. Given a penetration γ_n and a wind mix α_n, the correlation between the wind and solar time series and the electrical demand determines the amount of backup energy E_n^B and capacity $\mathcal{K}_n^B$ required to cover the demand and maintain system stability.

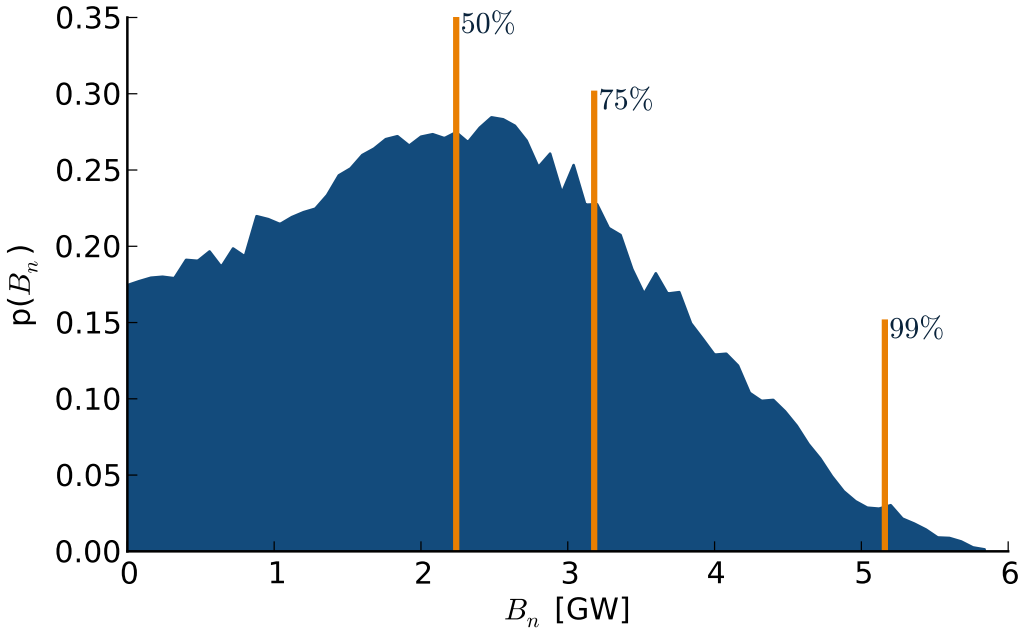

Figure 1: Probability distribution of the backup power required by Denmark, given $\gamma_n = 1.0$, $\alpha_n = 1.0$. Vertical lines indicate capacities of the 50%, 75%, and 99% quantiles.

Organization

In the following chapters, we will take the weather-driven approach together with this simple nodal modelling in order to uncover some properties of a highly renewable European electricity system. Each chapter is built around a peer-reviewed publication or submitted mansucript, with an extended introduction which places it in the context of the general research line.

Chapter 1, titled **Power flows**, explains how the nodal modelling can be taken as part of a network, and how elements of this network can interact to further reduce the individual nodes' backup energy (E_n^B). To arrive at these results, a flow algorithm needed to be devised which allowed for constraints along the links while being as close as possible to the real physical flow. We find that the backup energy E_n^B can easily be reduced with even moderate increases on transmission capacity, while reductions in $\mathcal{K}_n^B$ do not happen with a simple geographical aggregation [1].

Chapter 2, titled **Export schemes**, explores different ways that the nodes can interact in order to minimise $\mathcal{K}_n^B$. A synchronised operation, in which every node provides the same amount of backup $B_n(t)$ or curtailment $C_n(t)$ relative to their own size, can reduce the sum of all nodes' backup capacities $\mathcal{K}_{\mathsf{EU}}^B$. Physical, geometric, and economical interpretations can be given as to why this synchronised operation achieves this goal. Link capacities become much larger under this export scheme, as nodes need to share more of their resources [2].

Chapter 3, titled **Flow tracing**, takes off from an issue presented by [2]: Which nodes are responsible for a given flow? While there is no such thing as green electricity,

it is possible to track the consumption of a MWh from a sink to a source and vice versa. Here we combine a modified flow tracing theory from electrical engineering, an algorithm for finding trade partners from graph theory, and our own nodal modelling to find the usage that a node makes of the transmission network, as well as the node's main trade partners [3].

The competing interests found in [1] and [2], namely, the reduction in balancing energy and capacity ($E^B, \mathcal{K}^B$) measured against the increased need for transmission ($\mathcal{K}^T$), triggers an economic discussion in chapter 4, titled **Cost sensitivity**. To avoid losing the generality provided by the weather-driven approach and our nodal modelling, this is done via a senstivity analysis, where variations in the cost of different elements are accounted for. We find that the backup reductions in E^B and $\mathcal{K}^B$ brought about by a synchronised operation are worth the added cost of transmission from $\mathcal{K}^T$ for values of $0.5 \leq \gamma \leq 1.3$. We show how sensitive ESA are to the cost assumptions, and identify wind capacities and backup fuel costs as the key factors that most affect the optimal system's properties [4].

Chapter 5, titled **Heterogeneity**, removes one of the major constraints kept so far in the study: the homogeneity of γ_n and α_n across all nodes. By allowing different VRES capacities to be installed in different nodes, further reductions to the key metrics, (E^B_{EU}, $\mathcal{K}^B_{\mathsf{EU}}$, and $\mathcal{K}^T$) can be attained. We use optimal portfolio theory, commonly used in finance to weight the risk against the expected returns of investments, to explore the space of combinations of γ and α. A genetic algorithm shines light into some of the more extremely heterogeneous European layouts, further reducing the total cost of energy produced by the system [5].

Finally, the **Conclusion** frames all results within the context of energy systems analysis in Europe. We present some of the most important outlooks for weather-driven modelling, and concretely explain how to expand the node model to encompass more energy sectors, such as heating and transportation.

Chapter 1

Power flows

Motivation

When examining the weather dataset from [23] using the model described in the previous chapter, we find that the backup energy (7) required by an an average individual country in Europe differs significantly from that required by an aggregate of all countries. That is,

$$E^B_{\text{ind.}} = \sum_n E^B_n \frac{\langle L_n \rangle}{\langle L_{\text{EU}} \rangle} \approx 0.24\,, \tag{10}$$

for individual countries, and

$$E^B_{\text{EU}} = \frac{\langle B_{\text{EU}} \rangle}{\langle L_n \rangle} \approx 0.15\,, \tag{11}$$

where we first add up all the countries' mismatch to produce

$$B_{\text{EU}}(t) = \begin{cases} |\Delta_{\text{EU}}(t)| & \text{if } \Delta_{\text{EU}}(t) \leq 0, \\ 0 & \text{otherwise} \end{cases}\,. \tag{12}$$

This means that if countries do not interact with one another they will expend an average of 24% of their average demand in backup energy. When countries are allowed to share their renewable resources $before$ backup energy is determined this number goes down to 15%. As seen in [31], the correlation of VRES – and of wind, especially – decreases as a larger geographical area is considered. When the wind is not blowing in point A, there is a higher chance to find it blowing the further away you go from A.

The difference between 24% and 15% (a reduction of around 40%) represents the maximum benefit that a sharing of renewables can achieve in terms of backup energy reduction. In order for this to be possible, a well-connected electricity transmission network is required. This opens up the driving questions of this chapter: How much transmission would be required to achieve this reduction in E^B? How does this

amount compare to current installed capacities? What benefit can be achieved by a constrained transmission capacity, smaller than the one required for the maximum reduction in E^B?

Methods

We take the node model we developed earlier to be part of a larger network with N nodes, interconnected by L links to allow energy trading. The residual mismatch defined in (6) needs no longer be equal to zero at all times, but can instead be the net exports that the node offers to the network,

$$\Phi_n = (G_n + B_n) - (L_n + C_n) = (E_n - I_n)\,, \tag{13}$$

where E_n are exports from node n and I_n imports to node n. Nodes with a positive residual mismatch $\Phi_n > 0$ are considered sources of energy, while nodes with a negative residual energy $\Phi_n < 0$ are sinks. The vector $\mathbf{\Phi}$ of size n defines the injection pattern of the network.

This new definition of the residual mismatch also leads us to the node balance equation, which must hold true for every node in the network at every instant:

$$G_n(t) + I_n(t) + B_n(t) = L_n(t) + E_n(t) + C_n(t)\,. \tag{14}$$

Figure 2 gives a visual representation of the possible events in a node. Given a combination of (γ_n, α_n), we can take generation and load (G_n, L_n) as a stimulus to the node. The node can then respond with either an internal management of its resources, by providing backup power or curtailing (B_n, C_n), or by using the electrical network to trade electricity with its neighbours (E_n, I_n).

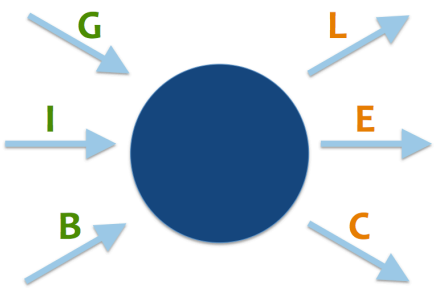

Figure 2: Node diagram with inputs from VRES generation G, electricity imports from other nodes I, and dispatchable backup generation B. Outputs to the node are curtailment of VRES C, exports to other nodes E, and local electricity demand L.

We can relate the exports and imports in a node to power flows $F_l(t)$ along all links via the $N \times L$ incidence matrix $\boldsymbol{K}$, whose entries $K_{n,l}$ are

$$K_{n,l} = \begin{cases} 1 & \text{if link } l \text{ starts at node } n, \\ -1 & \text{if link } l \text{ ends at node } n, \\ 0 & \text{otherwise .} \end{cases} \quad . \tag{15}$$

Summing up the flows into and out of a node results in the net exports,

$$E_n - I_n = \sum_{l=1}^{L} K_{l,n} F_l \,. \tag{16}$$

This can be interpreted as having the flows determine the net exports and imports into a node, or as having the injection pattern $\boldsymbol{\Phi}$ building a system of equations for finding the flows $\boldsymbol{F}$ as

$$\boldsymbol{\Phi} = \boldsymbol{K}\boldsymbol{F} \tag{17}$$

Electricity networks

We want to find the flows described by a given injection pattern as in (17), while being as similar as possible to the physical flows found in an electricity network. Each of the N nodes in a given interconnected network (for example, Figure 2.2) can be described by four variables: real power mismatch $\mathcal{P}$, reactive power mismatch $\mathcal{Q}$, the voltage V and the voltage phase angle δ. Solving the power flow and finding the power levels of buses and lines requires solving two sets of equations, one for the active and one for the reactive power at each node n [32].

$$\mathcal{P}_n = \sum_{m=1}^{N} |V_n||V_m|(\mathcal{G}_{n,m}\cos\delta_{n,m} + \mathcal{B}_{n,m}\sin\delta_{n,m}) \,, \tag{18}$$

$$\mathcal{Q}_n = \sum_{m=1}^{N} |V_n||V_m|(\mathcal{G}_{n,m}\sin\delta_{n,m} - \mathcal{B}_{n,m}\cos\delta_{n,m}) \,, \tag{19}$$

where $\delta_{n,m} = \delta_n - \delta_m$ is the difference of the phase angles at nodes n and m, and $\mathcal{G}_{n,m}$ and $\mathcal{B}_{n,m}$ are the real and imaginary parts of the admittance of the links connecting them, respectively. The goal here is to find the vector of the phase angles $\boldsymbol{\delta}$, as this defines the flow between two links via

$$F_{n,m} = \mathcal{B}_{n,m}(\delta_n - \delta_m) \,, \tag{20}$$

or

$$\boldsymbol{F} = \boldsymbol{K}^{\mathsf{T}}\boldsymbol{\delta} \tag{21}$$

when we assume that $B_{n,m} = 1$ for all node pairs (n,m) directly connected by a link.

For large systems, calculating these phase angles in real-time can be troublesome. A DC approximation, as evaluated in [33], simplifies the problem significantly and

is equivalent to the real solution under certain assumptions. For a system in steady state – with no fluctuations in voltage or power levels – so that $V_n = V_m = 1$; with no active power losses on the lines so that $G_{n,m} = 0$; and a sufficiently small difference between phase angles so that $\sin(\delta_{n,m}) \approx \delta_{n,m}$, we can reduce equations (18), and (19) to

$$\mathcal{P}_n = \sum_{m \neq n}^{N} B_{n,m}(\delta_n - \delta_m) = \sum_{m \neq n}^{N} B_{n,m}\delta_n - \sum_{m \neq n}^{N} B_{n,m}\delta_m = \sum L_{n,m}\delta_n \tag{22}$$

where

$$L_{n,m} = \begin{cases} -B_{n,m} & \text{if } n \neq m \\ \sum_{m \neq n} B_{n,m} & \text{if } n = m \end{cases}. \tag{23}$$

This leaves $\mathcal{P}$ as the total power supplied to or extracted from the system, corresponding to our injection pattern $\boldsymbol{\Phi}$. For unitary impedances $B_{n,m} = 1$, $\boldsymbol{L}$ is the Laplace matrix

$$\boldsymbol{L} = \boldsymbol{K}\boldsymbol{K}^{\mathsf{T}} \tag{24}$$

where $\boldsymbol{K}$ is the incidence matrix of the network from (15), so that (22) can be rewritten as

$$\boldsymbol{\Phi} = \boldsymbol{K}\boldsymbol{K}^{\mathsf{T}}\boldsymbol{\delta} \tag{25}$$

The system of equations given by (25) is underdefined, as $\boldsymbol{L}$ is singular. We can proceed in three different ways in order to find $\boldsymbol{\delta}$ and then $\boldsymbol{F}$. The first and simplest solution is to simply set an arbitrary node n' as a reference, so that $\delta_{n'} = 0$. A more elegant approach is to use the Moore-Penrose pseudoinverse for $\boldsymbol{L}$, allowing for a direct solution of (25)[1].

A third way is to use (21) and (25) to circumvent the usage of $\boldsymbol{\delta}$ and obtain (17) again. In order to guarantee that we see the same physical flows that would be described by (21), we can instead use the minimum dissipation principle, a property of potential flows. The way a potential defines a flow in equation (21) can be related to electric flows of the form $i = \frac{1}{R}u$, where the current i caused by the difference in potential u follows the path which minimises losses. Losses are related to the square of the current, so that, by analogy, minimising $\boldsymbol{F}^{\mathsf{T}}\boldsymbol{F}$ should provide the same results. See [32] and section 1.2 for more information. This means that, as long as we minimise the square of the flows while ensuring (17), we are describing a physical flow.

Power flow as an optimisation problem

We want to find the minimal amount of backup that a node requires. This optimal backup $\boldsymbol{B}^*$ leads to an injection pattern $\boldsymbol{\Phi}$, which in turn causes some flows $\boldsymbol{F}$ in the system. This can be stated as a two-step optimisation problem:

[1]Although $\boldsymbol{L}$ is not invertible, a matrix $\boldsymbol{L}^+$ can be found with many of the properties of the inverse. For more details, see [34, 35]

$$\begin{aligned} \text{step 1}: \quad & \min\left(\sum_n B_n(t)\right) && (26)\\ \text{subject to}: \quad & \boldsymbol{\Phi} = \boldsymbol{K}\boldsymbol{F}, \\ & \boldsymbol{F}_- \leq \boldsymbol{F} \leq \boldsymbol{F}_+ \\ \text{step 2}: \quad & \min\left(\sum_l F_l^2(t)\right) && (27)\\ \text{subject to}: \quad & \boldsymbol{\Phi} = \boldsymbol{K}\boldsymbol{F}, \\ & \boldsymbol{F}_- \leq \boldsymbol{F} \leq \boldsymbol{F}_+ \\ & \sum_n B_n = \sum_n B_n^* \end{aligned}$$

The first step finds the minimum total amount of backup that the system can survive with at a given time, given some constraints $\boldsymbol{F}_-, \boldsymbol{F}_+$ on each link. The second step takes this total amount and uses the minimum dissipation principle to determine the flow along each link. Note that the constraint in the second step is $\sum_n B_n = \sum_n B_n^*$ and not $B_n = B_n^*$. This means that we find the total amount that has to be exported and imported, but we do not define individual backups, nor the actual injection pattern $\boldsymbol{\Phi}$. This is defined with the second step, as a consequence of finding the most localised flow.

This optimisation is repeated for every hour in the 8-year lapse, producing a flow time series for every link. The total transmission capacity required

$$\mathcal{K}_{\mathsf{EU}}^T = \sum_l^L \mathcal{K}_l^T \,, \tag{28}$$

is, like in the case of backup capacities $\mathcal{K}_n^B$, defined not by the maximum value, but by high quantiles; see equation (9). In the case of a bidirectional flow (see Figure 1.4), we must choose between the 0.5% and the 99.5% quantile of the probability distribution of the flow in order to find a capacity sufficient for at least 99% of the time:

$$\mathcal{K}_l^T = \max\left\{-Q_{0.5\%}, Q_{99.5\%}\right\} \,, \tag{29}$$

where

$$x = \int_{-\infty}^{Q_x} p_l(F_l)\,\mathrm{d}F_l \,. \tag{30}$$

See section 1.4 for more details.

Main findings

We model first a fully renewable Europe with $\gamma_n = 1.0$ for all n and $\alpha_n = \alpha_n^*$, where α_n^* is a country-specific optimal mix which minimises the amount of backup energy

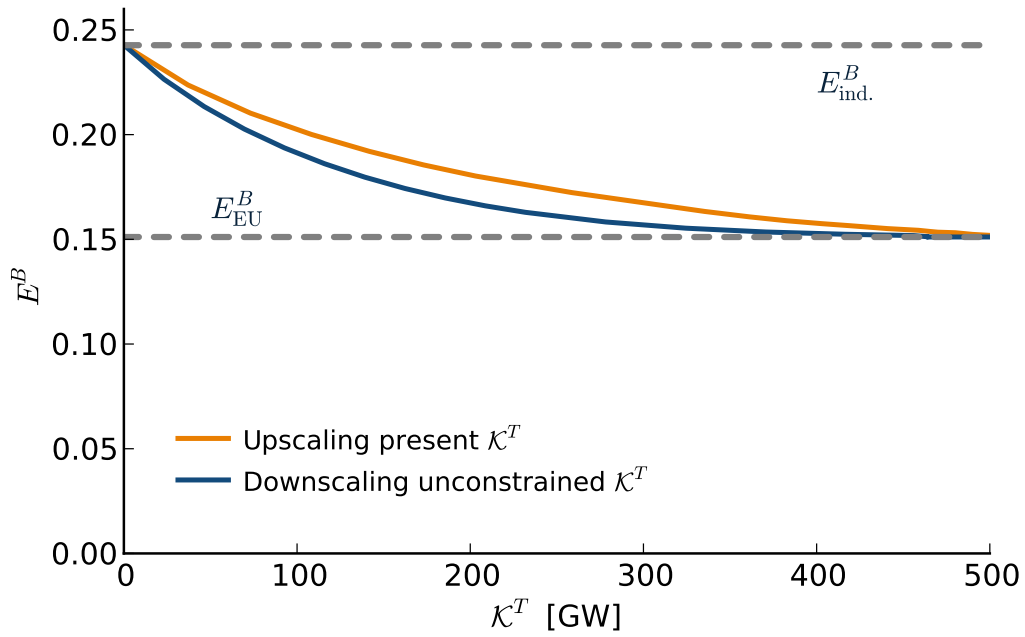

Figure 3: Total backup energy used in Europe E^B, normalised to mean annual consumption, as a function of the total installed transmission capacity $\mathcal{K}^T$, assuming a penetration of $\gamma_n = 1$ and an optimal wind mix $\alpha_n = \alpha^*$ for all countries. The orange line indicates a linear upscaling of present capacities (~ 73 GW), while the blue line indicates a linear downscaling of the capacities found by the unconstrained flows. The dashed lines indicate the energy required by an average disconnected country ($E^B_{\text{ind.}}$) and an aggregated Europe (E^B_{EU}).

needed for that country when it is not connected to its neighbours. We constrain link capacities to those registered by European Network of Transmission System Operators for Electricity (ENTSO-E) for 2011 [36], plus newer links not published in their latest capacity layout, such as the one between Great Britain and the Netherlands [37], and the Netherlands and Norway [38]. We find that the current capacity layout already provides roughly a third of the potential benefit, reducing backup energy to $E^B_{\text{ind.}} \approx 0.21$ (Figure 3).

By looking at the unconstrained flow, we can identify the links that are most used, so that a re-distribution of capacities could provide a greater benefit than a simple upscaling of existing ones. The benefit of increased transmission decreases sharply until around 4 to 5 times the current capacity, when we reach the 99% quantile, which provides over 90% of the total benefit. Nearly ten times as much capacity would be required to allow for the unconstrained flow of electricity in a fully renewable Europe.

Transmission needs across a fully renewable European power system

Rolando A. Rodriguez[a], Sarah Becker[b], Gorm B. Andresen[a], Dominik Heide[c], Martin Greiner[a]

a Department of Engineering and Department of Mathematics, Aarhus University, Denmark

b Frankfurt Institute for Advanced Studies (FIAS), Johann Wolfgang Goethe Universität, Germany

c Deutsches Zentrum für Luft- und Raumfahrt (DLR), Germany

Abstract

The residual load and excess power generation of 30 European countries with a 100% penetration of variable renewable energy sources are explored in order to quantify the benefit of power transmission between countries. Estimates are based on extensive weather data, which allows for modelling of hourly mismatches between the demand and renewable generation from wind and solar photovoltaics. For separated countries, balancing is required to cover around 24% of the total annual electricity consumption. This number can be reduced down to 15% once all countries are networked together with unconstrained interconnectors. The reduction represents the maximum possible benefit of transmission for the countries. The total Net Transfer Capacity of the unconstrained interconnectors is roughly 11.5 times larger than current values. However, constrained interconnector capacities 5.7 times larger than the current values are found to provide 98% of the maximum possible benefit of transmission. This motivates a detailed investigation of several constrained transmission capacity layouts to determine the export and import capabilities of countries participating in a fully renewable European electricity system.

keywords: renewable energy system, power transmission, constrained power flow, wind power generation, solar power generation, large-scale integration

1.1 Introduction

The sustainability of the world's energy supply is strongly dependent on the successful integration of renewable sources. Variable Renewable Energy Sources (VRES), such as wind and solar energy, promise to be key elements in future energy systems [9, 10, 12, 13, 39]. The nature of VRES makes them hard to integrate into an electrical system that was built on more or less predictable loads with dispatchable generation. In small penetrations, the variations can be absorbed without much consequence, but will be harder to ignore in a future, highly renewable, macro energy system. The spatio-temporal dispersion of the weather patterns that define the output of wind and solar energy will lead to fluctuating mismatches between regional demand for and generation of electricity. This will give rise to new challenges for countries with a high penetration of VRES, such as the need for back-up conventional balancing, flexible demand, dispatchable renewable sources such as hydroelectric reservoirs or biomass, increased transmission capacities to neighbouring regions and energy storage [10, 13]. In order to understand and to design the future energy systems with dominant shares of VRES, we need to let the weather decide.

For the optimal integration of VRES in future 100% renewable electricity systems, one wishes to make as much use as possible of renewables while minimising the need for conventional balancing, both in the installed power capacity required and the energy expended [26]. Additionally, we wish to minimise the need for storage [23, 24] and transmission capacities [27, 28]. In determining lower bounds on the need for storage and transmission, the synergies between these factors and the need for balancing must be well understood [25, 40]. In this article, we focus on determining the synergy between transmission and balancing.

There is a conflict between the need for maximising the integration of fluctuating VRES and minimising the expansion of the transmission system. Several studies have assessed the need for a larger transmission network [10, 41–43]. Despite the planned investments in grid strength, the European Network of Transmission System Operators for Electricity (ENTSO-E) has identified 100 bottlenecks in their network development plan [44], with 80% of them due to integration of renewables. By looking at characteristic weather patterns and possible wind and solar power generation across Europe, potential transmission between regions have been estimated. This has been done for Germany [45], and with an economic approach for Europe [27, 40]. A similar study has looked at regional aggregation and transmission in the United States [14]. Estimates on the size of an ideal transmission grid are large, such as 20 GW for the link between France and Spain [43], which is over 15 times larger than the current interconnector capacity.

Starting from the same large weather database as presented in [23–25], we estimate the potential output of wind and solar photovoltaic energy for any given country in a 30-node representation of Europe. In Section 1.2, we introduce a model which calculates the local mismatches between VRES generation and load in this set of interconnected countries, and which distributes the excess generation in a way that maximises the use of renewables. An efficient usage of renewables also minimises the need for balancing energy E coming from conventional dispatchable resources. Section 1.2 also explains how this optimal distribution of VRES excess generation can be found by performing a novel generalisation of DC power flow calculations with constrained interconnectors. It also determines the interplay between installed transmission capacity and the benefit coming from transmission. In Section 1.3, the DC power flow model is applied to the case of a future, 100% renewable Europe. A minimum E that each country can attain through an optimal mix of wind and solar is found, and then compared to that of a fully connected, unconstrained Europe. The total E resulting from this unconstrained flow leads to the maximum benefit of transmission, when countries can make the most use of the renewable excess generation of their neighbours. By applying the constrained DC power flow calculation we find a precise relation between the installed transmission capacity and the required total balancing energy E. Section 1.4 discusses the limits to import and export capabilities, and the reduction of conventional power capacities. The conclusion is presented in Section 1.5.

1.2 Methodology

The following is a method to determine power flows in a power system with a large amount of VRES generation, and the benefit they bring by reducing the need for balancing. Power flow calculations are detailed for unconstrained and constrained cases.

Definitions

For a node n representing a country, the hourly VRES generation and the electrical load will generally not be equal. The hourly mismatch between the load L_n and the combined output of wind G_n^W and solar G_n^S generation in a 100% renewable system is defined as [23]

$$\Delta_n(t) = \left(\alpha_n^W \frac{G_n^W(t)}{\langle G_n^W(t)\rangle} + (1-\alpha_n^W)\frac{G_n^S(t)}{\langle G_n^S(t)\rangle}\right)\cdot\langle L_n(t)\rangle - L_n(t)\ . \quad (1.1)$$

Here, t represents the hourly timestep and α_n^W the wind share at node n. Time-averaged means are denoted by $\langle . \rangle$. The VRES generation is normalised to its mean and scaled to the mean value of the load. Under

this scaling, VRES generate as much energy, on average, as is consumed by the load. The mean of the mismatch $\langle \Delta_n \rangle = 0$, but, due to the fluctuations of the generation and the load, $\Delta_n(t)$ will almost always be either positive in case of excess generation or negative in case of deficit generation.

The negative part of the mismatch defines the positive-valued residual load of a country,

$$\Delta_n^-(t) = \max\left\{-\Delta_n(t), 0\right\} \ , \tag{1.2}$$

which needs to be balanced by other dispatchable generation sources. The positive part of the mismatch is positive-valued excess power

$$\Delta_n^+(t) = \max\left\{\Delta_n(t), 0\right\} \ , \tag{1.3}$$

which must either be exported or curtailed. The time averages of (1.2) and (1.3) are identical, $\langle \Delta_n^- \rangle = \langle \Delta_n^+ \rangle$.

Unconstrained DC power flow

Assuming that the nodes are connected by links, the transmission of energy would follow Kirchhoff's rules for electric flow. Given a directed graph consisting of N nodes and L links with zero global mismatch, that is

$$\sum_{n=1}^{N} \Delta_n = 0 \, , \tag{1.4}$$

the DC approximation to the full AC power flow [32] unambiguously defines the flow between two neighboring nodes n and m as

$$F_{n \to m} = b_{nm}(\delta_n - \delta_m) \, , \tag{1.5}$$

where b_{nm} is the susceptance of the connecting link and δ_n and δ_m are the voltage phase angles of the connected nodes n and m, respectively. The relative phase angles thus determine the potential flow between all nodes in the graph, and can be found by solving the system of N equations

$$\Delta_n = \sum_{n=1}^{N} B_{n,m}\delta_m \, . \tag{1.6}$$

The elements of the susceptance matrix B are defined by

$$B_{n,m} = \begin{cases} -b_{nm} & \text{if} \quad n \neq m \\ \sum_{m \neq n}^{N} b_{nm} & \text{if} \quad n = m \end{cases} \tag{1.7}$$

The DC approximation defined by (1.4), (1.5), and (1.6) is valid as long as the network is in steady state, the resistances of the links can

be neglected and no significant voltage phase shifts occur between the nodes [33]. Another consequence of the zero-resistance assumption is that the susceptances do not depend on the length of the links and can be uniformly chosen to be equal to one. This means that the $N \times N$ matrix B becomes exactly identical to the matrix product of the $N \times L$ incidence matrix K,

$$B = K \cdot K^T \,, \tag{1.8}$$

where K is

$$K_{n,l} = \begin{cases} 1 & \text{if link } l \text{ starts at node } n, \\ -1 & \text{if link } l \text{ ends at node } n, \\ 0 & \text{otherwise .} \end{cases} \tag{1.9}$$

Equations (1.5) and (1.6) can then be expressed as

$$F = K^T \cdot \delta \tag{1.10}$$

and

$$\Delta = K \cdot K^T \cdot \delta = K \cdot F \,. \tag{1.11}$$

The last equation expresses local flow conservation at each node.

The power flows (1.5) resulting from the DC power flow equations (1.4) and (1.6) can also be derived from the constrained quadratic mimization objective

$$\begin{aligned} \min_{F} \quad & F^T F \\ \text{s.t.} \quad & K \cdot F = \Delta \,. \end{aligned} \tag{1.12}$$

This can be shown by using a vector of N Lagrange multipliers λ to find the minimum of the constrained function

$$\Lambda = \frac{1}{2} F^T F - \lambda^T (KF - \Delta) \tag{1.13}$$

via

$$\frac{\partial \Lambda}{\partial F} = F^T - \lambda^T K = 0 \,, \tag{1.14}$$

which leads to

$$F = K^T \lambda \,. \tag{1.15}$$

This last result has the same form as (1.10), meaning that the Lagrange multipliers λ can be interpreted as the voltage phase angles δ.

The two formulations (1.4)-(1.6) and (1.12) are fully equivalent. We will now use the second approach to generalise the unconstrained DC power flow to the dominating situation

$$\sum_{n=1}^{N} \Delta_n \neq 0 \,,$$

when the combined mismatch of all nodes is not zero. In case of a negative sum, some nodes with a negative mismatch will not be able to import enough and will be required to balance the remainder from their own dispatchable sources:

$$B_n(t) = -\min\left\{\left[\Delta_n(t) - \sum_{l=1}^{L} K_{n,l} F_l(t)\right] \,,\, 0\right\} \,. \tag{1.16}$$

Likewise, in case of an overall positive mismatch, some nodes will not be able to export all of their excess energy and will be required to curtail:

$$C_n(t) = \max\left\{\left[\Delta_n(t) - \sum_{l=1}^{L} K_{n,l} F_l(t)\right] \,,\, 0\right\} \,. \tag{1.17}$$

By their definition, both B_n and C_n are positive at all times.

The balancing B_n, the excess energy C_n and the flows F_l at all nodes and links are now determined by a two-step optimization procedure. The first priority is the minimization of the overall balancing for each hour:

$$B_{\mathsf{min}}(t) = \min_{F_l} \sum_{n=1}^{N} B_n(t) \,, \tag{1.18}$$

which guarantees a maximum usage of VRES across all nodes. Since this does not yet determine the flows in a unique manner, they are fixed in a second step,

$$\begin{aligned} \min_{F_l} \quad & \sum_{l=1}^{L} F_l^2 \\ \text{s.t.} \quad & \sum_{n=1}^{N} B_n = B_{\mathsf{min}} \,, \end{aligned} \tag{1.19}$$

which minimises the quadratic flows with the constraint of keeping the total balancing at its minimal value found in the first step. The two steps ensure that we arrive at the most localised DC power flows which allow an optimal sharing of renewables between exporters ($\Delta_n > 0$) and importers ($\Delta_n < 0$). The following constrains are implicitly fulfilled by the two-step optimisation (1.18), (1.19):

$$\begin{aligned} &\text{if} \quad \Delta_n < 0, \quad \text{then} \quad 0 \le B_n \le -\Delta_n \\ &\text{if} \quad \Delta_n > 0, \quad \text{then} \quad 0 \le C_n \le \Delta_n \,; \end{aligned} \tag{1.20}$$

a violation would lead to additional flows, increasing the squared flow sum (1.19).

Constrained DC power flow

Today's transmission grids are constrained by the Net Transfer Capacities (NTC). These constraints are based not only on the physical properties of the interconnectors, the Total Transfer Capacities (TTC), but also on the strength of the grid on either sides of the link and on the security policies of the participating countries [46]. As a result, transmission over links is constrained with different values in each direction.

The problem, as stated in equation (1.19), can be further generalised by adding limits $f_l^- \leq F_l \leq f_l^+$:

$$\begin{aligned} \text{Step 1:} \qquad & \min_{F_l} \quad \sum_{n=1}^{N} B_n \equiv B_{\mathsf{m}in} \\ & \text{s.t.} \quad f_l^- \leq F_l \leq f_l^+ \\ \text{Step 2:} \qquad & \min_{F_l} \quad \sum_{l=1}^{L} F_l^2 \\ & \text{s.t.} \quad f_l^- \leq F_l \leq f_l^+ \\ & \qquad \sum_{n=1}^{N} B_n = B_{\mathsf{min}} \ . \end{aligned} \tag{1.21}$$

The first step can be solved linearly with the help of a slack variable, whereas the second step is a quadratic programming optimization problem. Solutions can be obtained with several computational solving tools. The high speed of the solvers generated by CVXGEN [47] made this tool well suited for our purposes.

Benefit of transmission

The constrained optimization (1.21) determines the power flows F_l on all links and, via (1.16), also the residual loads B_n on all nodes. It is important to note that the resulting power flows and residual loads depend on the transmission capacity layout $\{f_l^{\pm}\}$ that constrains the power flows. Each layout $\{f_l^{\pm}\}$ will result in a mean annual balancing energy

$$E = \frac{1}{Y} \sum_{t=1}^{T} \sum_{n=1}^{N} B_n(t) \tag{1.22}$$

which is the sum over all country-specific balancing needs at all times, divided by the number of years Y in the dataset of length T. The case of zero transmission capacity layout $f^{\pm} = 0$ results in zero power flows, so that the mean annual balancing energy

$$E(f_l^{\pm} = 0) = \frac{1}{Y} \sum_{t=1}^{T} \sum_{n=1}^{N} \Delta_n^-(t) \tag{1.23}$$

can be expressed as the country sum over the individual negative mismatches (1.2). Unconstrained power flows represent the other extreme and are the result of an infinitely strong layout. The resulting annual balancing energy

$$E(\infty) = \frac{1}{Y} \sum_{t=1}^{T} \max \left(-\sum_{n=1}^{N} \Delta_n(t) \ , \ 0 \right) \tag{1.24}$$

can be obtained without a flow calculation, simply by allowing countries' mismatches to be summed before determining the amount of balancing required. Similarly, intermediate layouts $\{f_l^{\pm}\}$ between the two extremes will result in an annual balancing energy $E(\infty) \leq E(f_l^{\pm}) \leq E(0)$.

A measure on how much a transmission capacity layout is able to reduce the annual balancing energy is defined by the benefit of transmission

$$\beta = \frac{E(0) - E(\{f_l^{\pm}\})}{E(0) - E(\infty)} \ . \tag{1.25}$$

The benefit of the zero transmission is thus $\beta = 0$, and that of the unconstrained layout is $\beta = 1$. Intermediate layouts will result in $0 \leq \beta \leq 1$.

1.3 Case study: Power transmission in a fully renewable Europe

The methodology developed in the previous section is applied to the case of a 30-node fully renewable European network. Each country is assumed to have a combined wind and solar power generation that is, on average, equal to its load. Country-specific optimal mixes are first determined. Then, the unconstrained formulation (1.19) for the power flow is used to estimate maximum transmission capacities on the interconnectors. Finally, the constrained power flow problem (1.21) is solved with different capacity layouts and the respective benefits of transmission β are determined.

Country specific optimal mixes

Focusing on wind and solar energy, VRES generation potentials were determined for 30 European countries from a large weather database, spanning eight years from 2000 to 2007 [23]. This includes both on- and off-shore regions with a spatial resolution of 47 km $\times$ 47 km. Weather measurements were used to determine wind and solar energy generation time series with an hourly resolution. To obtain the absolute power output for a country, capacity scaling factors were applied to each grid cell belonging to the country to be aggregated. The scaling factors

ISO	Country	$\langle L \rangle$ (GW)	ISO	Country	$\langle L \rangle$ (GW)	ISO	Country	$\langle L \rangle$ (GW)
DE	Germany	54.2	FI	Finland	9.0	RS	Serbia	3.9
FR	France	51.1	CZ	Czech Republic	6.7	IE	Ireland	3.2
GB	Great Britain	38.5	AT	Austria	5.8	SK	Slovakia	3.1
IT	Italy	34.5	GR	Greece	5.8	BA	Bosnia & Herz.	3.1
ES	Spain	24.3	RO	Romania	5.4	HR	Croatia	1.6
SE	Sweden	16.6	BG	Bulgaria	5.1	LT	Lithuania	1.5
PL	Poland	15.2	PO	Portugal	4.8	EE	Estonia	1.4
NO	Norway	13.7	CH	Switzerland	4.8	SI	Slovenia	1.4
NL	Netherlands	11.5	HU	Hungary	4.4	LV	Latvia	0.7
BE	Belgium	9.5	DK	Denmark	3.9	LU	Luxembourg	0.7
						EU	Europe	345.5

Table 1.1: Country specific average hourly load, detrended to their values for the year 2007.

reflect the assumed installed wind and solar capacity at that location. Historical data for the electricity demand was used to generate hourly load time series for all 30 countries covering the same 8 years from 2000 to 2007. The time series for each country were then detrended to correct for the approximately 2% annual increase in electricity demand. Average loads for the countries can be seen in Table 1.1.

The distribution of the mismatch is shown in Figure 1.1 for three different countries, with three different choices for the mixing parameter ranging from fully solar ($\alpha_n^W = 0.0$) to fully wind ($\alpha_n^W = 1.0$). It is evident that the mismatch distributions depend on the mixing parameter α_n^W, and that no mix will completely eliminate the positive and negative mismatches. Our optimisation objective is to minimise the average negative mismatch with respect to the wind share α_n^W. Since the average negative mismatch $\langle \Delta_n^-(t) \rangle = \langle \Delta_n^+(t) \rangle$ is identical to the average excess power, this is equivalent to the minimisation of average excess generation. The optimal mixing parameters are shown in Figure 1.2(a). Compared to the average optimal wind mix $\alpha_n^W \approx 0.71$, southern countries have a slightly smaller and northern countries a slightly larger value.

For an average country, the minimised average residual load amounts to 24% of its average load (see Figure 1.2(b)). This implies that although the average wind and solar power generation are equal to the average load, 24% of it is generated at the wrong time. This amount has to be covered by dispatchable sources.

The absolute values of the mismatch quantiles are shown in Figure 1.2(c). Higher values in the quantiles imply larger deviations of VRES generation from the mean load. The 1% and 10% quantiles give an indication of the required balancing capacities resulting from the residual load time series defined by (1.2). The 90% and 99% quantiles are also shown and can be interpreted as the curtailed energy resulting from the

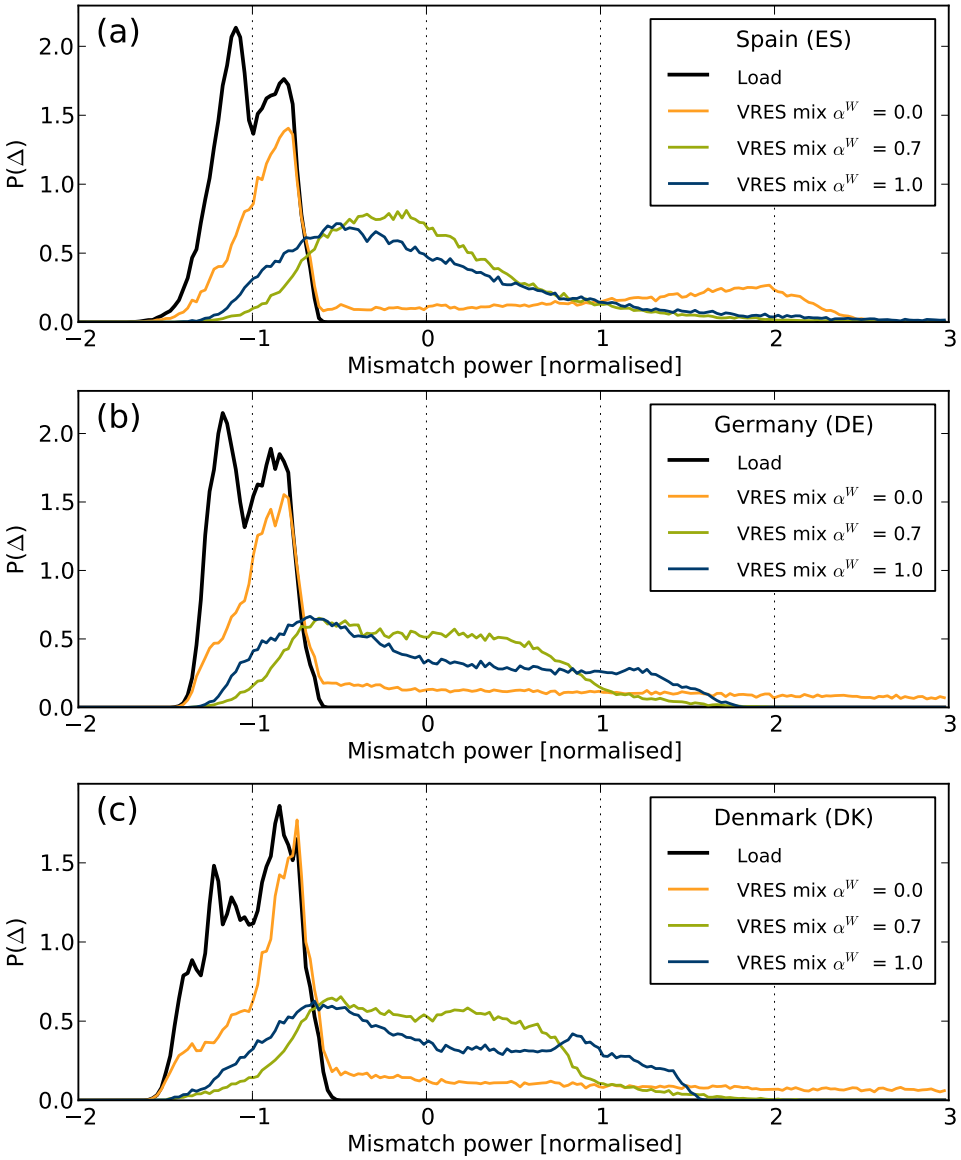

Figure 1.1: Mismatch distributions for (a) Spain, (b) Germany and (c) Denmark with no cross-border transmission, for a fully renewable system. Values are normalised to the country specific mean load (see Table 1.1). The different colours represent the wind shares $\alpha_n^W = 0.0, 0.7, 1.0$. For comparison, the distribution of the normalised load is also shown.

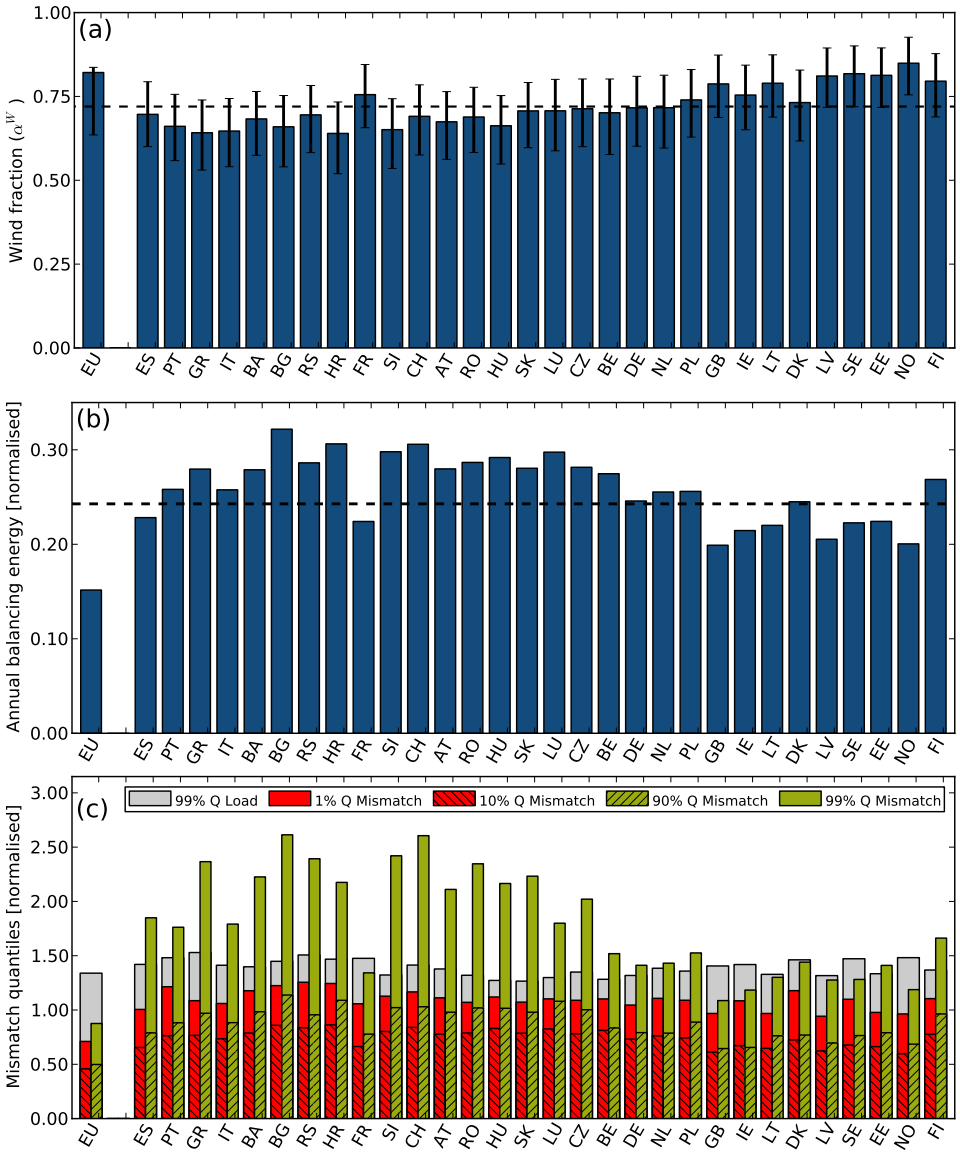

Figure 1.2: (a) Optimal mix minimising the average residual load calculated independently for each country and for aggregated Europe. Countries are ordered by the latitude of their geometric centre. Error bars show mixes that produce average residual loads which are larger by 1% compared to the optimum. The dashed line indicates the optimal mix averaged over all countries. (b) Minimum average residual load for each country, obtained with the optimal mixes from (a), in units of the country specific average hourly load (see Table 1.1). The dashed line indicates the residual load averaged over all countries. (c) The 1% (red), 10% (striped red), 90% (striped green), 99% (green) quantiles of the mismatch time series are based on the optimal mix from (a). As a reference the 99% quantiles (grey) of the load time series are also indicated.

excess time series defined by (1.3). Whereas the 90% quantiles are only a little larger than the 10% quantiles, the 99% quantiles turn out to be significantly larger than the 1% quantiles. For the larger fraction of the countries the 99% mismatch quantile is also larger than the 99% load quantile. These are the expected results when looking again at the asymmetry of the mismatch distributions of Figure 1.1.

We now compare the results for individual countries to those of the aggregated EU. The latter is assumed to have an unconstrained transmission between all countries, so that all excess generation can be shared with other countries. When each country has its optimal mix of renewables installed, the average residual load for all individual countries amounts to 24% of the average load, shown as the dotted line in Figure 1.2(b). However, once all countries are aggregated, each with its own optimal mix, the resulting average residual load turns out to be $\langle \Delta^-_{\mathrm{EU}} \rangle = 15\%$. This is in full agreement with the results found in [23]. This means that the largest reduction in its need for balancing energy that the average country can expect from its embedding into Europe is of the order of 40%, and sets an upper bound on what an ideal transmission system can do to reduce the need for balancing energy in Europe. While the Europe-wide optimal wind mix of $\alpha^W_{EU} = 0.82$ would result in smaller need for balancing, the bars showing mixes resulting in balancing energies within 1% of the minimum hint at a shallow optimum. For a more extensive discussion on country-specific optimal mixes, readers are directed to [6].

Unconstrained power flow

We now determine how much transmission capacity is needed for a layout to behave as though it was unconstrained. We apply the problem, as defined in equation (1.19), to a network representing 30 European countries and the links between them. The topology of the network is based on the layout reported by ENTSO-E for winter 2010-2011 [36], as well as from individual reports for links not found on ENTSO-E's report [37, 38], and is initially assumed to have no capacity constraints; see Figure 1.3.

Power flows and local balancing were calculated for every hour in the eight year span, assuming the country-specific optimal wind mixes α^W_n. The distribution of the resulting non-constrained power flow along a selected link is shown in Figure 1.4. The maximum unconstrained power flow from France to Spain amounts to 38 GW, which is larger than the combined average loads of Spain and Portugal by a factor 1.3. In the other direction the maximum flow is 75 GW, which is 1.5 times the mean load in France.

We define the Unconstrained layout as that in which all links have

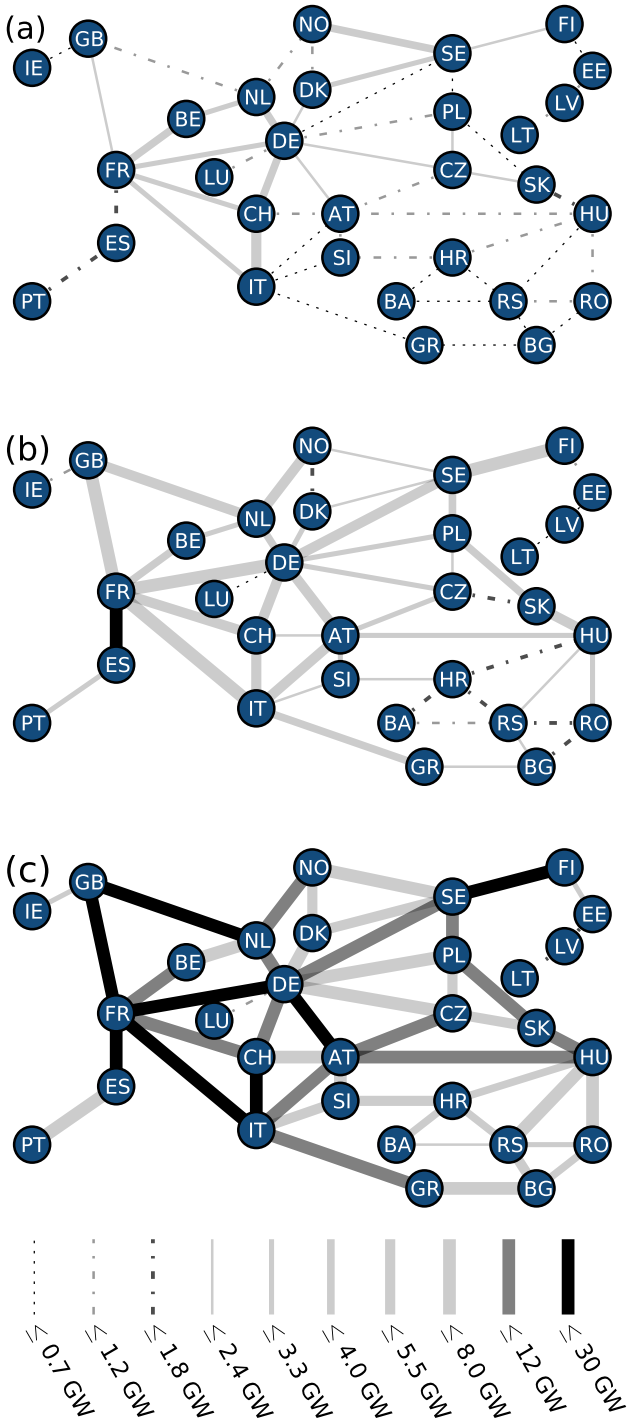

Figure 1.3: Transmission network topology and link capacity, with the links as of 2012 [36–38]. (a) Present layout capacities. (b) Intermediate layout, with a total capacity 2.3 times larger. (c) 99% Quantile layout, with 5.7 times the total capacity of (a). All three layouts are described in detail in Table 1.3. Line thickness represents the larger NTC of the interconnector.

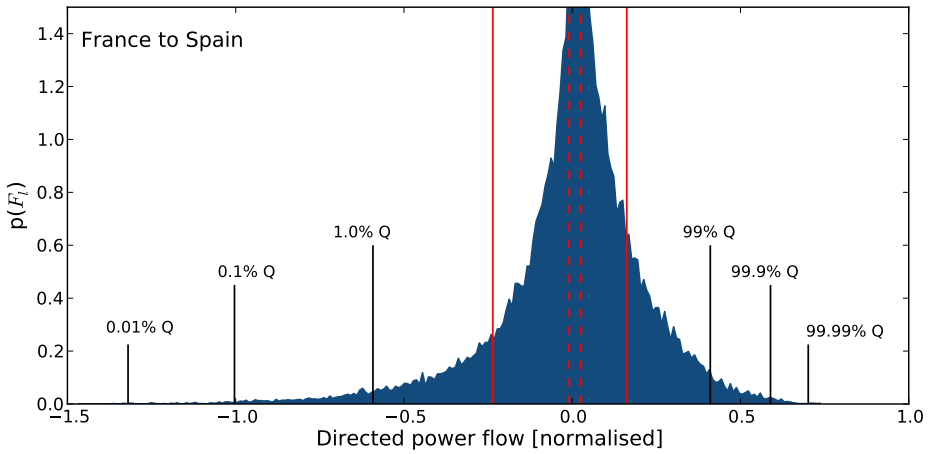

Figure 1.4: Distribution of unconstrained, non-zero power flows between France and Spain, normalised to the mean load in France (see Table 1.1). Several low- and high-quantiles are marked for illustration. The dashed red lines represent current capacities. The solid red lines show capacities as defined by the Intermediate layout. Zero-flow events occur around 46% of the time, and are not shown.

capacities equal to the maximum recorded exchange, so that power can flow unconstrained along the interconnectors. By construction, these give rise to the full benefit of cooperation, as they allow the interactions between countries to be identical to one in which they are all aggregated. The sum of the transmission capacities

$$T_C = \sum_{l=1}^{L} \max\left\{|f_l^-|, |f_l^+|\right\} \tag{1.26}$$

over the larger NTC value of each interconnector in the present layout adds up to around 73 GW. With 840 GW the Unconstrained layout capacities are 11.5 times larger. These unconstrained capacities are determined by single, one-hour events over eight years of data. Therefore, we consider the 1% and 99% quantiles of the flow distributions to define a reduced, directed capacity layout, which we call the 99% Quantile layout; see again Figure 1.4. This means that power will flow unobstructed for 98% of the time. The remaining 2% corresponds to around one week per year. The 99% Quantile layout comes with 395 GW in total and is roughly half as large as the Unconstrained layout, but still 5.7 times larger than today's interconnector capacities. See Table 1.3.

Constrained power flow

To determine what fraction of the benefit of transmission is obtained with a non-ideal, limited transmission capacity, we deal with constrained

Layout	Total transmission capacity [GW]	E [TWh]	E (percentage of annual consumption)	Benefit β of transmission
Zero transmission	0	735	24.3 %	0.0%
Present layout	73	636	21.0 %	35.5 %
Intermediate layout	158	539	17.8 %	70.8 %
99% Quantile layout	395	464	15.3 %	97.6 %
Unconstrained layout	840	457	15.1 %	100.0 %

Table 1.2: Studied layouts with their total installed transmission capacities, the required total European balancing energy E in absolute and relative terms, and the benefit of transmission β.

power flows as defined in (1.21). This allows the determination of a compromise between the reduction in balancing energy and the increase in total transmission capacity.

As can be seen in Table 1.2, the 99% quantile capacities provide, with $\beta = 97.6\%$, most of the benefit of the Unconstrained layout with less than half of the total installed capacity. The layout defined by these 99% quantiles can be seen in Figure 1.3(c). It is also noteworthy that today's capacities already provide 35.5% of the benefit of transmission, if applied to this scenario. In order to find out how the benefit scales with increasing transmission capacities, ways of interpolating between today's system and the larger layouts are now defined.

Interpolation A is an upscaling of present capacities with a linear factor a. That is, for a directed link l, the limits are defined by

$$f_l^{\mathsf{A}} = \min\left\{a f_l^{\mathsf{today}}, f_l^{99\%Q}\right\} , \tag{1.27}$$

where f_l^{today} represents the NTC of the link as of 2012 and $f_l^{99\%Q}$ those of the 99% Quantile layout.

Interpolation B involves a linear reduction of the 99% quantile capacities with factor b, that is

$$f_l^{\mathsf{B}} = b f_l^{99\%Q} . \tag{1.28}$$

Interpolation C defines the capacity layout

$$f_l^{\mathsf{C}} = f_l^{c\mathsf{Q}} , \tag{1.29}$$

which allows unconstrained flow for a percentage c of time, as shown by the different quantiles in Figure 1.4. Here, more capacity is allocated to more transited links than to less used ones.

Figure 1.5 shows the average balancing energy required by all nodes for different transmission layouts, following all three interpolations. We use the larger of the NTC on each link direction as a proxy to estimate the total installed capacity shown on the x-axis.

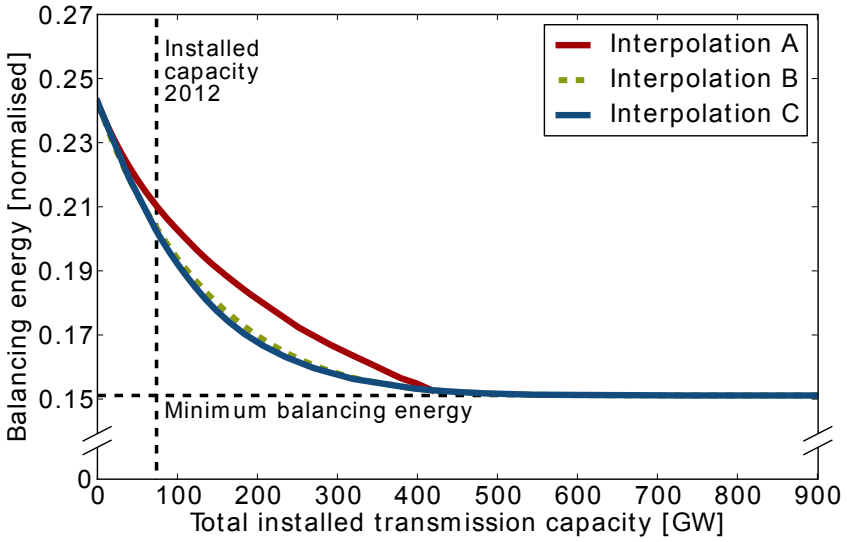

Figure 1.5: Balancing energy as a function of the total installed transmission capacity for different interpolations, normalised to the total annual consumption. The vertical dashed line indicates the total installed transmission capacity as of 2012, and the horizontal dashed line the total balancing required for the unconstrained flow. Notice that the intersection with the y-axis is congruent with the results shown in Figure 1.2 for the average balancing required.

Today's existing transmission capacity already provides a reduction in balancing energy from 24% to 21% of the annual consumption, providing 35% of the possible benefit of transmission. This is not as much as a more efficient distribution of the resources could have achieved. With the same total amount of transmission capacities, layouts B and C lead to a balancing energy of 20% of the annual consumption, with the benefit of transmission being 45%. An increase of today's total capacities by a factor of 2 in the way described by interpolations B or C, from 73 GW to 158 GW, will double the benefit of transmission to 70%, reducing the balancing energy to about 18% of the annual consumption. This new layout is between today's transmission capacities and the capacities defined by the 99% quantiles. Hence, we denote it as the Intermediate layout. It can be seen in Figure 1.3(b), and its capacities are also listed in Table 1.3. Overall results for the Intermediate layout are presented in Table 1.2.

Notice that some of the capacities under the Intermediate layout are smaller than the ones in the present one. The link between Norway and Sweden, for instance, is $f^{\text{today}}_{\text{NO-SE}} = 3.90$ GW while $f^{\text{inter}}_{\text{NO-SE}} = 2.26$ GW. This is due to the fact that the Intermediate layout is presented as a reduction of the 99% quantiles, and not as an expansion of the present one.

1.4 Discussion: country perspectives

After having quantified how much the strengthening of the interconnectors between the countries reduces the total balancing energy of Europe, we are now interested in what the different transmission capacity layouts imply for the import/export capabilities and the balancing power capacities of the single countries.

Limits to export and import capabilities

Let us have a look again at Table 1.2. Compared to the Zero transmission layout, the Unconstrained layout reduces the European balancing energy by 37.8%, from 727 TWh to 452 TWh. It is caused by the power flows from countries with an excess power generation to those with a deficit. The 37.8% can also be interpreted as the maximum capability for imports and exports. This number can not become larger since it is already based on the unconstrained transmission layout. It draws the limit to the benefit that geographical dispersion of VRES can bring to Europe. For the constrained transmission layouts the import/export capabilities are smaller. The relative reduction in balancing energy is 12.9%, 26.4% and 36.6% for the present, the intermediate and the 99% quantile transmission layouts, respectively.

So far, the reduction in balancing energy has been discussed for total Europe only. For the single countries the reduction does not need to be the same, although the average over all countries has to reproduce Europe's reduction in balancing energy. Figure 1.6 illustrates the time-averaged country-specific residual loads for the different transmission capacity layouts. Apparently, some countries have better import capabilities than others. Most of the small middle and southern countries show a pronounced reduction of balancing energy from the present to the intermediate transmission capacity layout. As to the larger countries, France benefits the most from imports, and Great Britain the least. Compared to the present transmission capacity layout, the intermediate transmission layout reduces the balancing energies between 2% (for Lithuania) and 25% (for Slovenia). For the 99% quantile transmission layout the respective reductions are in the range between 17% (for Lithuania) and 37% (for Greece).

Figure 1.6 also shows the country-specific average excess powers for the various transmission capacity layouts. For some countries like Great Britain, Ireland, the Netherlands, Romania, Croatia and Portugal the average excess powers turn out to be smaller than their average residual loads. With the further extension of the present transmission capacity layout, these countries will be able to export more than what they will be able to import. Other countries like Switzerland, Austria and Czech Republic will become strong importers. It is interesting to note that the

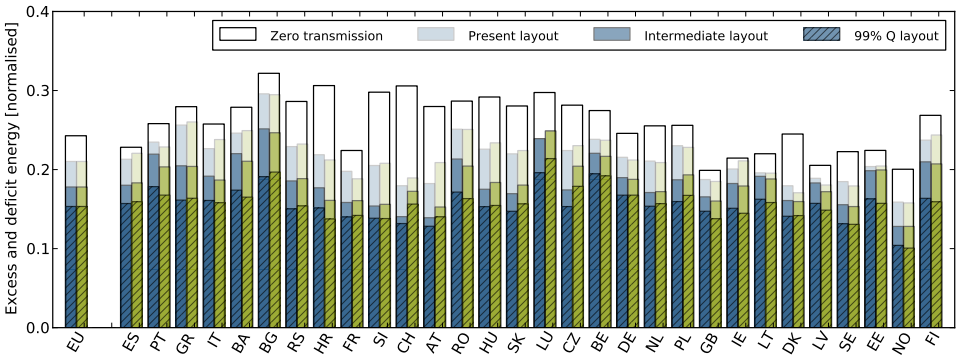

Figure 1.6: Country-specific average residual loads (blue) and excess energies (green) on the Zero transmission layout, the Present layout, the Intermediate layout and the 99% Quantile layout. Residual loads and excess energies are normalised by the average load. Bars are not stacked. The optimal wind mixes a_n^W from Figure 1.2 (a) have been used for each country. Note, that the residual loads for the Zero transmission layout are identical to those shown in Figure 1.2 (b).

stronger transmission capacity layouts quite naturally lead to stronger import/export imbalances for the countries. Please refer to [6] for an extended discussion on countries' export and import capabilities on the road to future energy systems.

Balancing power capacities

Figure 1.7 shows the distributions of non-zero mismatches for three selected countries, as they change for different transmission capacity layouts. The central part of the distributions are lowered as the transmission capacity layouts become stronger. This connects nicely to the results on the reduction of average residual load and excess power, which have been discussed in the previous subsection. While the central part of the distribution, lying between -1 and $+1$ times the mean load, noticeably shrinks with increasing transmission layouts, the tails, lying below -1 and above $+1$ remain unaffected. Referring to Figure 1.2(c), this implies that the 99% quantiles of the residual load and the excess power for the non-zero transmission capacity layouts are not reduced when compared to those for the zero transmission capacity layout. In other words, it appears that increased transmission does not affect the maximum balancing power, and that Europe has to keep its present dispatchable power generation capacity.

However, this would be a pre-mature conclusion. The objective of the current power flow modelling, as presented in Section 1.2, has been first to reduce the overall balancing energy the most using only export of excess generation, and then to determine the most localised power flow across the network. The objective has not been to reduce the high

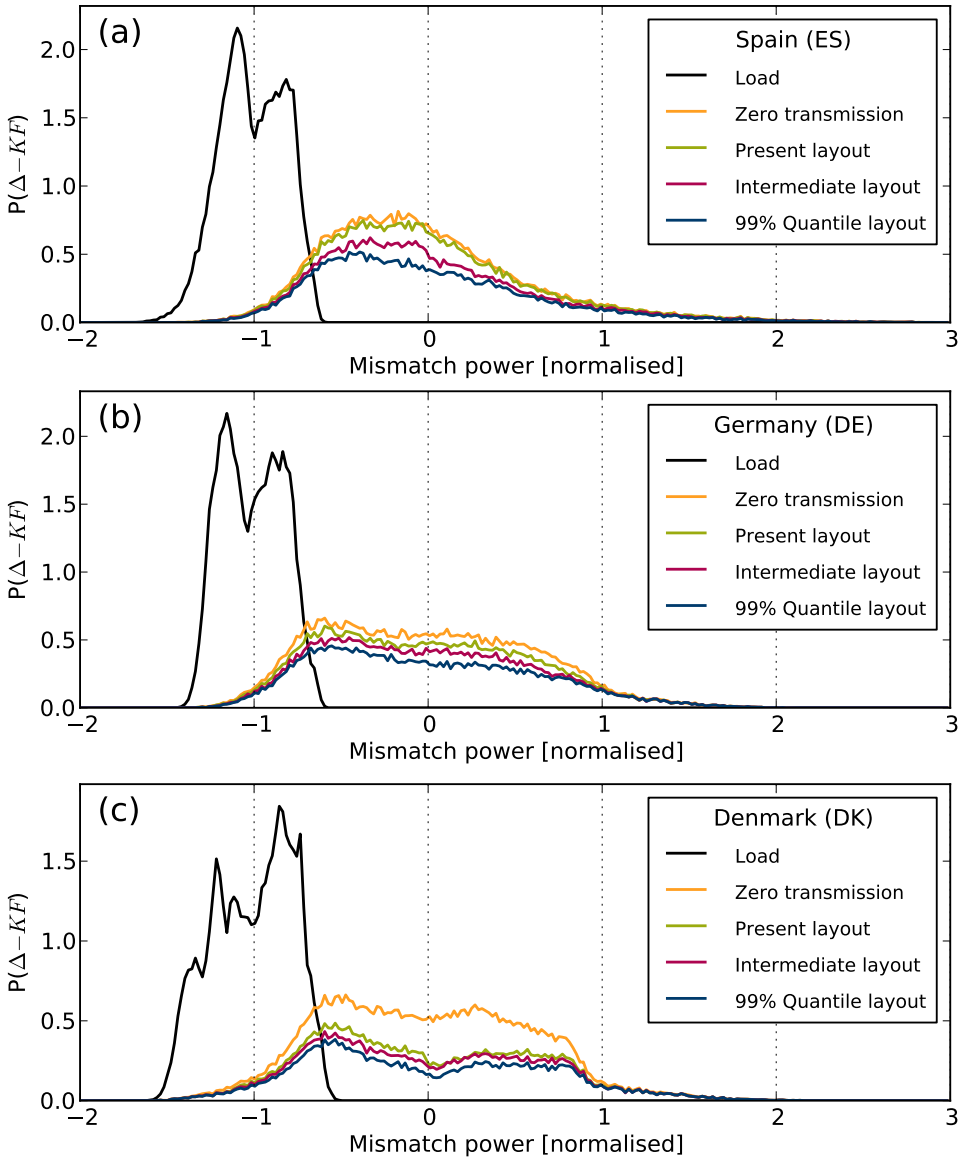

Figure 1.7: Normalised non-zero distributions for residual load (below zero) and excess generation (above zero). (a) Spain, (b) Germany and (c) Denmark, with a country-specific optimal mix of wind and solar. Apart from the zero transmission scenario (orange), three layouts are shown: the Present layout (green), the Intermediate layout (purple) and the 99% Quantile layout (blue). For comparison, the distribution of the normalised load (black) is also shown.

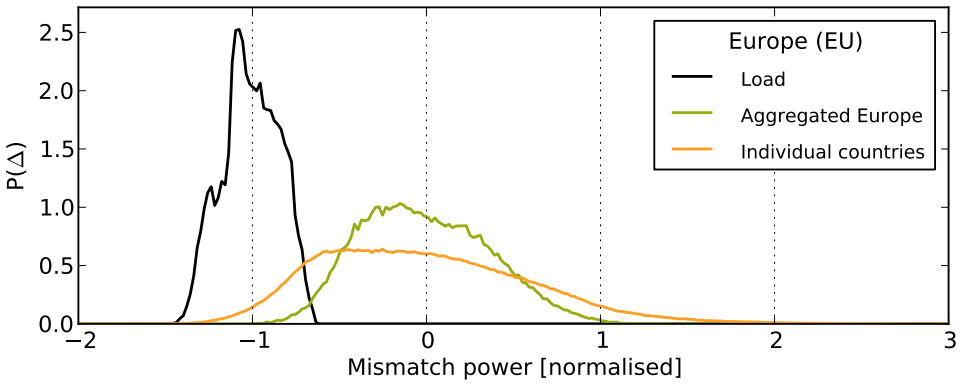

Figure 1.8: Normalised non-zero mismatch distribution for Europe resulting from the unconstrained transmission scenario (green) and for an average country in the zero transmission scenario (orange). For comparison, the distribution of the normalised European load (black) is also shown.

quantiles of the residual load at each node of the network. In other words, the reduction of balancing power capacities has not been prioritised in the current power flow modelling. Figure 1.2(c) gives an indication about how much the balancing power capacities can be reduced in principle. The first bar of this figure shows the 1% quantile of the mismatch for an aggregated Europe. With 73% of the average European load it is significantly smaller than 108%, which holds true for an average independent single country. This is also nicely visualised in Figure 1.8, which shows the respective mismatch distribution for Europe with unconstrained transmission and for an average country in the zero transmission scenario. Compared to the single-country distribution, both tails of the European distribution are significantly shifted towards zero mismatch – making the mismatch distribution narrower. The explanation for this reduction in the overall balancing capacities lies in the sharing of balancing capacities between countries.

This effect of shared balancing is not taken into account in the current power flow modelling, where after import of excess renewable power the countries balance their remaining deficit fully by themselves. Shared balancing implies that countries are allowed to import part of their remaining deficit from balancing capacities of other countries, which are not fully used at the same time. This of course also leads to additional power flows. A self-consistent treatment of power-flow modelling with shared balancing capacities will not be given here. Other ways of reducing peak balancing power could include demand flexibility, the use of energy storage, and penetration of renewables larger than 100%. For the moment we will leave all of this open for future investigations.

1.5 Conclusion

We have quantified the benefit of the far-future pan-European transmission system when, by assumption, all countries have reached a 100% penetration of combined wind and solar power generation. Two extreme transmission scenarios, Zero and Unconstrained, can be treated without any power flow calculations. For the scenario with zero inter-connectors, the countries can be discussed separately. Their annual balancing energy, which is required to cover the negative mismatches between their renewable power generation and their load, depends on the wind share α_n^W of VRES power generation, becomes minimal at $\alpha_n^W \approx 0.71$ (with a small dependence on the geographical latitude), and then results to be around 24% of their annual electricity consumption. For the scenario with infinitely strong inter-connectors and no transmission losses, all country-specific mismatches can be directly aggregated into an overall European mismatch. This leads to a required balancing energy that is only 15% of the total annual European electricity consumption. The difference 24% - 15% between the outcomes of the two extreme scenarios represents an upper limit on the benefit that a pan-European transmission system can provide. In other words, no transmission layout is able to further reduce the required balancing energy.

In order to estimate the benefit of transmission capacities constrained between zero and infinity, a novel modelling approach has been presented, which calculates the constrained power flows for a pan-European network. Based on highly resolved spatio-temporal weather data, it first minimises the all-European residual load, so that as much of the overall renewable power generation is used as possible. In a second step, the square sum over all flows is minimised, leading to a very local flow pattern. This process allows us to avoid making assumptions regarding market-economic policies. This novel modelling approach reveals that an infinitely strong European transmission network should be 11.5 times as strong as today's total inter-connector capacities. A capacity layout five times as large as today's provides 98% of the benefit of transmission, which is almost as good as the infinitely strong layout for the reduction of required balancing energy. For weaker transmission networks, the relationship between the need for balancing energy and the total capacity of the transmission layout turns out to be non-linear and convex. A good compromise between these two conflicting objectives, i.e. on the one hand reducing the balancing energy as much as possible and on the other to increase the transmission capacities as little as possible, appears to be an Intermediate layout with total transmission capacities being twice as large as today's capacities. This Intermediate layout leads to a 70% benefit of transmission. Compared to the Zero transmission layout it reduces the required European balancing energy from 24% to 18% of

the annual consumption. This reduction from 24% to 18% also implies that an average country participating in the pan-European transmission network can only import around a quarter of its own balancing needs, and that the remainder must come from its own balancing resources.

The presented findings have focused on the transmission needs in a fully renewable European power system. The penetration of combined wind and solar power generation has been assumed to be exactly 100%. Of course, this can be generalised to penetrations below 100%, and thus provide information on the required ramp-up of transmission needs all the way from today's penetration to the far-future 100% penetration [6]. In this respect, also a modification of the network topology should be discussed, like for example the addition of new links across the North Sea. In order to reduce the need for balancing energy further below the discussed 15% limit of the annual electricity consumption, one could look at renewable penetrations above 100% and discuss more synergies between balancing, transmission and storage. Although outside of the scope of the present work, a cost-optimal system layout, including VRES, balancing, transmission and storage capacities, needs to be explored.

Acknowledgements: The authors thank Uffe Poulsen and Morten G. Rasmussen for insightful discussions. S.B. gratefully acknowledges financial support from O. and H. Stöcker, and G.B.A. financial support from DONG Energy and The Danish National Advanced Technology Foundation.

Appendix

Link	Present Layout (GW)	Intermediate Layout (GW)	99 % Q Layout (GW)	Unconstrained Layout (GW)
AT ⇄ CH	0.47 1.20	2.26 2.05	5.65 5.13	14.06 11.50
AT ⇄ CZ	0.60 1.00	3.23 2.78	8.08 6.94	15.75 12.08
AT ⇄ HU	0.80 0.80	2.31 3.23	5.78 8.09	10.38 19.56
AT ⇄ DE	2.00 2.20	5.27 4.26	13.17 10.64	28.33 17.36
AT ⇄ IT	0.22 0.28	3.39 4.10	8.48 10.25	15.38 21.55
AT ⇄ SI	0.90 0.90	1.96 2.66	4.90 6.64	7.92 15.53
FI ⇄ SE	1.65 2.05	5.86 4.13	14.64 10.31	24.54 15.32
FI ⇄ EE	0.35 0.35	0.98 1.16	2.45 2.91	4.28 5.12
NL ⇄ NO	0.70 0.70	4.03 4.20	10.07 10.50	19.31 19.94
NL ⇄ BE	2.40 2.40	2.87 3.05	7.17 7.62	12.88 16.28
NL ⇄ GB	1.00 1.00	4.71 5.08	11.77 12.70	26.99 25.03
NL ⇄ DE	3.00 3.85	3.59 3.48	8.98 8.70	19.10 19.57
BA ⇄ HR	0.60 0.60	1.42 0.91	3.54 2.28	7.22 3.85
BA ⇄ RS	0.35 0.45	0.96 0.72	2.39 1.79	4.16 4.03
FR ⇄ BE	3.40 2.30	3.39 3.26	8.49 8.15	19.11 13.89
FR ⇄ GB	2.00 2.00	6.03 6.49	15.07 16.24	31.20 27.63
FR ⇄ CH	3.20 1.10	4.27 3.94	10.69 9.84	26.02 25.90
FR ⇄ DE	2.70 3.20	6.67 6.18	16.67 15.46	35.41 31.28
FR ⇄ IT	2.58 0.99	6.51 7.52	16.27 18.80	36.46 40.46
FR ⇄ ES	1.30 0.50	8.39 12.11	20.98 30.28	37.67 75.44
NO ⇄ SE	3.60 3.90	2.26 2.18	5.64 5.46	11.96 13.57
NO ⇄ DK	0.95 0.95	1.69 1.49	4.22 3.73	8.18 7.59
GB ⇄ IE	0.45 0.08	1.03 0.92	2.59 2.29	4.50 4.34
PL ⇄ CZ	1.80 0.80	2.11 2.12	5.28 5.30	8.93 11.42
PL ⇄ DE	1.10 1.20	2.67 2.60	6.69 6.50	12.87 12.42

Table 1.3.a: Interconnector capacities for different layouts.

Link	Present Layout (GW)	Intermediate Layout (GW)	99% Q Layout (GW)	Unconstrained Layout (GW)
PL ⇄ SE	0.00	3.23	8.07	18.51
	0.60	3.66	9.14	16.96
PL ⇄ SK	0.60	2.70	6.76	11.10
	0.50	3.39	8.49	16.79
BG ⇄ GR	0.55	2.21	5.53	14.41
	0.50	1.94	4.85	10.49
BG ⇄ RO	0.60	1.35	3.37	7.09
	0.60	1.02	2.56	5.11
BG ⇄ RS	0.45	2.03	5.08	11.09
	0.30	1.26	3.16	5.82
GR ⇄ IT	0.50	4.00	9.99	20.46
	0.50	2.66	6.66	11.69
PT ⇄ ES	1.50	2.47	6.18	12.35
	1.70	1.87	4.68	7.79
CH ⇄ DE	3.50	4.55	11.37	21.86
	1.50	4.13	10.34	16.66
CH ⇄ IT	4.17	3.64	9.10	14.92
	1.81	4.90	12.24	26.52
HR ⇄ HU	0.80	1.46	3.66	7.26
	1.20	1.10	2.76	4.89
HR ⇄ RS	0.35	0.85	2.14	3.24
	0.45	1.32	3.31	7.42
HR ⇄ SI	1.00	2.09	5.21	12.94
	1.00	1.60	3.99	7.09
RO ⇄ HU	0.70	3.07	7.68	16.10
	0.70	1.94	4.84	7.45
RO ⇄ RS	0.70	1.30	3.26	5.68
	0.50	0.79	1.98	3.82
CZ ⇄ DE	2.30	2.91	7.27	16.52
	0.80	2.58	6.44	12.49
CZ ⇄ SK	2.20	1.28	3.21	5.46
	1.20	1.74	4.34	8.76
HU ⇄ RS	0.60	1.67	4.18	6.47
	0.70	2.32	5.79	13.11
HU ⇄ SK	0.60	4.31	10.76	24.98
	1.30	3.30	8.26	13.65
DE ⇄ SE	0.60	3.93	9.83	16.70
	0.61	4.38	10.94	20.40
DE ⇄ DK	1.55	2.61	6.51	12.12
	2.08	2.77	6.92	12.94
DE ⇄ LU	0.98	0.25	0.63	0.91
	NRL	0.34	0.86	1.51
SE ⇄ DK	1.98	1.87	4.67	8.40
	2.44	1.66	4.16	7.24
IT ⇄ SI	0.16	2.18	5.45	12.26
	0.58	1.99	4.97	12.72
EE ⇄ LV	0.75	0.58	1.45	2.57
	0.85	0.67	1.68	3.08
LV ⇄ LT	1.30	0.41	1.01	1.73
	1.50	0.48	1.21	2.16

Table 1.3.b: Interconnector capacities cont. (NRL, No Realistic Limit)

Chapter 2

Export schemes

Motivation

In the previous chapter, we explored the benefit that a sufficiently large transmission grid offers in terms of reduced backup energy E^B. By being able to shift excess generation to where it is needed, countries can make more efficient use of their resources. We saw that around 5 times as much capacity has to be installed in order for the average balancing energy of individual countries $E^B_{\text{ind.}}$ to be equal to the balancing energy required by a hypothetical, 'copper plate' Europe, E^B_{EU}.

The same is not true of backup capacities, determined by high quantiles of the backup probability distribution. Figure 4 shows the reduction in $\mathcal{K}^B_{\text{ind.}}$ with increases in $\mathcal{K}^T_{\text{EU}}$, from that of the disconnected system to that of the fully connected one. The total backup capacity for the individual countries $\mathcal{K}^B_{\text{ind.}}$ does not reach the limit that is set by the backup capacities of aggregated Europe $\mathcal{K}^B_{\text{EU}}$. These results are disappointing, since they point at a possibility to reduce the amount of fuel coming from conventional resources, but not a reduction of conventional capacities.

The reason for this stems from the optimisation targets we have set. Step one, which minimises the total backup energy (26), does not spread out the duty of backup to other nodes. Backup power from the local node is just as good as that from the neighbour's, and importing backup would incur additional flows, which are punished by step two (27). When we aggregate Europe as a single entity, nodes share backup resources from a common source. This triggers the driving question for this chapter: Is there an export scheme to trade backup energy, so that the total need for backup capacity can be reduced?

Methods

Throughout this chapter we compare the properties and consequences of three export schemes, illustrated in Figure 5 below. The figure shows a set of three interconnected

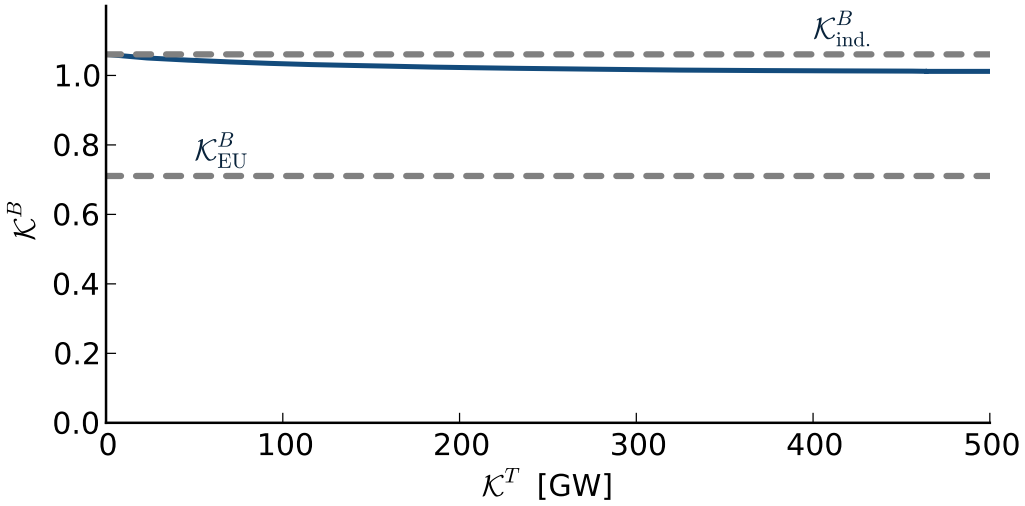

Figure 4: Total backup energy capacity in Europe $\mathcal{K}^B$, normalised to mean hourly demand, as a function of the total installed transmission capacity $\mathcal{K}^T$. We assume a penetration of $\gamma_n = 1$ and an optimal wind mix $\alpha_n = \alpha^*$ for all countries. The dashed lines indicate the energy required by an average disconnected country ($\mathcal{K}^B_{\text{ind.}}$) and an aggregated Europe ($\mathcal{K}^B_{\text{EU}}$).

nodes in a system with a global negative mismatch $\sum_n \Delta_n < 0$, meaning that additional backup must be provided to cover the deficit in generation.

The first panel, 5(a), shows the Zero export scheme, in which nodes do not trade any resources. The second panel, 5(b), shows the Localised export scheme which was the subject of Chapter 1 and [1], dominated by the optimisation problem defined in (26) and (27). In this case, the objective is to utilise as little backup as possible (9 units). Excessive flows are punished, so the most effective way of doing this is to give three additional units to each of the neighbouring nodes, who must then provide their own additional backup. The last panel, 5(c), shows the proposed new scheme, termed Synchronised export scheme. In this case, the total backup duties are equally shared between the nodes. In the actual implementation we distribute them according to the size of the country, so that all countries curtail or provide

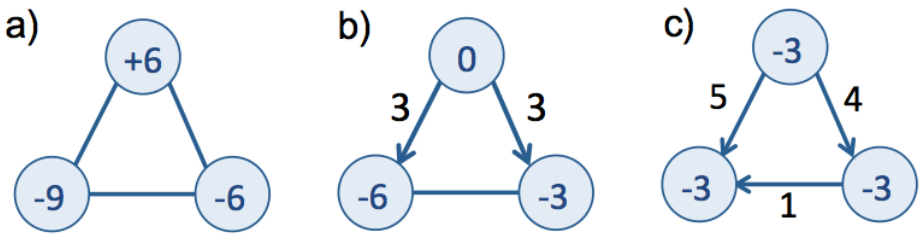

Figure 5: Three export schemes: zero transmission (a), localised (b), and synchronised (c). There is a global mismatch of -9, which must be covered by some or all of the nodes.

backup with the same amount proportional to their mean load.

This behaviour can be achieved by a modification to the first step in the optimisation problem from the Localised scheme, by minimising the sum of the square of the backup power and curtailment, instead of the simple sum:

$$\begin{aligned} \text{step 1}: \quad & \min\left(\sum_n \frac{(B_n(t)-C_n(t))^2}{\langle L_n\rangle}\right) && (31)\\ \text{subject to}: \quad & \boldsymbol{\Phi} = \boldsymbol{K}\boldsymbol{F}, \\ \text{step 2}: \quad & \min\left(\sum_l F_l^2(t)\right) && (32)\\ \text{subject to}: \quad & \boldsymbol{\Phi} = \boldsymbol{K}\boldsymbol{F}, \\ & B_n = B_n^*\,. \end{aligned}$$

Flow constraints will no longer be considered for simplicity, but they could easily be added. Note that, in this case, we enforce $B_n = B_n^*$ in the second step instead of just $\sum_n B_n = \sum_n B_n^*$. This is because the Synchronised export scheme's first step *does* uniquely define the injection pattern $\boldsymbol{\Phi}$. There are analytical, geometric, and even economic interpretations that help explain why this is a good idea.

Geometric interpretation

Going back to the general statement of the node from equation (14), we can group terms by

$$\boldsymbol{\Omega} = \boldsymbol{B} - \boldsymbol{C}\,; \qquad \boldsymbol{\Delta} = \boldsymbol{G} - \boldsymbol{L}\,; \qquad \boldsymbol{\Phi} = \boldsymbol{E} - \boldsymbol{I}\,, \tag{33}$$

so that we can rewrite the node equation as

$$\boldsymbol{\Omega} + \boldsymbol{\Delta} = \boldsymbol{\Phi}\,. \tag{34}$$

We can display each of these vectors in an N-dimentional space (shown for $N = 2$ countries in Figure 6), where the positive side of the axes shows a positive power imbalance $p_i > 0$ and the negative side a negative imbalance $p_i < 0$. The vector $\boldsymbol{n}$ in the top right quadrant marks a diagonal where the power from country p_a is equal to the power from country p_b. The vector $\boldsymbol{L}$ has components $\langle L_a\rangle$ and $\langle L_b\rangle$, and the dashed line it marks has points where the relative load between a and b is equal, $p_a/\langle L_a\rangle = p_b/\langle L_b\rangle$. We can plot the mismatch $\boldsymbol{\Delta}$ as a vector from the origin. The top right quadrant shows mismatches where $\Delta_i > 0$ for all i, whereas points to the right of the dotted line show global positive mismatches $\sum_i \Delta_i > 0$. The vector $\boldsymbol{\Delta}$ shows a negative global mismatch, since $\sum_i \Delta_i < 0$. We can plot a vector representing the injection pattern, or the transfer of mismatch from one country to the other. This vector $\boldsymbol{\Phi}$ must fulfil $\sum_i \Phi_i = 0$, since we consider no losses and no country can receive more or less than what another country sends. This constraint can be enforced by making sure that $\boldsymbol{\Phi}$ is perpendicular to $\boldsymbol{n}$. It is clear that, unless

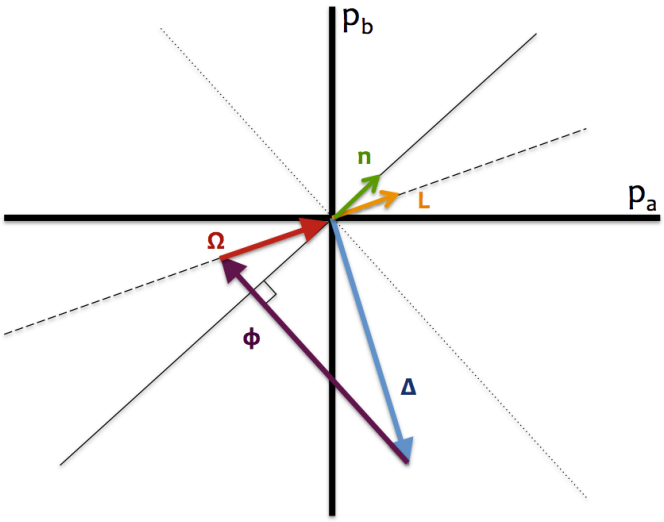

Figure 6: Geometric representation of the power balance between two nodes a and b, inspired by [48]. Vectors are used to indicate the mismatch Δ, the injection pattern Φ, and the backup/curtailment Ω. The solid line indicates equal magnitudes between p_a and p_b, the dashed line equal magnitudes relative to their mean load L_a and L_b, and the dotted line is used to show perpendicularity to the solid line, so that $p_a = -p_b$.

$\boldsymbol{\Delta}$ is also perpendicular to $\boldsymbol{n}$ (meaning that a country has in excess the same amount as the other has in deficit), some additional backup or curtailment $\boldsymbol{\Omega}$ will be required.

If we allow $\boldsymbol{\Phi}$ to stop at the y-axis where $p_a = 0$, then country a will have given b all of its excess, leaving $\boldsymbol{\Omega} = \Omega_b$. Alternatively, we can allow it to continue until the solid line that marks $p_a = p_b$, leaving $\Omega_a = \Omega_b$, but if the countries have very different sizes, this might imply a smaller country providing backup outside of its capabilities. We instead project $\boldsymbol{\Delta}$ onto the line marked by $\boldsymbol{L}$, with the constraint that the projecting vector $\boldsymbol{\Phi}$ must be perpendicular to $\boldsymbol{n}$. This means that both countries will provide the same amount of backup with respect to their mean loads.

The magnitude of $\boldsymbol{\Omega}$ is then the euclidean distance between $\boldsymbol{\Delta}$ and $\boldsymbol{\Phi}$ with the constraint that $\sum_i \Phi_i = 0$, or

$$\min \sum_i \frac{(\Phi_i - \Delta_i)^2}{\langle L_i \rangle}, \tag{35}$$

which is equivalent to (31).

Analytical interpretation

We want the backup power of individual countries $B_n(t)$ to more closely resemble that of an aggregated Europe $B_{\mathrm{EU}}(t)$, so that it results in the reduced need for backup capacity $\mathcal{K}^B_{\mathrm{EU}}$. We claim that this can be achieved by a minimisation of the

sum of the square of the backup power:

$$\min \sum_n \frac{(\Phi_n - \Delta_n)^2}{\langle L_n \rangle}\,, \tag{36}$$

under the constraint that

$$\boldsymbol{\Phi} = \boldsymbol{K}\boldsymbol{F}\,, \tag{37}$$

which is to say that the sum of all exports must equal the sum of all imports

$$\sum_n \Phi_n = 0\,. \tag{38}$$

We replace the terms

$$\delta_n = \Delta_n / l_n\,; \qquad \phi_n = \Phi_n / l_n\,, \tag{39}$$

where $l_n = \sqrt{\langle L_n \rangle}$, while rephrasing the constraint as

$$\sum_n \phi_n \cdot l_n = 0\,, \tag{40}$$

to maintain the original requirement on net flows.

We can find an equation that is equivalent to our minimisation while obeying the constraint in (38) by using Lagrange multipliers. We define a function $z(\boldsymbol{\phi})$

$$z(\boldsymbol{\phi}) = \sum_n (\phi_n - \delta_n)^2 + \lambda \sum_n \phi_n \cdot l_n \tag{41}$$

and derive with respect to an entry ϕ_m

$$\frac{\mathrm{d}z}{\mathrm{d}\phi_m} = 2(\phi_m - \delta_m) + \lambda \cdot l_m\,. \tag{42}$$

By making (42) equal to zero, we find

$$\phi_m = \delta_m - \frac{\lambda \cdot l_m}{2}\,, \tag{43}$$

which means that we can rewrite the constraint as

$$\sum_n \phi_n \cdot l_n = \sum_n l_n \left(\delta_n - \frac{\lambda \cdot l_n}{2}\right) = 0 \tag{44}$$

and find

$$\lambda = 2\frac{\sum_n l_n \cdot \delta_n}{\sum_n l_n^2}\,. \tag{45}$$

Going back to (43), we can replace the value of the multiplier λ to find an equation that obeys the constraint in (38):

$$\phi_m = \delta_m - \frac{\sum_n l_n \cdot \delta_n}{\sum_n l_n^2} \cdot l_m\,. \tag{46}$$

Switching back to our original vectors, we get

$$\frac{\Phi_m}{\sqrt{\langle L_m \rangle}} = \frac{\Delta_m}{\sqrt{\langle L_m \rangle}} - \frac{\sum_n \Delta_n}{\sum_n \langle L_n \rangle} \cdot \sqrt{\langle L_m \rangle} \tag{47}$$

$$\Phi_m = \Delta_m - \left(\frac{\sum_n \Delta_n}{\sum_n \langle L_n \rangle} \right) \langle L_m \rangle \,. \tag{48}$$

The term in parenthesis is simply the European mismatch Δ_{EU} divided by the European mean load $\langle L_{\mathsf{EU}} \rangle$,

$$\Delta_m - \Phi_m = \Omega_m = \left(\frac{\Delta_{\mathsf{EU}}}{\langle L_{\mathsf{EU}} \rangle} \right) \langle L_m \rangle \,. \tag{49}$$

This means that all countries m provide backup or curtailment with an equal amount Ω_m proportional to their mean load. Adding these up together covers the European mismatch.

Market interpretation

When dealing with the issue of efficient use of resources, an economic theory is bound to be of interest. The supply and demand curve, which can be used to define the marginal cost of procuring goods, helps define the merit order in energy supply (see Figure 7). The merit order is used to make sure that the resources with the lowest marginal cost of generation are dispatched first to satisfy the demand. A supply and demand curve will stack, on the x-axis, the generation capacity of all available resources at a given time. When the curve that defines the demand for electricity joins the one defined by the supply, the marginal cost of the last unit generated defines the price to be paid to all the generators below that point [49].

In a supply and demand curve built to satisfy all of the load $L_n(t)$, resources with zero or near zero marginal costs (wind, solar photovoltaics, hydro lakes) would be placed first in line. Since we are dealing with a high degree of renewables and only wish to cover the residual load, we subtract VRES generation from the initial demand and consider only the backup needs.

Although, as mentioned above, the price of the last unit of backup required $\mathrm{d}\mathcal{C}_n(B_n)$ will be the price paid for all produced electricity, the total cost of producing that electricity is

$$\mathcal{C}_n = \int_0^{B_n} \mathrm{d}\mathcal{C}_n(B_n) \,. \tag{50}$$

The localised export scheme used in [1] and described in Figure 5(b) assumes a constant marginal cost of electricity for all countries, independent of the amount of backup being provided. This means that, when deciding where to procure the next unit of power, a node might as well choose its own generation over its neighbours, as the cost is the same and it implies less flow. In reality, nodes that are already providing a large amount of backup might prefer to import some of the cheaper capacity from their neighbours, if possible.

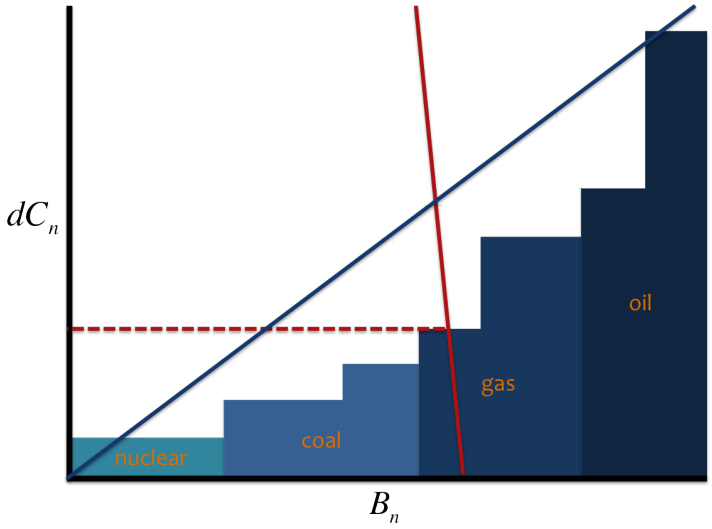

Figure 7: Example of a supply and demand curve, where available power is arranged by marginal cost. The red line indicates electricity demand, and the dashed line indicates the price paid for that demand. The blue line indicates a linear approximation, using $\mathrm{d}\mathcal{C}_n(B_n) = f\frac{B_n}{\langle L_n\rangle}$.

The diagonal shown in Figure 7 proposes an approximation of the supply curve to a linear function

$$\mathrm{d}\mathcal{C}_n(B_n) = f\frac{B_n}{\langle L_n\rangle}\,. \tag{51}$$

Working under the assumption that the supply curve in all countries follows the above implies a couple of things. Firstly, that all nodes have a roughly similar distribution of installed dispatchable power capacities relative to their mean loads. We know this not to be strictly true. France, for example, possesses a larger than average nuclear power capacity, and Norway relies almost exclusively on hydro power. Secondly, that there is a similar cost factor f accross all countries. This means that providing a new MW of power when France's dispatchable capacities are operating at 60% costs is exactly the same as providing it from one of its neighbours, if that neighbour is also operating at 60%.

Real supply curves appear to be quadratic rather than linear, but we believe that, as a first approach, a linear approximation can reveal interesting dynamics. Under the relation in (51), the integral in (50) summed across all countries becomes

$$\mathcal{C}_n = \int_0^{B_n} f\frac{B_n}{\langle L_n\rangle} = \frac{f}{2}\cdot\frac{B_n^2}{\langle L_n\rangle}\,. \tag{52}$$

A minimisation of the total cost of providing backup to the system would be, again, identical to (31).

Main findings

Using the same systems as in [1], we model a fully renewable electricity system with $\gamma_n = 1$ for all n, using three export schemes: the zero exports, the localised exports as in [1], and the synchronised exports proposed in the previous section. Figure 2.6 shows the reduction in backup capacity $\mathcal{K}^B$ for these three export schemes. The reduction achieved by the synchronised scheme is more than twice what the localised reaches, since nodes are sharing their backup capacities.

The probability distribution histogram that shows the behaviour of backup capacities looks identical for all countries (Figure 2.4), since they all provide backup or curtailment simultaneously. This, however, leads to higher flows along all links, as can be seen in Figure 2.9. Depending on the mixing parameter α, the synchronised export scheme can use up to twice as much installed transmission capacity $\mathcal{K}^T$. This opens up two important lines of research which are approached in [3] and [4] and can be summarised with a few questions: Are all countries equally responsible for the flow of renewables in a network? Which nodes benefit most from the existence of a link? Is the decrease in backup capacity worth the increased need for transmission?

Selfish vs. cooperative exports across a fully renewable pan-European power network

Rolando A. Rodriguez[a], Magnus Dahl[b], Martin Greiner[a,c]

a Department of Mathematics, Aarhus University, Denmark

b Department of Physics and Astronomy, Aarhus University, Denmark

c Department of Engineering, Aarhus University, Denmark

Abstract

Compared to no or very limited power transmission, unconstrained power flows across a fully renewable pan-European electricity network significantly reduce the overall amount of required annual backup energy, but not necessarily much of the required backup capacities. The reduction of the backup capacities turns out to be very sensitive on the choice of export scheme determining the power flows. Two selfish export schemes are discussed, which export only renewable excess power, but no backup power, and are compared to a cooperative export scheme, which exports renewable excess power and also backup power. It turns out that the cooperative export of local backup power to other countries is crucial to significantly save on installed backup capacities.

keywords: renewable energies, energy system, power transmission, pan-European transmission grid,

2.1 Background

Todays macro energy systems, mainly based on conventional fossil and nuclear resources, will in the future increasingly rely on renewable resources. At the moment it is not really clear what will be the best transitional pathway between the current and the future energy system. In this respect it makes sense to think backwards, which means in a first step to get a good understanding of fully renewable energy systems [1, 12, 13, 15–18, 23–25, 27, 31, 40, 50–55] and then in a second step bridge to todays energy system [6, 26]. Since wind and solar power generation are expected to be dominant, the fluctuating spatio-temporal weather patterns will determine the design of fully renewable energy systems. Based on state-of-the-art high-resolution meteorological data [30], spatio-temporal modelling, and the physics of complex networks [56, 57], some fundamental properties of a fully renewable pan-European power system have already been derived. Amongst such characteristics are the optimal mix of wind and solar power generation [23, 24], the optimal combination of storage and balancing [25], the optimal extension of the transmission network [1, 6], and the optimal ramp down of conventional power generation during the transitional phase [26]. These results indicate that the pathways into future energy systems will be driven by an optimal systemic combination of technologies.

The benefit of transmission in fully renewable energy networks has been discussed in [1]. The backup energy, which integrates over the usage of backup units in order to balance temporal deficits of the renewable power generation, turns out to be a strongly convex function of the overall transmission line capacities. For a fully renewable pan-European power system with zero interconnector capacities the required backup energy decreases from 24% of the annual electricity consumption down to 15% with sufficiently large unconstrained transmission capacities. Most of this reduction is already achieved with transmission capacities which are 3-4 times larger than today's interconnector strengths. Although backup energy quickly decreases with increasing transmission capacities, it has been observed that the backup capacities are not similarly reduced [1].

The objective of this paper is to generalise the interplay between backup and transmission used in [1], and to discuss its potential for a combined reduction of backup energy and capacity in a fully renewable energy network. Figure 2.1 gives an illustration of this objective. The first node in the triangular network (a) generates more renewable power than what it consumes; it has two units of renewable excess power. The other two nodes do not generate enough renewable power compared to what they consume, and have a deficit of 3 and 2 units, respectively. In (b), which is the export scheme used in [1], the source node exports one

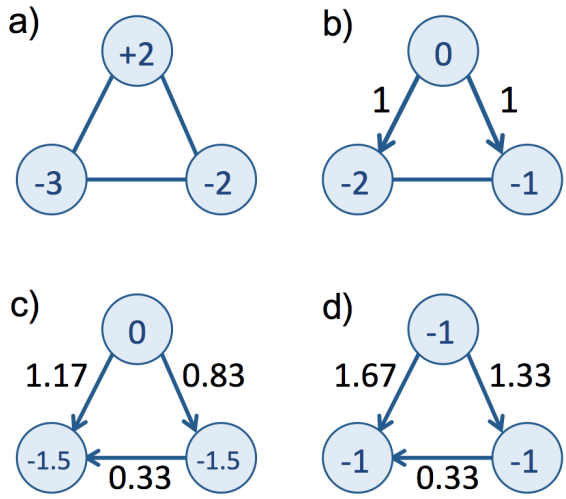

Figure 2.1: The network with one source and two sinks can be balanced via different export schemes: (a) zero exports, (b) maximum export of renewable excess power with minimum overall power flow, (c) maximum export of renewable excess power with maximum reduction of local backup, (d) combined export of renewable excess and backup power with maximum reduction of local backup.

excess unit to each of the two sink nodes, which then still have to balance two and one units, respectively. In (c) the source node also exports its two excess units, but now in such a way that after their imports the two sink nodes have to balance the same amount of 1.5 units. In (d) the source node exports three units, which is more than its own excess power. Two units go to the second node and one unit to the third node. All three nodes are then left to balance one unit.

Behind scheme (b) is the minimum squared flow principle. After the maximum export of the source node's excess power the resulting power flows through the network are minimal. Since the role of the three nodes might swap due to the fluctuating weather patterns, (b) leads to a network-wide backup energy of three units, a backup capacity of two units per node and a transmission capacity of one unit per link. In (c), after the maximum export of the source node's excess power, the resulting flow leads to an equal usage of backup capacity for the sink nodes. The scheme (c) also leads to a network-wide backup energy of three units, but when compared to (b) the backup capacity per node is only 1.5 units, whereas the transmission capacity per link has increased to 1.17 units. The shared backup principle of (d) requires all nodes to balance the same amount after the imports and exports have taken place. It also keeps the network-wide backup energy to three units. The backup capacity at each node is reduced to one unit, and the transmission capacities of the links are increased to 1.67 units.

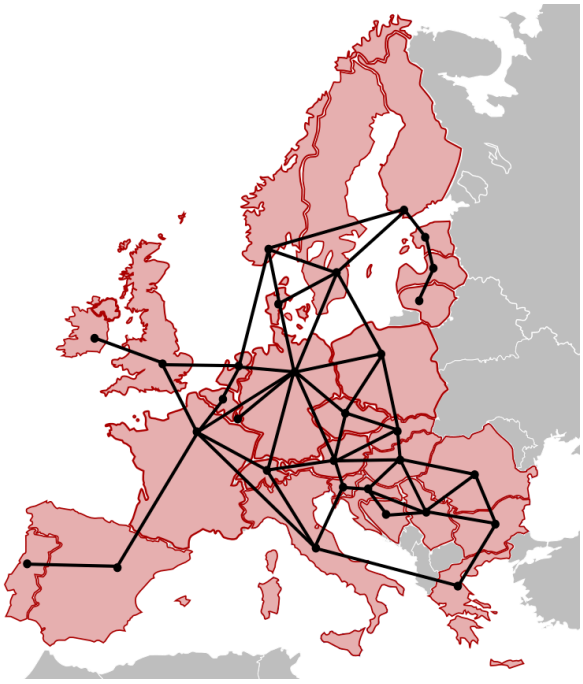

Figure 2.2: A simplified pan-European transmission network, where countries are treated as ideal nodes and are linked by interconnectors.

The three export schemes illustrated in Figure 2.1(b-d) will be formalised in the following Methods section. The Results and Discussion section will use a simplified pan-European transmission network (see Figure 2.2) to quantify the differences between the three export schemes with respect to backup energy, backup capacity and transmission capacities. A conclusion will be given in the last section.

2.2 Methods

Renewable power generation

We define a country n to have a fully renewable power system once the average power generation from renewable sources $\langle G_n^{\mathrm{RES}} \rangle = \langle L_n \rangle$ matches the average load. The renewable power generation

$$G_n^{\mathrm{RES}}(t) = G_n^W(t) + G_n^S(t) \tag{2.1}$$

is assumed to be dominated by wind and solar photovoltaics. Other renewable sources are either neglected (like run-of-river hydro) or considered as part of the backup system (like dispatchable hydro storage lakes and biomass). The ratio

$$\alpha_n = \langle G_n^W \rangle / \langle L_n \rangle = 1 - \langle G_n^S \rangle / \langle L_n \rangle \tag{2.2}$$

defines the mixing parameter between wind and solar power generation.

Realistic time series for the wind and solar PV power generation, including consistent spatio-temporal correlations, have been obtained from a recently developed renewable energy atlas [23, 30]. The atlas is based on weather data from high-resolution forecast models. The data extends over several years with hourly time resolution and has a spatial grid cell resolution of approximately $40\times40\mathrm{km}^2$ covering all of Europe. The conversion from weather data to potential wind and solar PV power generation is done on a grid cell level and then aggregated to country level. The load time series $L_n(t)$ have been taken from historical records with hourly resolution. For more details see [23, 24].

Backup energy and power

Although equal on average, the renewable power generation of a fully renewable country will be larger than the load for roughly half of the times, and smaller for the other half. The country then might want to export ($T_n > 0$) or import ($T_n < 0$) power. This defines the residual mismatch

$$\Delta_n(t) = G_n^{\mathsf{RES}}(t) - L_n(t) - T_n(t) \ . \tag{2.3}$$

If $\Delta_n(t)$ is negative, the country needs to balance an amount $B_n(t) = -\min(\Delta_n(t), 0)$ with own backup power plants, and if positive the country needs to curtail $C_n(t) = \max(\Delta_n(t), 0)$.

Due to fluctuations in the renewable power generation, the load and the export power, the backup power $B_n(t)$ changes from one hour to the next. When multiplied with the number of hours $T = 8760$ per year, the average backup power is equal to the annual backup energy $E_n^B = \langle B_n \rangle T$. We take the 99% quantile $\int_0^{C^B} p(B)dB = 0.99$ of the backup power distribution as a measure for the backup capacity C_n^B.

Equation (2.3) leads to the conservation law

$$G_n^{\mathsf{RES}}(t) + B_n(t) = L_n(t) + T_n(t) + C_n(t) \ , \tag{2.4}$$

which holds locally at every country. Based on the assumption of lossless transmission, a second conservation law holds globally for the networked countries:

$$\sum_n T_n(t) = 0 \ . \tag{2.5}$$

Power transmission

In the high-voltage DC approximation [32], the AC power flows along the interconnectors between the countries are directly determined from

the net exports:

$$\begin{aligned} T_n &= \sum_{m=1}^{N} B_{nm}\delta_m \ , \\ f_{n\to m} &= b_{nm}(\delta_n - \delta_m) \ . \end{aligned} \tag{2.6}$$

Inversion of the first equation gives the voltage phase angles δ_n at all nodes. Their differences determine the power flows $f_{n\to m}$ along the links $n\to m$ between neighbouring nodes. Assuming zero link resistances and no dependence on link lengths, the elements of the susceptance matrix $B_{nm} = (\sum_k b_{nk})\,\delta_{nm} - b_{nm}$ can be set equal to the adjacency matrix $b_{nm} = a_{nm}$ of the network graph.

Since the exports $T_n(t)$ are a function of time, the power flows $f_l(t)$ will also fluctuate with time. The low and high quantiles $q = \int_{-\infty}^{F(q)} p(f)df$ of the unconstrained flow distributions $p(f)$ are a measure for the required interconnector strengths $C_l^T = \max(-F_l(0.01), F_l(0.99))$. The total interconnector capacity $C^T = \sum_l C_l^T$ of the pan-European transmission network is given by the sum over all links.

Export schemes

Next, four different export schemes are outlined. They include zero export, two selfish exports of only renewable excess power, and cooperative export with additional export of backup power.

Zero export

The zero-export scheme is expressed by

$$T_n = 0 \ , \tag{2.7}$$

and is illustrated in Figure 2.1(a). Each country then has to fully balance or curtail the mismatch between its renewable power generation and its load.

Selfish export I

Rather than full curtailment, countries with surplus renewable power generation may want to export as much of it as possible to other countries

with a current deficit:

$$\begin{aligned} \text{exporters}: &\quad 0 < T_n(t) \leq \max(G_n^{\mathsf{RES}}(t) - L_n(t), 0) \;, \\ \text{importers}: &\quad 0 > T_n(t) \geq \min(G_n^{\mathsf{RES}}(t) - L_n(t), 0) \;, \\ \text{objective 1}: &\quad \min\left(\sum_n B_n(t)\right) \;, \\ \text{objective 2}: &\quad \min\left(\sum_l f_l^2(t)\right) \;. \end{aligned} \tag{2.8}$$

Two steps need to be taken to assign exporters and importers. The first objective is to use as much excess renewable power as possible to reduce the overall balancing power. In case that the overall export strengths are larger than the overall import needs, this objective makes sure that all importers will be fully served, but there is still the freedom to select different subsets of exporters. This freedom is fixed by the second objective, where the transmission system operator requires the power flows on the network to be as localised as possible. Those nodes which are at the end left unable to export everything have to locally curtail.

In case of larger overall import needs, all export opportunities will be used by the first objective, and the second objective fixes the subset of importers. Those nodes which have not been able to import enough then have to locally balance for themselves. Compare again with Figure 2.1(b). Note also that from one time instance to the next the role of exporters and importers might change.

This export scheme has been employed in two previous publications [1, 6]. Here we call it a selfish export scheme because exporters are not willing to export more than their excess renewable power generation.

Selfish export II

The third export scheme is almost the same as the previous one, except that the first objective is replaced by

$$\text{objective 1}: \quad \min\left(\max_n \frac{B_n(t)}{\langle L_n \rangle}\right) \;. \tag{2.9}$$

It gives priority to importers with the largest relative deficit power and allows to reduce the backup capacities. Compare with Figure 2.1(c).

Cooperative export

A very different export scheme forces all countries into a completely synchronised residual mismatch (2.3):

$$\Delta_n(t) = \beta(t)\langle L_n \rangle \;, \tag{2.10}$$

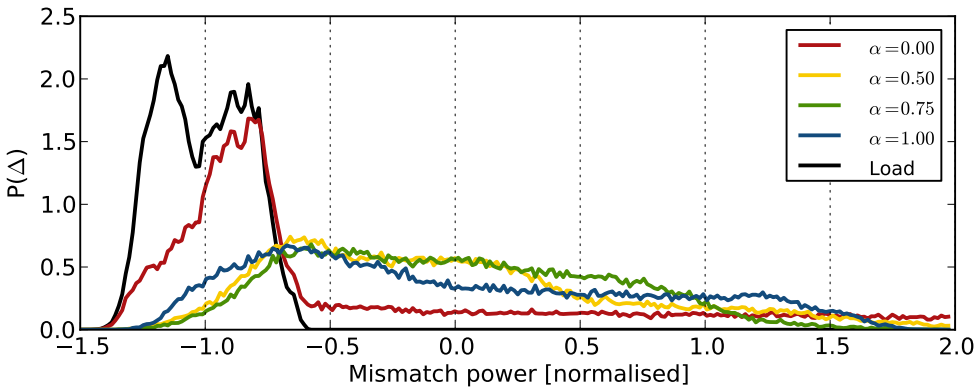

Figure 2.3: Distributions of residual mismatches (2.3) for Germany resulting from the zero export scheme with four different mixing parameters $\alpha_{\mathrm{GER}} = 0.0$ (red), 0.5 (yellow), 0.75 (green), 1.0 (blue). For comparison, the negative load distribution (black) is also shown. Mismatches and load have been normalised to the average load $\langle L_{\mathrm{GER}} \rangle$.

where due to (2.3) and (2.5)

$$\beta(t) = \frac{\sum_n (G_n^{\mathrm{RES}}(t) - L_n(t))}{\sum_n \langle L_n \rangle} \,. \tag{2.11}$$

After exports and imports, every node is balancing ($\beta < 0$) or curtailing ($\beta > 0$) the same amount relative to its own average load as all the other nodes. This requires cooperation. For example in case of $\beta < 0$, nodes with excess renewable power generation not only export their excess to other countries, but also balancing power from their own backup capacities; see again Figure 2.1(d).

2.3 Results and Discussion

Residual mismatch distributions

The distribution $p(\Delta_n)$ of the residual mismatch (2.3) depends strongly on the mixing parameter α_n between wind and solar power generation. This is illustrated in Figure 2.3 for the zero export scheme (2.7). Although zero on average, the distributions are very broad. For a solar-only Germany with $\alpha_{\mathrm{GER}} = 0.0$, the mismatch ranges from -1.4 to 4.7 times the average load. For a wind-dominating Germany with $0.5 \leq \alpha_{\mathrm{GER}} \leq 1.0$, the normalised mismatch values are between -1.3 and 2.0.

The negative part of the mismatch distribution is of particular importance. Its average determines the average backup power, which is proportional to the annual backup energy. Its tail characterises the most extreme backup power needs, which determine the required backup ca-

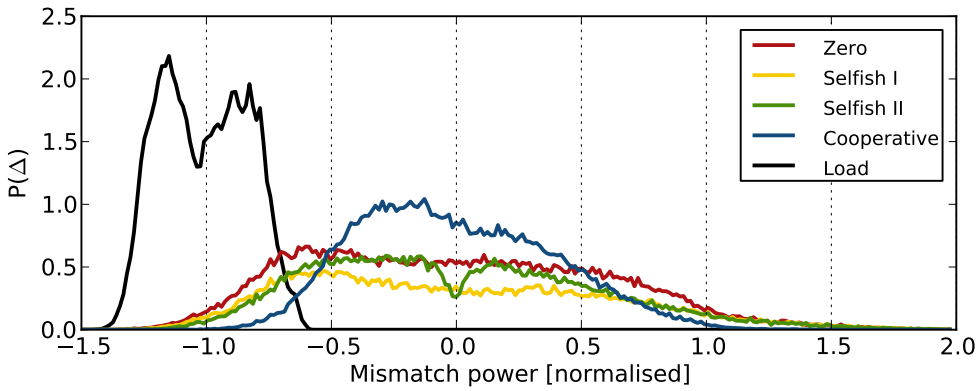

Figure 2.4: Distributions of residual mismatches (2.3) for Germany with $\alpha_{\mathrm{GER}} = 0.7$ resulting from the zero (red), the two selfish (yellow, green) and the cooperative (blue) export schemes. For comparison, the negative load distribution (black) is also shown. Mismatches and load have been normalised to the average load $\langle L_{\mathrm{GER}} \rangle$. The residual mismatch distributions resulting from the two selfish export schemes are shown without their singular peak at $\Delta_{\mathrm{GER}} = 0$.

pacities. From these perspectives, a mixing parameter around $\alpha \approx 0.75$ appears to be most favourable.

For $\alpha_n = 0.7$, Figure 2.4 shows the dependence of the residual mismatch distribution on the three non-zero export schemes (2.8)-(2.10), where each country is allowed to import and export from all 30 European countries. Contrary to the cooperative export scheme, the two selfish schemes produce a lot of $\Delta_n = 0$ events. The resulting singular peak has been removed in the illustrated distributions, but can still be observed indirectly as the integrated area below those two normalised distributions is smaller than for the other two distributions resulting from the zero and the cooperative export scheme. When compared to the zero export scheme, the two selfish export schemes are able to lower the frequency of negative residual mismatches, causing a decrease of the average backup power. See Figure 2.5. The residual mismatch distribution resulting from the cooperative export scheme changes in a different way, also leading to a reduction of the average backup power. Contrary to the two selfish export schemes, the cooperative export scheme also lowers the negative tail of the residual mismatch distribution and therefore significantly reduces the required backup capacity. See Figure 2.6.

Backup energy and capacity

The average backup power $\langle B_n \rangle$, which is proportional to the annual backup energy, reveals a pronounced dependence on the mixing parameter α_n between wind and solar power generation. See again Figure 2.5. For $\alpha_n = 0.0$ we get the expected $\langle B_n \rangle \approx 0.5 \langle L_n \rangle$, because of the miss-

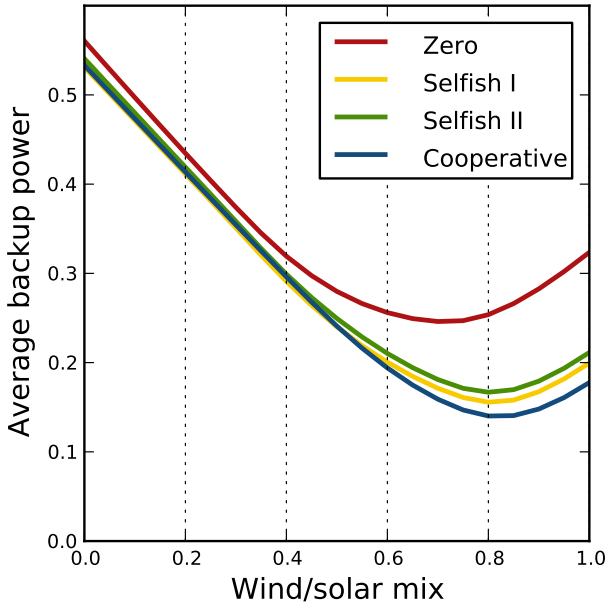

Figure 2.5: Average backup power as a function of the renewable mixing parameter α_{GER} for Germany resulting from four different export schemes. The average backup power has been normalised to the average load $\langle L_{\mathrm{GER}} \rangle$.

ing solar power generation during nights. The zero export scheme (2.7) produces the minimum $\langle B_n \rangle \approx 0.24 \langle L_n \rangle$ at $\alpha_n \approx 0.7$. Both values are averages over all countries. The country-specific values vary weakly [1]. The two selfish and the cooperative export schemes (2.8)-(2.10) shift the minimum mix value to $\alpha_n = 0.8$. The average backup power reduces to $\langle B_n \rangle \approx 0.14 \langle L_n \rangle$. This is 42% less than for the zero export scheme. With a strong pan-European transmission grid the countries are able to significantly reduce their annual backup energy.

The two selfish and the cooperative export schemes (2.8)-(2.10) have a different impact on the average backup power for the different countries. For Germany with a mixing parameter in the range $0.6 \leq \alpha_n \leq 1.0$, the first selfish export scheme leads to a slightly larger reduction of the average backup power when compared to the second selfish scheme. This is because the first scheme allows Germany to import more on average than the second scheme. See Figure 2.7, where the top level shows the average imports $\langle \max(-T_n, 0) \rangle$ for all countries. The cooperative export scheme leads to a significantly larger average import. However, this does not lead to a further reduction of the average backup power because the country is then also exporting backup power.

For some countries other than Germany the two selfish export schemes (2.8)-(2.9) lead to a smaller average backup power than from the cooperative export scheme (2.10). This is explained by the observation that

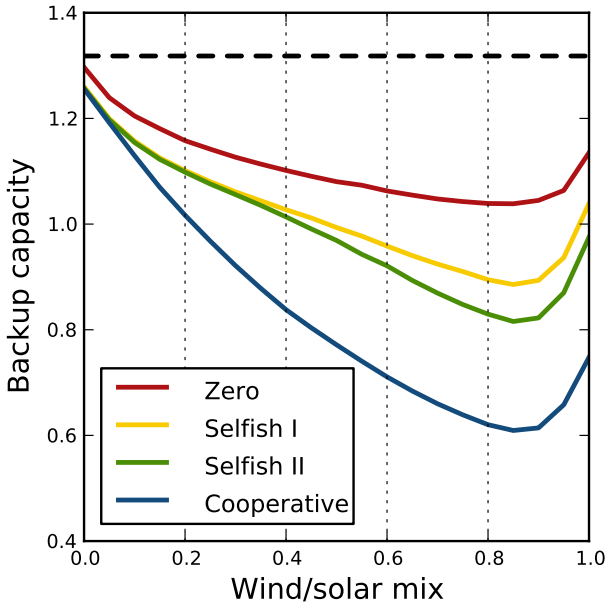

Figure 2.6: Backup capacity as a function of the renewable mixing parameter α_{GER} for Germany resulting from four different export schemes. The backup capacity has been normalised to the average load $\langle L_{\mathrm{GER}} \rangle$. For reference, the 99% quantile of the German load distribution is shown as the black dashed line.

the sum $\sum_n \langle B_n \rangle$ is identical for the three export schemes. All three schemes use the same amount of overall renewable excess power, which is as much as possible. This is clear for the two selfish export schemes. For the cooperative export scheme this follows from equation (2.11). Consult also again Figures 2.1(b-d).

The lower panel of Figure 2.7 shows the average net exports $\langle T_n \rangle = -\langle \Delta_n \rangle$ for the different countries. The average net export is the difference between average export and average import. Except for a minus sign, it is equal to the mean of the residual mismatch (2.3). For the cooperative export scheme (2.10) the net exports are zero for all countries. However, this is not the case for the two selfish export schemes (2.8) and (2.9). For big countries like Germany, France and Great Britain with $\alpha_n = 0.7$ it turns out to be of the order $\langle T_n \rangle / \langle L_n \rangle \approx -0.004$. Those countries become net importers. The biggest relative net importers are the two Nordic countries Norway and Sweden with $\langle T_n \rangle / \langle L_n \rangle \approx -0.023$. Spain and Italy are net exporters of the order $\langle T_n \rangle / \langle L_n \rangle \approx 0.014$. With $\langle T_n \rangle / \langle L_n \rangle \approx 0.023$ the strongest relative net exporters are the smaller countries in South Europe. Of course, due to (2.5), the overall country sum over all net exports and net imports is again $\sum_n \langle T_n \rangle = 0$.

The backup capacity C_n^B also shows a strong dependence on the mixing parameter. See Figure 2.6. For all four export schemes (2.7)-(2.10) it

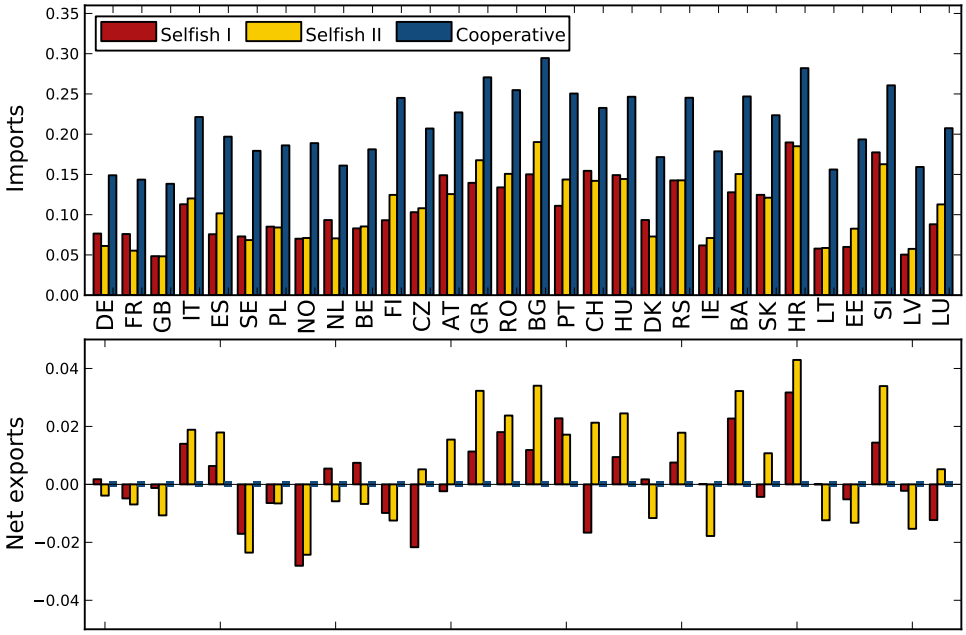

Figure 2.7: (Top) average imports $\langle \max(-T_n, 0) \rangle$ and (bottom) average net exports $\langle T_n \rangle$ for all countries following from the two selfish and the cooperative export schemes (2.8)-(2.10). The renewable mixing parameter $\alpha_n = 0.7$ has been used, and the imports and net exports have been normalised to the average loads $\langle L_n \rangle$.

takes a minimum at $\alpha_n = 0.85$. Compared to the value $1.32\langle L_n \rangle$ of the 99% quantile of the German load, the backup capacity $C_n^B = 1.04\langle L_n \rangle$ at $\alpha_n = 0.85$ resulting from the zero export rule is not much smaller. Without transmission, a 100% renewable country needs an enormous amount of backup capacity. The two selfish and the cooperative export schemes have a bigger impact on the reduction of the backup capacities. For Germany with $\alpha = 0.85$, the first selfish export scheme leads to $C_n^B = 0.89\langle L_n \rangle$, the second selfish scheme to $C_n^B = 0.82\langle L_n \rangle$, and the cooperative scheme to $C_n^B = 0.61\langle L_n \rangle$. For the other countries the relative backup capacities resulting from the two selfish export schemes are slightly different than the German values. See Figure 2.8. The cooperative export scheme leads to identical relative backup capacities for all countries. This is no surprise since the cooperative export scheme (2.10) with (2.11) enforces a synchronised balancing between all countries.

Since equation (2.11) describes the all-European mismatch we arrive at a strong conclusion: the cooperative export scheme leads to the largest possible reduction in overall backup capacities. No other export scheme is able to reduce the backup capacities further. For mixes between $0.70 \leq \alpha_n \leq 0.95$, the cooperative export scheme leads to backup capacities

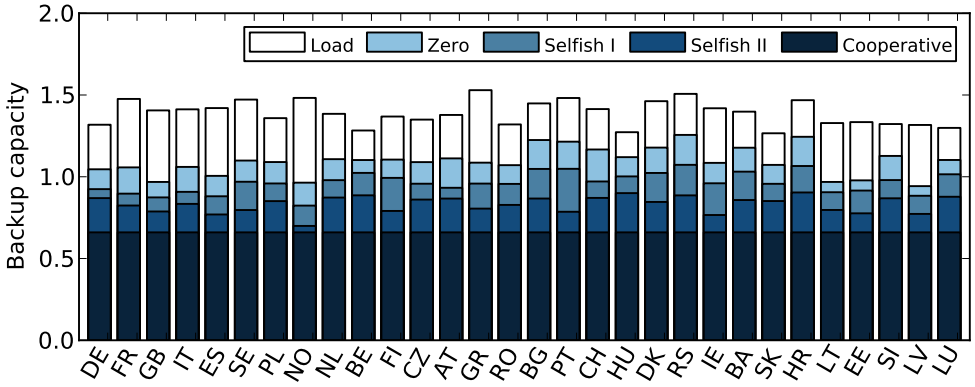

Figure 2.8: Backup capacities for all European countries resulting from four different export rules. The renewable mixing parameter $\alpha_n = 0.7$ has been used, and the backup capacities have been normalised to the average loads $\langle L_n \rangle$. For reference, the 99% quantile of the load distributions is also shown.

which are only half of the high load quantiles, the latter representing more or less the backup capacities of our current electricity system.

Transmission capacities

Reference [1] has shown that the unconstrained total interconnector capacities become relatively large. Almost the same European country network as in Figure 2.2 had been used with a mixing parameter around $\alpha_n \approx 0.71$, and only the first selfish export scheme had been discussed. The total interconnector capacities turned out to be $C^T = 395$ GW, which is about a factor 5.4 larger than the present European layout; see Table 1.2 in [1].

Figure 2.9 extends the previous findings to the full range $0 \leq \alpha_n \leq 1$ of the mixing parameter, and to the second selfish and the cooperative export schemes. The two selfish export schemes produce very similar total interconnector capacities. The minimum capacities are reached at $\alpha_n = 0.35$. For the solar only $\alpha_n = 0$ the transmission capacities are larger because of the strong East-West power flows in the mornings and evenings, and because of the strong seasonal South-North flows. For the other extreme, the wind-only $\alpha_n = 1$, the transmission capacities become even larger. This is caused by strong power flows between decorrelated regions separated by distances larger than the observed correlation length of about 500 km for the wind power generation [31, 54].

The cooperative export scheme leads to a minimum at a slightly larger $\alpha_n = 0.42$. Over the whole range $0 \leq \alpha_n \leq 1$ the total interconnector capacities required from the cooperative scheme are a factor of 1.35-1.70 larger than for the two selfish schemes. For $\alpha_n = 0.7$ the cooperative scheme produces $C^T = 550$ GW, whereas it is only $C^T = 400$

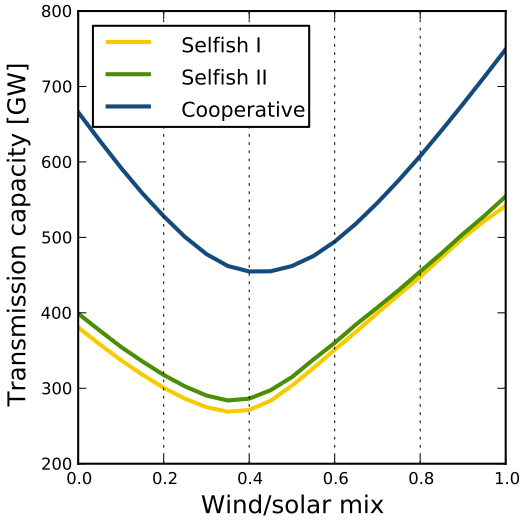

Figure 2.9: Overall interconnector capacities C^T of the unconstrained European transmission grid as a function of the renewable mixing parameter α_n.

GW for the selfish schemes. This difference is easily explained by the extra exports of backup power caused by the cooperative scheme (see again Figure 2.7), which cause more power flows and result in higher required transmission capacities (see again Figures 2.1(b-d)).

2.4 Conclusion

Fully renewable networked power systems have been discussed, for which their average renewable power generation is equal to their average load. Such systems still require backup generation units to cover the occurring temporal deficits of fluctuating renewable power generation to match the load. The amount of backup capacity depends on the export schemes applied to the transmission network. Compared to no exports at all, the export of local renewable excess power, which we have dubbed as selfish, leads to some reduction of the overall backup capacities. Significantly more reduction is achieved when also local backup power is allowed to be exported. For a fully renewable pan-European transmission grid such a cooperative export scheme leads to backup capacities which are only half of the maximum loads.

In its present form the cooperative export scheme is based on a completely synchronised residual mismatch across the network. No other export scheme is able to reduce the backup capacities further. However, it requires larger transmission capacities when compared to the selfish export schemes. From an economic perspective this is not necessarily a drawback, since costs for backup capacities are usually one order of

magnitude bigger than transmission costs. It will be interesting to explore other cooperative export schemes, including market-like schemes, which might be able to reduce also the transmission capacities. Such an exploration could be based on the minimisation of an overall cost objective, which not only includes backup and transmission capacities, but also renewable power generation capacities. These findings will have an impact on the future strategies of planners and policy makers.

Chapter 3

Flow tracing

Motivation

The increased penetration of renewables in the European network will almost certainly entail larger flows between countries [10]. Regions with uncorrelated weather patterns can become trading partners, with a mutually beneficial exchange of excess energy, enabling both parties a higher penetration of renewables. Given the long distances involved, the pathways connecting such two regions will affect countries in between, or even parallel to the trade route. This is already the case in Scandinavia, where Denmark lies in the way between its larger neighbours, Sweden and Germany, and in central Europe, where large flows between Germany and Austria saturate the Czech system due to natural parallel flows.

Saturated links will cause a price difference in nodal or area-based markets [58], so that the Transmission System Operators (TSOs) on both sides of the link can profit from the difference. This is not the case when the link is not saturated, and the only profit is the usage fee that the interconnector's owner specifies for usage, a metric that is complicated by the presence of parallel flows. A more concise way of determining the parties responsible for a flow will facilitate new metrics to decide on what stake a producer or consumer has on a link.

While it is true that, for a grid-connected consumer, there is no such thing as 'green' electricity, there is such a thing as power coming from renewable sources. That is, there is a way to know exactly how much of the power delivered to a bus in an electricity system is due to a specific source in that system. Figure 8 shows an example, where the additional presence of a must-run source (one with zero marginal cost) causes an additional flow in the system. In Figure 8(a), two dispatchable sources (blue and red) are feeding two pure sinks with no flow between them. In Figure 8(b), the presence of an additional must-run source (yellow) causes downwards regulation of power in either one or both dispatchable sources. The sinks, which previously were fed by $either$ blue or red are now fed by a mixture of some or all the sources. The magnitude of a given source, its topological location in the grid, the shape of the

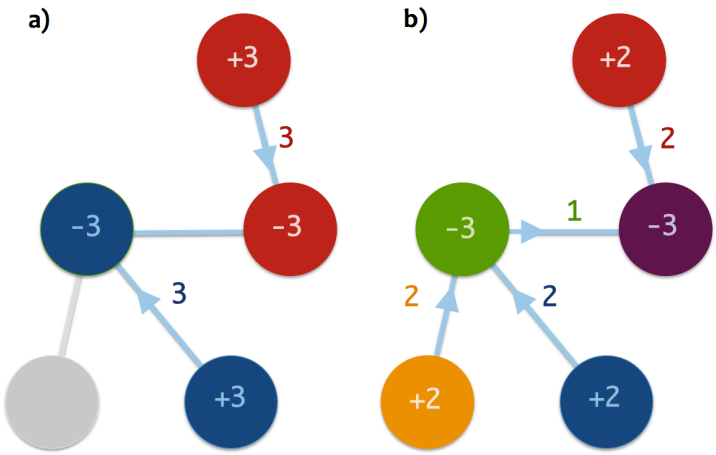

Figure 8: Tracing electricity exports. In (a), two node pairs are balanced. In (b), non-dispatchable generation provides two extra units, causing downwards regulation and an additional flow.

grid, and the magnitude of the other sources within the system all affect the ratio of energy at the sink that can be tracked to the original source. In other words, the system layout and the injection pattern can help us determine the origin and the path of a unit of energy consumed by a load.

Methods

The method of tracing the flow of electric power follows from an assumption of homogeneity: the power leaving a bus (node) is a homogeneous mixture of the power entering it. In Figure 10 above, we can interpret this as meaning that the power leaving the green node is an even mixture of yellow and blue. This simple rule, combined with graph theory and algebraic operations, can reveal all the interactions between sinks and sources.

The algorithm is easiest to explain from a graph theory perspective. Given a network with potential flows (see Figure 8), we are guaranteed at least one pure source and one pure sink [59]. If we begin by looking at a pure source (for example, the blue source) and 'colouring' its contribution to the injection pattern, we can follow the presence of its exports in all the nodes downstream from it. At the green sink, the exports from the blue and yellow nodes are mixed evenly, and then sent on to the purple sink. The purple sink receives additional imports from the red source. At the purple sink, one can then discern power originating from red, blue, and yellow sources. In this simple example, it is straightforward to identify import/export partners and link usages. The algorithm becomes complicated for larger networks, so that an algebraic expression might turn useful.

This graph-theory approach has been previously described in [60], though in a

purely qualitative way. A very similar algorithm to track the downstream exports was earlier and independently described in [61], focused on finding the portfolio of a sink's imports in an electricity system. The authors of [59] give a rigorous mathematical proof of the validity of the algorithm presented in [61], and point at its equivalence to [60]. Even though the operations performed in these articles are clearly dealing with vectors and matrices, none of them describe them in this simple manner. We believe that they can be stated succinctly in a few lines, and that this new visualisation allows for a faster solution.

We introduce a power mix matrix $\boldsymbol{P}$, with elements $P_{n,m}$, which represent the presence of power from node n in node m. This mix can be defined from

$$\boldsymbol{P} = \boldsymbol{P}((\boldsymbol{K}\boldsymbol{F}_+)\boldsymbol{K}^\intercal)_- + \boldsymbol{\Phi}_+ \,, \tag{53}$$

where the subindex in Φ_+ indicates the positive entries in Φ. Details of how one can arrive at this solution can be found in Section 3.3. This system of equations can be solved for $\boldsymbol{P}$ either iteratively or through a (costly) inversion

$$\mathbf{P} = \boldsymbol{\Phi}_+[\mathbb{I} - ((\boldsymbol{K}\boldsymbol{F}_+)\boldsymbol{K}^\intercal)_-]^{-1} \,. \tag{54}$$

Exploiting a property of networks with potential flows, that at least one pure source and one pure sink can be found, allows for an easier solution of (53). The presence of a pure source, as indicated in the example above, means that the equations can be solved from one end of the system to the other. Once the power mix $\boldsymbol{P}$ has been found, it is trivial to find the matrix of exports $\boldsymbol{E}$

$$\boldsymbol{E} = \boldsymbol{P}\boldsymbol{\Phi}_- \tag{55}$$

and of link usages for exports $\boldsymbol{H}$

$$\boldsymbol{H} = \boldsymbol{P} \cdot (\boldsymbol{K}\boldsymbol{F})_+ \,. \tag{56}$$

Imports can be found by transposing $\boldsymbol{E}$, while link usages for imports require an upstream recalculation of the problem. See Section 3.3 for more details.

Main findings

We apply the flow tracing algorithm to an unconstrained 8-year calculation for a European power system with $\gamma_n = 1.0$ and $\alpha_n = \alpha^*$ for all nodes n. Whereas a study of the correlations would have shown potential trading partners, by actually studying the network dynamics we can see which countries actually interact the most, and in what way. Figure 3.3 shows an example for Germany. Italy and France are shown to be Germany's most important trade partners in a fully renewable Europe, due to their proximity, the size of their mean load, and the low correlation their resources have with Germany's. We can also identify important links for Germany, and indirect links that are used due to parallel flows, mainly those connecting its first neighbours.

Given the high penetration of wind in the system (where $\alpha^* \approx 0.8$ for all nodes, see [1] for more details), we expected to see evidence of the oft discussed north-south exchange of wind for solar resources. While such dynamics might be visible in shorter time spans or with a higher nodal resolution, average flows seem to indicate that the dominating flow pattern is flow from the periphery of Europe towards the larger nodes (Germany, France, Great Britain)

This algorithm also allows us to compare the stakes that a node has on the network calculated in different manners. The current stake that a country has can be approximated by the links directly connected to it divided by two. A measure of a country's actual usage, as shown in Figures 3.4, 3.5, and 3.8, could help identify new ways of distributing the investment cost for a new pan-European high capacity transmission network.

While a main motivation of this paper was the determination of this usage factor, the algorithm developed to achieve it has many potential uses, some of which will be discussed in the Conclusions. The algorithm could help TSOs, policy makers, planners, and energy traders identify key links and partnerships to exploit, and identify the role of VRES within a country's electricity system. Readers will recall the exchange between CEPOS [62] and CEESA [63] in 2009, where the exports of wind energy from Denmark were debated. While both parties raised interesting points about the way electricity is traded, taxed, and accounted for in the system, and of what the actual benefit of a high share of renewables in the Danish system is, a technical issue at the core of the argument, whether or not one could track exports to wind power plants, has a clear technical answer, and was largely ignored.

Tracing the flow of energy in a highly renewable Europe

Rolando A. Rodriguez[a], Anders B. Thomsen[a], Gorm B. Andresen[b], Martin Greiner[a,b]

a Department of Mathematics, Aarhus University, Denmark

b Department of Engineering, Aarhus University, Denmark

Abstract

In a future European power system with large amounts of VRES (variable renewable energy sources), power transmission over long distances can reduce the variability of the total generation, and increase the integration of renewable energy in the electricity consumption. In this paper, we apply minimum dissipation power flow modelling and sink-source tracing to determine the most important trade partners and transmission lines for the exchange of renewable energy. The analysis is based on an 8-year-long, high-resolution European dataset of hourly wind and solar power generation as well as hourly load data. The official National Renewable Energy Action Plans of the EU countries are used to determine VRES penetrations for 2020, and scaled up logistically to a final penetration of 100% for later years. Based on these results, we discuss three mechanisms to quantify the stakes and the relative interest that each of the countries have in a strong common European transmission network. We find that a measure that depends on a country's actual usage of the transmission system leads to significantly different distribution of interests from measures that depends on the country's total consumption or its total transmission capacity to neighbouring countries.

keywords: renewable energies, power tracing, wind power generation, pan-European transmission grid,

3.1 Introduction

The European Union and most other European countries have set ambitious targets for renewable energy for 2020 [11], and the official goal is to supply nearly all electricity from renewable sources by 2050 [64, 65]. A very large fraction will have to come from variable renewable energy sources (VRES), especially wind and solar photovoltaic energy sources [12], where energy production generally does not follow the demand.

A strong international transmission system can help alleviate this problem as excess generation in one location may be allocated residual load in another. In [1], the benefit of a strong European transmission system has been quantified. In an optimised endpoint scenario, where each country has an average generation from wind and solar power equal to its load, a strong transmission network leads to a maximum reduction in the need for dispatchable backup energy of 33% when compared to a case without any transmission at all. For this to be realised, around five times today's transmission capacity is required.

Building a strong international transmission grid is both expensive and politically complicated. Furthermore, it may not be obvious what consequence it has for each individual country. In this paper, we present a methodology for determining which parts of the grid will benefit any particular country most, and which countries are compatible trade partners. This is largely determined by correlations between excess wind and solar energy and residual load, but is also affected by distance in the network, as a nearby trade partner is more attractive than one further away.

The methodology is based on an 8-year-long, high-resolution European dataset of hourly wind and solar power generation as well as hourly load data. Our modelling consists of a combination of minimum dissipation power flow modelling and self-consistent sink-source tracing. Since we model generation and flows between all countries simultaneously, it includes the effect of multiple simultaneous sources and sinks for excess wind and solar electricity. Considering the correlations between pairs of countries such as Danish and German wind power generation, as in [63, 66], gives part of the answer, but discards the aspect of competition that different countries might have for trade partners.

We apply our methodology to show how the stake that individual countries have in a strong common grid may develop towards a fully renewable European power system, and results are presented for the years leading to a hypothetical, fully renewable 2050. For these years, we show which transmission links and countries are of particular interest to each of 30 countries. In addition, we define and discuss three different measures to quantify the stakes that each country has in a strong common grid.

The self-consistent sink-source assignment used in this paper is based on similar methods developed in [59–61] to decompose the combined power flow from a portfolio of power plants into a combination of flows from each individual plant. In power transmission analysis it is known as the AP-method (Average Participation Method) (see e.g. [67]). Here, we give the method a simple algebraic representation and apply it to trace the transfer of wind and solar energy from source countries with excess energy to sink countries with a residual load. The analysis is performed for each hour in the 8-year-long data set, and by combing the results for all hours, a map of the most frequent import and export partners and transmission channels used by each individual country emerges.

We do not include transmission of dispatchable backup power as this tends to obfuscate the discussion (see e.g. [62, 63]), but it is well documented that a strong transmission network enables individual balancing areas to be combined, and significantly reduce the total need for fast reacting and other power reserves [14]. Furthermore, including exchange of backup energy in the flow calculation will increase the total flow in the system.

This paper is organised as follows: In Section 3.2, the key definitions of the weather-driven modelling are introduced as well as three different measures that indicate the relative interest each of the countries have in a strong common European transmission network. Section 3.3 details the flow tracing algorithm, expands on its application to finding trade partners and describes a generalisation that allows the identification of the vital links for exports and imports. Section 3.4 uses the end-point scenario of 2050 to showcase the differences between the stake quantification mechanisms. The pathway to this hypothetical, fully renewable future is examined in Section 3.5, and the participation of different countries in the European power grid is analysed before Section 3.6, which concludes the paper.

3.2 Motivation

We model a system of interconnected nodes, where each node represents a European country. The hourly generation of electricity from VRES in the country can be defined as

$$G_n(t) = \gamma_n \cdot (\alpha_n \cdot G_n^W + (1 - \alpha_n) \cdot G_n^S) \cdot \langle L_n \rangle, \tag{3.1}$$

where γ_n is the share of renewables in country n and α_n is a factor that determines the wind to solar ratio in the VRES power mix. When $\gamma_n = 1$, the mean renewable generation $\langle G_n \rangle$ will be equal to the mean load $\langle L_n \rangle$, but due to the variations from wind and solar, there will

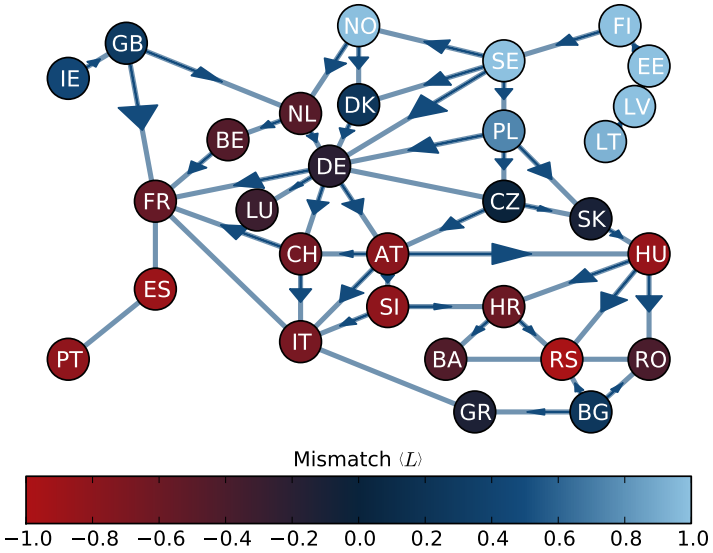

Figure 3.1: Example hour of the modelled power system for a winter night, for a fully renewable system in 2050, showing power flows and the countries' mismatch Δ_n, normalised to the mean load $\langle L_n \rangle$ of the country. Countries with an excess are shown in light blue, countries with a deficit in red. Link lengths and arrow areas are not drawn to scale.

usually be a non-zero mismatch

$$\Delta_n(t) = G_n(t) - L_n(t). \tag{3.2}$$

In reality, the electricity system must be perfectly balanced at all times. We introduce the possibility for nodes to perform curtailment of generation $C_n(t)$ or to provide additional backup power $B_n(t)$ from dispatchable sources, such as conventional fossil fuels or hydroelectric sources. This allows us to define the residual mismatch

$$\Delta'_n(t) = G_n(t) - L_n(t) + B_n(t) - C_n(t). \tag{3.3}$$

Interconnectors between countries allow for the trading of electricity, so that the nodal balance equation that must be maintained can be generalised to

$$G_n(t) + B_n(t) + I_n(t) = L_n(t) + C_n(t) + E_n(t), \tag{3.4}$$

or

$$\Delta'_n(t) = E_n(t) - I_n(t) \tag{3.5}$$

where $I_n(t)$ and $E_n(t)$ are the sum of imports and exports, respectively. The net imports into a node can be found from the flow along all links

$F(t)$ by

$$E_n - I_n = \sum_{l=1}^{L} K_{n,l} F_l \,. \tag{3.6}$$

Here, the incidence matrix **K** relates the vector of the flows at all links to the net imports at all nodes. It holds the information of the network structure:

$$K_{n,l} = \begin{cases} 1 & \text{if link } l \text{ starts at node } n, \\ -1 & \text{if link } l \text{ ends at node } n, \\ 0 & \text{otherwise .} \end{cases} \tag{3.7}$$

Using the same large weather data as in [23, 25, 26], and the flow modelling introduced in [1, 6], we can simulate the mismatches and flows for a given European electricity system with a high penetration of renewables γ. These flows can be calculated from a physical solution to the unconstrained energy flow in an electrical network. As previously found, ensuring an efficient usage of renewables requires a larger interaction between the countries than at present [10]. These larger flows lead to larger required interconnectors, the capacity of which can be determined by looking at high quantiles of the flows in either direction. We can determine the net transfer capacity of a link l by

$$T_l^C = \max\{|F_l^{0.5\%}|, |F_l^{99.5\%}|\}, \tag{3.8}$$

where $F_l^{\mathsf{Q}\%}$ represents the Q^{th} quantile of the flow along a link F_l. In this way, extreme events are ignored, and we find a capacity sufficient to cover transmission needs for at least 99% of the time. These capacities are still not small, a transmission system that makes full use of renewables would be around five to six times as large as the present one [1]. Even for a partially expanded transmission system, substantial investments would have to be made by the participating countries or TSO's.

It can be said that all nodes in a network are stakeholders in the transmission system connecting them. More than one stake distribution mechanism can be designed to determine the stake that a country has in the system – how many MW of the transmission system should one country be responsible for. A first guess, which we term **node proportional** is to weight the total transmission capacity by the node's mean load:

$$M_n^1 = \frac{\langle L_n \rangle}{\langle L_{\mathsf{EU}} \rangle} \sum_l T_l^C. \tag{3.9}$$

This mechanism assigns the same stake to all countries proportional to their size, and is fair under the assumption that all countries export/import the same, and that all links cost the same to build and operate. Large countries, or countries whose generation from VRES is strongly correlated with that of the rest of Europe (and so get few chances for export), could be unfairly taxed under this mechanism.

A second approach is a simple distribution of the links connecting a country with its neighbours.

$$M_n^2 = \frac{1}{2} \sum_l T_l^C \cdot |\mathbf{K}_{n,l}|. \tag{3.10}$$

This approach takes all the links a country is directly in contact with and adds up half of their capacities, so we call it **link proportional**. This might not immediately come across as unfair, as the TSO's in each country will split the profit of the price different between regions, and so they will both benefit. However, a price difference only exists when the link is saturated, and so this stake distribution mechanism is unfair to pathway countries – countries that lie in the route between two larger interacting countries – as flows below the link's capacity carry smaller profits for the countries or the TSO's.

A fairer stake allocation mechanism would measure a country's usage of each link. We can define usage as flows coming from or going to a country, since both exports and imports offer some degree of advantage to both of the involved countries. This presents a new question: In a network of interconnected nodes, how do we know from which node has a flow originated? In a real life electrical network, it is impossible to ensure that the MW you consume came from the source you bought it from. All producers contribute their production into the common grid to ensure that the frequency and voltage levels are maintained between operational parameters.

In the example power flow in Figure 3.1, which shows the modelled network in a winter night, energy is flowing from northern countries with an excess and into southern countries with a deficit. It is possible, for this hour, to identify pathways countries (f.x., Denmark lies in the way between the nordic countries and Germany) as well as parallel flows (the flow between Germany and Austria causes and is limited by the flow between the Czech Republic and Austria). While the responsible parties for a flow in some of the links is unambiguous, such as the case between Ireland and Great Britain, other cases are not so clear. It is not clear, for example, how much of the flow across Denmark and Poland is caused by Swedish exports into Germany. These issues trigger the implementation of a flow-tracing algorithm, which can allow us to produce a better, **usage proportional**, stake distribution mechanism:

$$M_n^3 = \frac{\langle U_{n,l} \rangle}{\langle U_{\mathsf{EU},l} \rangle}. \tag{3.11}$$

where U_n represents the total usage in MW – and therefore stake – that country n makes of the network. The following section explains how to determine said usage.

3.3 Methodology

Flow tracing – node usage

An algorithm to determine the flow of power in an electrical network has been developed by [61]. This algorithm decomposes the grid into sinks and sources, allowing to determine the portfolio of sources feeding a sink and vice versa. In electrical engineering, it is known as the average participation method [67]. In this section we show a simplified method to find both the usage of nodes and links for exports and imports, using a faster solution similar to [60]. To find the final destination and origin of energy exports and imports, one can either follow exports from source to sink (downstream) or trace the imports from sink to source (upstream). While both approaches can identify trading partners, finding what path these transactions took – and thus what usage of the network they incurred – has to be done for both upstream and downstream calculations.

In the downstream flow tracing, we use the term $power\,mix$ $(\vec{p}_n)$ to identify the presence of foreign generation in a node's local available energy for own usage or export. The power mix of a node that is a pure source or exporter consists of 100% of its own generation, while the power mix of a node with a local negative mismatch consists of 100% of foreign generation. We begin by identifying the own contribution λ_n of a node to an N-node, L-link network, assuming that only renewable excess generation is exported.

$$\lambda_n = \begin{cases} \Delta'_n & \text{if } \Delta'_n > 0, \\ 0 & \text{otherwise} \end{cases} . \tag{3.12}$$

Similarly, the upstream 'contribution' to consumption $\widetilde{\lambda}_n$ – which is really the country's net imports – can be stated as

$$\widetilde{\lambda}_n = \begin{cases} -\Delta'_n & \text{if } \Delta'_n < 0, \\ 0 & \text{otherwise} \end{cases} . \tag{3.13}$$

For net exporters this amount represents the whole of the local energy presence, but for other nodes in the network it will be only a part of their local power mix

$$\vec{p}_n = [\, p_{n,1} \;\ldots\; p_{n,j} \;\ldots\; p_{n,N} \,]^{\mathsf{T}} , \tag{3.14}$$

where N is the total number of nodes in the network. The power mix in n is built by adding the power mix of the incoming flows to n and its own local generation

$$\vec{p}_n = \sum_{j \neq n} F_{j \to n}\, \vec{p}_j + \lambda_n\, \vec{e}_n \,. \tag{3.15}$$

The vector $\vec{e}_n$ is one filled with zeros, apart from $e_{n,n} = 1$.

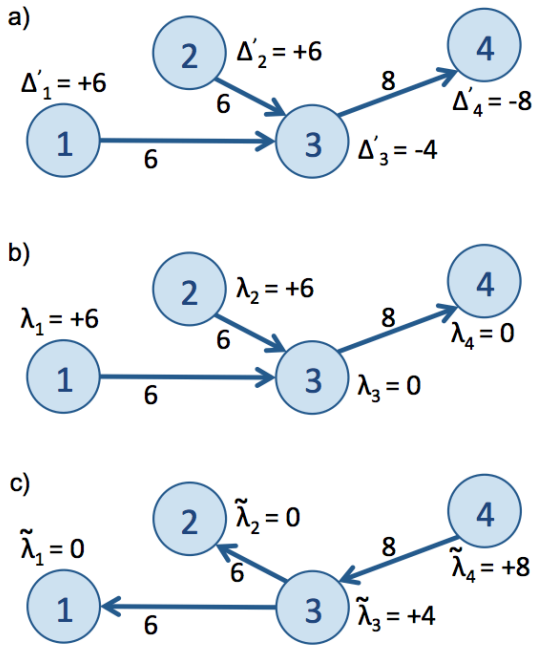

Figure 3.2: Illustration of flow tracing algorithms. The example system with residual loads is shown in (a), the downstream search in (b) and the upstream search in (c).

The power mix is normalised so that

$$\sum_j p_{n,j} = \sum_j f_{j,n} + \lambda_n = 1\,, \tag{3.16}$$

and thus, every entry $p_{n,j}$ represents the percentage of the local available energy in node n coming from node j.

Figure 3.2(a) shows a 4-node network connected with 3 links, and their residual loads at a given time. Nodes 1 and 2 act as sources with a positive residual load Δ' while nodes 3 and 4 are sinks with $\Delta' < 0$. Figure 3.2(b) shows countries' own contributions λ_n to the downstream power mix. For net exporters like node 1 and 2, the entries of the power mix are $p_{n,j} = 0,\ \forall\ j \neq n$, and $p_{n,n} = 1$.

Since it is not known beforehand which nodes are present in which other nodes, the whole network must be solved simultaneously with the system of equations generalised from (3.15)

$$\mathbf{P} = \mathbf{P}((\mathbf{K}\mathbf{F}_+)\mathbf{K}^\intercal)_- + \Lambda\,. \tag{3.17}$$

Here, Λ is the matrix with diagonal entries λ_n and $\mathbf{F}$ is a matrix with the flows contained in F as diagonal entries. As seen in (3.6), the term $\mathbf{KF}$ shows all inflows and outflows, which can be decomposed into a matrix

with only the outflows and one with all the inflows,

$$\mathbf{KF} = \mathbf{KF}_+ - \mathbf{KF}_- \ . \tag{3.18}$$

The term $(\mathbf{KF}_-)\mathbf{K}_+^\intercal$ relates the outflows of all nodes as inflows into another, as does the summation term in equation (3.15), while maintaining same normalisation as in (3.16). The matrix $\mathbf{P}$ contains the downstream power mixes of all nodes, so that

$$\mathbf{P} = \begin{bmatrix} | & & | & & | \\ \vec{p}_1 & \cdots & \vec{p}_n & \cdots & \vec{p}_N \\ | & & | & & | \end{bmatrix} . \tag{3.19}$$

This can be solved by a simple matrix inversion

$$\boldsymbol{P} = \Lambda[\mathbb{I} - ((\boldsymbol{K}\boldsymbol{F}_+)\boldsymbol{K}^\intercal)_-]^{-1} \ , \tag{3.20}$$

which becomes costly for large systems. One can also exploit a property of electrical networks: in a finite network under a physical flow, there should always be at least one pure source and a pure sink [59]. That means that at least one of the equations given by (3.17) is trivially solvable, leading to a well defined system solvable without the need for inversion. A similar algorithm based on graph theory is explained in [60], though without a mathematical representation.

In the case illustrated in figure 3.2, solving the above leads to

$$\boldsymbol{P} = \begin{bmatrix} 1 & 0 & 1/2 & 1/2 \\ 0 & 1 & 1/2 & 1/2 \\ 0 & 0 & 0 & 0 \\ 0 & 0 & 0 & 0 \end{bmatrix} \tag{3.21}$$

since all the power in all the nodes originates from nodes 1 and 2.

From the downstream power mix matrix $\boldsymbol{P}$, a matrix $\boldsymbol{E}$ that details exports and imports can be obtained by multiplying $\boldsymbol{P}$ with a diagonal matrix with entries equal to the $upstream$ contributions to consumption, $\widetilde{\Lambda}$

$$\boldsymbol{E} = \boldsymbol{P}\widetilde{\Lambda} \ . \tag{3.22}$$

Using the upstream contributions from Figure 3.2(c), this is

$$\boldsymbol{E} = \begin{bmatrix} 1 & 0 & 1/2 & 1/2 \\ 0 & 1 & 1/2 & 1/2 \\ 0 & 0 & 0 & 0 \\ 0 & 0 & 0 & 0 \end{bmatrix} \begin{bmatrix} 0 & 0 & 0 & 0 \\ 0 & 0 & 0 & 0 \\ 0 & 0 & 4 & 0 \\ 0 & 0 & 0 & 8 \end{bmatrix} , \tag{3.23}$$

$$\boldsymbol{E} = \begin{bmatrix} 0 & 0 & 2 & 4 \\ 0 & 0 & 2 & 4 \\ 0 & 0 & 0 & 0 \\ 0 & 0 & 0 & 0 \end{bmatrix} . \tag{3.24}$$

The lower two rows show, as expected, that the two sinks have no net exports. The first two rows show that each of the sources in the network exports 2 and 4 units to nodes 3 and 4, respectively. This can be transposed to find a similar matrix for imports, **I**,

$$\boldsymbol{I} = \boldsymbol{E}^{\intercal} = \begin{bmatrix} 0 & 0 & 0 & 0 \\ 0 & 0 & 0 & 0 \\ 2 & 2 & 0 & 0 \\ 4 & 4 & 0 & 0 \end{bmatrix} . \tag{3.25}$$

Flow tracing – link usage

J. Bialek, in [61], points out that the it is possible to trace the flow of power from the node-power mixes, but does not explicitly show an algorithm. D. Kirschen, in [60], does suggest an algorithm, but does not express it in mathematical terms. Here, we show an algebraic representation of the operations required to find the usage that a node makes of a link.

Once the downstream power mix for all nodes ($\boldsymbol{P}(t)$) has been defined at a given hour, the power mix of the links $\boldsymbol{H}(t)$ which shows export usage can be determined as

$$\boldsymbol{H} = \boldsymbol{P} \cdot (\mathbf{KF})_{+} , \tag{3.26}$$

which assigns the power mix of emitting nodes to the outgoing power flowing along a link. The L columns of $\boldsymbol{H}$ each contain the export usage of each node of that link. In the example from figure 3.2, this is

$$\boldsymbol{H} = \begin{bmatrix} 1 & 0 & 1/2 & 1/2 \\ 0 & 1 & 1/2 & 1/2 \\ 0 & 0 & 0 & 0 \\ 0 & 0 & 0 & 0 \end{bmatrix} \begin{bmatrix} 6 & 0 & 0 \\ 0 & 6 & 0 \\ 0 & 0 & 8 \\ 0 & 0 & 0 \end{bmatrix} , \tag{3.27}$$

$$\boldsymbol{H} = \begin{bmatrix} 6 & 0 & 4 \\ 0 & 6 & 4 \\ 0 & 0 & 0 \\ 0 & 0 & 0 \end{bmatrix} , \tag{3.28}$$

which matches our expectations, as it shows node 1 using link 1 to export 6 units and link 3 to export 4 units, and node 2 using link 2 to export 6 units and link 3 to export 4 units.

The usage of links for import $\widetilde{\boldsymbol{H}}$ cannot be obtained from a simple transposition of $\boldsymbol{H}$, but must instead be calculated from

$$\widetilde{\boldsymbol{H}} = \widetilde{\boldsymbol{P}} \cdot (\boldsymbol{KF})_{-} . \tag{3.29}$$

The terms in these equation come from an upstream re-calculation of the problem, where the flows along links and the role of sinks and sources is reversed, as illustrated in Figure 3.2(c).

We have expressed $\boldsymbol{P}$ and $\widetilde{\boldsymbol{P}}$ in normalised values, while the values of $\boldsymbol{H}$ and $\widetilde{\boldsymbol{H}}$ are directly expressed in MW. This allows a direct relation to the term $\langle U_n \rangle$, which expresses, in MW, how much of the installed capacity of the network can be attributed to node n

$$\langle U_n \rangle = \frac{\sum_t^T}{T} \sum_l^L \Big(H_{l,n}(t) + \widetilde{H}_{l,n}(t) \Big) \tag{3.30}$$

where $H_{l,n}$) is the n^{th} element of the power mix of link l, and T is the time period over which power flows are tracked. This finally allows us to calculate the usage a node makes of the whole network and thus the usage proportional pricing mechanism, M_n^3.

3.4 Transmission participation in 2050

As a test case, we look at a nearly fully renewable network for a hypothetical scenario. We use the flow tracking algorithm to identify the usage of links caused by the physical flows of renewable energy between countries. Trading between countries happens only when one of them has an excess in renewable generation and the other a deficit. As an example, the energy exports and imports of Germany are tracked and shown in Figure 3.3. This figure shows countries which receive or emit at least 1% of the energy generated or consumed in Germany. Links important to germany are likewise coloured according to the percentage of German energy they carry.

In this highly renewable future, France, iItaly and Sweden together account for around 50% of German exports and imports, while Denmark is accountable for less than 1% of German exports or imports. These patterns emerge as a consequence of the correlation of weather patterns in different countries (which determines the generation from VRES), as well as from the position of nodes in the network and the size of their mean loads. Denmark, for instance, has only a fourth of the mean load of Sweden.

This flow tracking algorithm reveals other interesting patterns arising from parallel flows in the network. Certain links connecting first neighbours of Germany are considerably important for the German market, such as those between the Czech Republic and Austria and Denmark and Sweden. By comparing the different usages that the nodes involved in these links make, we can make an estimate of the benefit that each derive from the installed capacities.

3.4. Transmission participation in 2050

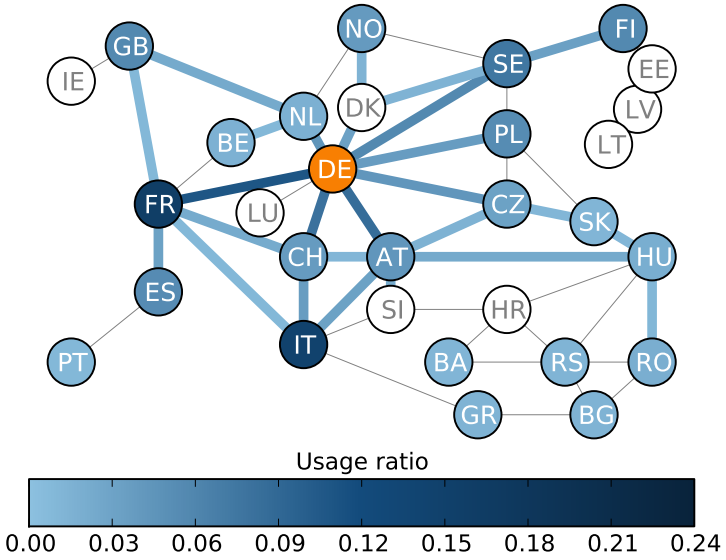

Figure 3.3: Trading partners and pathways for Germany. Scale for both nodes and links shows the percentage of German energy going to or coming from neighbouring countries and links. Some nodes appear islanded, since only links with a usage higher than 1% are drawn.

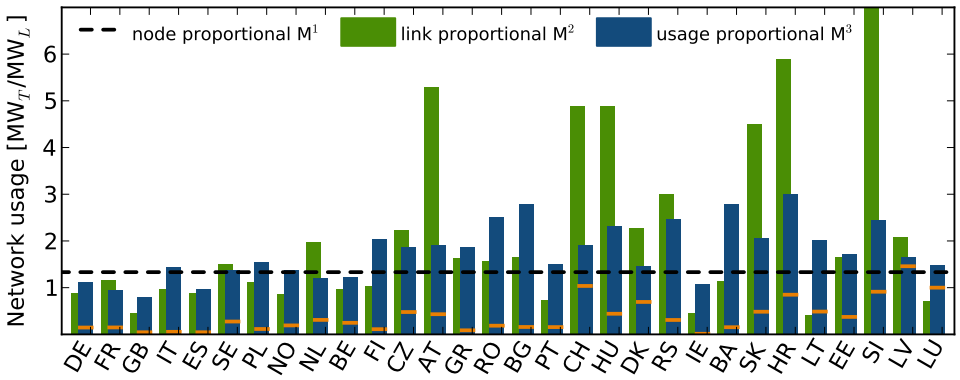

Figure 3.4: Contribution to the grid in MW_T / MW_L. That is, how many MW of grid is a country using per MW of internal mean load, under the link proportional M^2 (green) and usage proportional M^3 (blue). All countries contribute the same amount relative to their mean loads under the node proportional method M^1, shown by the dashed line. The thin orange lines show a country's stake (M^2) in present installed capacities according to [36].

After considering the usage that a country makes of the total network, it is possible to estimate the stake on the network held by a country under the usage proportional mechanism M^3 . Figure 3.4 shows how many MW of transmission capacity a country is 'responsible' for under the different investment distribution mechanisms. The importance of figuring out which nodes benefit most from the network becomes patent when comparing the results. Under M^1 (dashed line), where the total usage is distributed evenly as a function of a countries' mean load, each country would, in average, contribute 1.34 MW of electric transmission per 1 MW of average mean load. Under the link proportional mechanism M^2 (green), where we split the capacity of the links directly connecting two nodes between them, we see that most of the larger countries use less of the network than would be expected from their size. A different picture appears under M^3 (blue). Pathway countries are easily recognised by having significantly lower investment responsibility under M^3 (blue) than M^2 (green).

These results have deep implications for the design of a future network. It is not enough to look at a country's connections or its mean load. The weather-dictated correlation between it and its neighbours, and between third countries, determines its import and export capabilities, and the degree to which it benefits from the presence of a transmission network.

Effects of line-length

So far, we have been using an oversimplified transmission network, where single links connect countries and where the impedance or length of these links is assumed to be uniform. In reality, most connections that are not HVDC are not single-links, but interconnected networks at different levels of voltage. As a measure of the grid strengthening which must take place, we now talk about MWkm, which relates the length and capacity of links which must be installed to provide a sufficiently large transmission. We use the distance between capitals as a proxy for the area of the grid that must be expanded. A more precise calculation would consider the impedance of the links. While this is easily achieved under our modelling framework, results in cite{Magnus1} point at just slightly quantitatively different result, with no significant quantitive differences.

Considering now the MWkm, as shown in Figure 3.5, some differences appear. Countries that use longer links are now responsible for larger amounts compared to the other nodes, which in average (M^1) must contribute 770 MWkm of transmission per MW of mean load. The usage of M^2 raises additional questions. Can a country be responsible for, or benefit from, grid expansions outside its borders? Current bottlenecks in the grid, such as the weak northern German HV transmission grid,

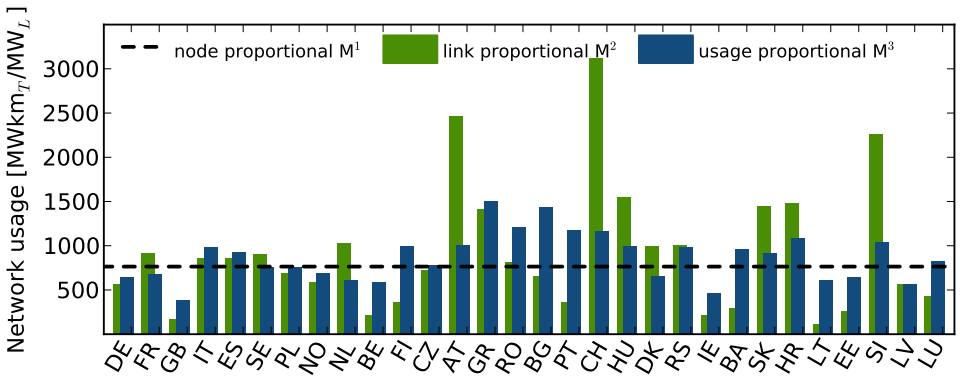

Figure 3.5: Contribution to the grid in $MWkm_T$ / MW_L. That is, how many MWkm of grid is a country using per MW of internal mean load, under M^2 (green) and M^3 (blue). All countries contribute the same amount relative to their mean loads under M^1, shown by the dashed line. Countries are arranged by the size of their mean loads.

impede Danish wind exports to central Germany. Pricing mechanisms like M^3 could help quantify the actual benefit that an expansion of the grid in this area represents for not only Germany or Denmark, but for all of Europe.

3.5 Path to a renewable Europe

Th previous test case is just the endpoint of a possible development of the European network. In [6], published renewable targets for 2020 for each country and a logistic interpolation (which best describe the deployment of new technologies) are used to we can plot the developmental pathways to a fully renewable Europe. Figure 3.6(a) shows the growth in VRES penetration for European countries and regions, for more details, see [6]. Every year, from 2020 until 2050, VRES capacities are expected to increase and, as a consequence, so will the transmission capacities required for full usage of renewable energy. Figure 3.6(b) shows (in blue) the increase in transmission, from close to 0 MW$_T$ / MW$_L$ to the 1.34 MW$_T$ / MW$_L$ arrived at in the previous section (see Figure 3.4). The different transmission buildups for which different countries are responsible (according to M^3_n) is shown in transparent lines, with a few exemplary exceptions.

A clear outlier in this figure is Greece, whose fast growth in transmission usage in Figure 3.6(b) (in light blue) is partly triggered by the fast growth in VRES penetration shown in Figure 3.6(a). The high national targets described in [6] define the logarithmic growth behaviour of the countries. The more recent political and economical developments might push towards a different behaviour for some countries.

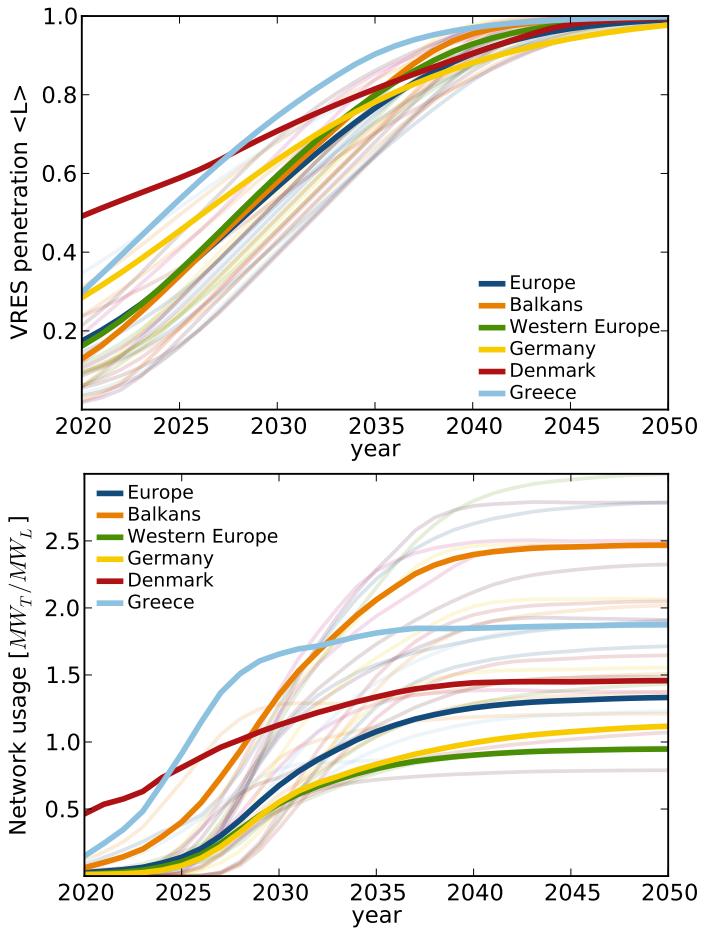

Figure 3.6: Development of the European electricity network from 2020 to 2050. Assumed penetration of renewables γ_n for different countries and regions, normalised to the mean load (top). Contribution to the grid in MW_T / MW_L. That is, how many MW of grid is a country using per MW of internal mean load, under M^3 for different countries and regions (bottom).

The initially high VRES penetration in Denmark (see Figure 3.6(a), in red) means that it has a higher usage of the network compared to other nodes (Figure 3.6(b), in red). This high initial usage also means that is has the slowest growth, as the years progress and the rest of Europe catches up. In fact, if the analysis of Section 3.4 were repeated for 2020, Denmark would be, by far, the country with the highest usage of the network, and would be responsible for installing around 5 MW of transmission for every 10 MW of mean national load. This is not at odds with the current installed capacity for Denmark under M^2, which can be seen in Figure 3.4 in orange lines. At present, there are around 5.4 GW of installed transmission capacity connecting Denmark with it's neighbours. Comparing half of these links, 2.7 GW, with the danish mean

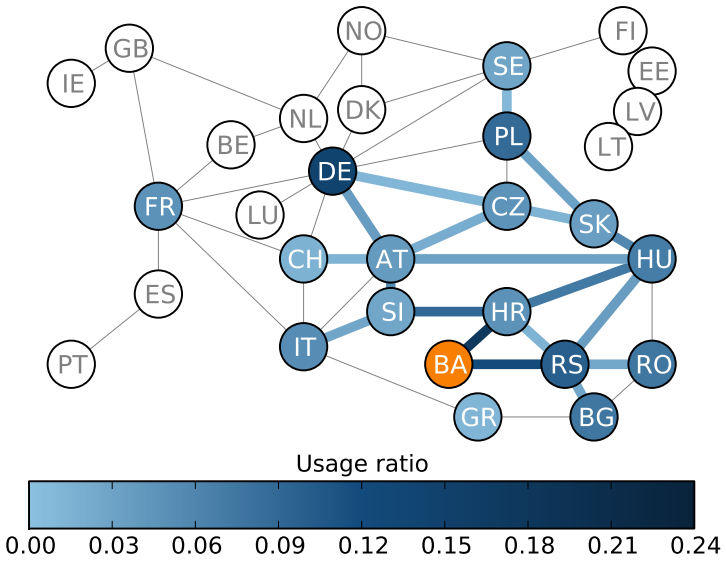

Figure 3.7: Trading partners and pathways for Bosnia Herzegovina. Scale for both nodes and links shows the percentage of energy going to or coming from neighbouring countries and links. Some nodes appear islanded, since only links with a usage higher than 1% are drawn.

load close to 4 GW means that, at present, Denmark is responsible for 0.7 MW_T / MW_L.

Examining the current stakes shown by the orange lines in Figures 3.4 and 3.8 shows that other countries seem to be presently well connected. The present stake that M^2 defines for countries like Switzerland, Latvia, Denmark, and Croatia exceeds in many cases 1 MW_T / MW_L. Comparing this with the year-by-year contribution shown in Figure 3.8 shows that many of these installed capacities would not be needed until 2030 or 2035.

Figure 3.6 shows that some outliers in this trend are Germany (in yellow) and the countries considered in Western Europe (France, Belgium, The Netherlands, Great Britain, and Ireland, in green), which use a smaller proportion of the network as a ratio of their mean load than countries in, for example, the Balkans (Bosnia Herzegovina, Bulgaria, Croatia, Serbia, and Greece, in orange). This follows the trend we saw in Figures 3.4 and 3.5, where the larger western countries have a smaller than average usage of the network. The larger geographical dispersion of their areas and the dispersion of their first neighbours means that most of their transmission happens in the links directly connected to them. This is easier to understand if we compare the usage map for Germany (Figure 3.3) to that of Bosnia Herzegovina, a country that makes higher than average usage of the network (Figure 3.7).

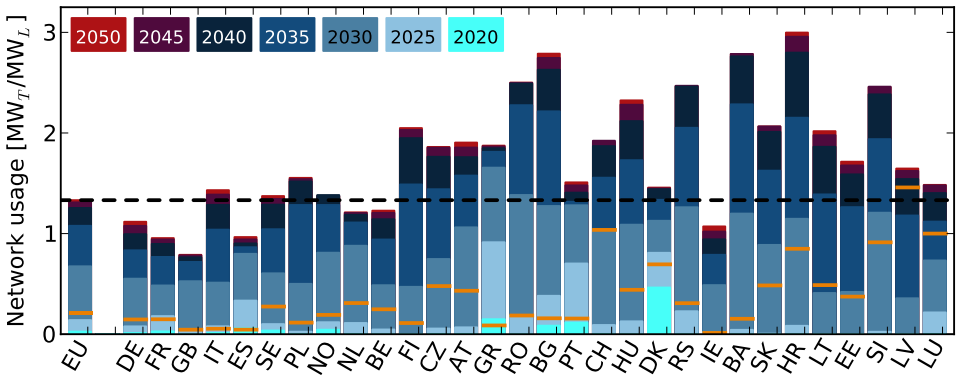

Figure 3.8: Contribution to the grid in MW_T / MW_L. That is, how many MW of grid is a country using per MW of internal mean load, under M[3]. Different color bars indicate when the investment should take place in order to account for growing VRES penetrations. All countries contribute the same amount relative to their mean loads under M[1], shown by the dashed line. Countries are arranged by the size of their mean loads.

The strong correlation that Bosnia has with its immediate neighbours means that it must make high usage of links two or sometimes three neighbours away to either export its excess or import the energy it needs. The node between HR and SI and the link between HR and HU each carry over 10% of exports from BA. In the German case, no secondary link carries more than 5% of the German trade. Furthermore, while for most of the Wester European countries, their main trading partner is a first neighbour, Germany is the top trading partner for many Balkan countries. In fact, Germany is one of the top three trading partners for over half the countries in Europe, meaning that the larger the distance that separates a country from Germany, the higher its network usage will tend to be. This can be seen for Bosnia & Herzegovina in Figure 3.7 and for all the countries in Table 3.1 in the Appendix.

The current installed capacity of VRES in Europe does not require a large transmission capacity to be effectively used, as can be seen in Figure 3.8. In fact, up until 2030, most countries would need to make no significant investment in transmission. Starting in that year, the larger countries countries start using a large percentage of the grid, disproportional to the size of their mean loads. Countries adjacent to large links, especially if their own mean loads are small, are disproportionally responsible for transmission investments. This is the case with Slovakia, Slovenia, Denmark and Switzerland. By 2040, most countries would be using close to their maximum of transmission capacity, with only a few additional expansions required until 2050. Full results are available as a table in the appendix.

3.6 Conclusion

While electricity cannot be traced – electrons cannot be traced to a wind turbine or a coal plant – power flows in an electric network are directly caused by the sink/source interactions. A power flow tracing algorithm can help identify the presence of power flowing out of a particular source in different sinks and links in the network. In this paper, we apply a power flow tracing algorithm to determine how the correlation of wind and solar power generation, in combination with electricity demand, determines the most attractive trading partners and pathways in a pan-European transmission grid.

The analysis shows that, in general, the current European transmission grid is sufficiently strong to support exchange of excess wind and solar energy until 2020, though individual links and country internal transmission bottlenecks may require strengthening. In the years after 2030, the expected increase in installed wind and solar capacity across the continent leads to a higher need for new transmission capacity in order to facilitate exchange of national excess from VRES.

As a hypothetical 2050 endpoint scenario, a European grid where all countries have a 100% penetration of wind and solar power is modelled. The analysis reveals that even in the case of such a homogeneous renewable scenario, not all countries hold the same stakes in a strong common transmission grid. By comparing the transmission capacity directly associated with a country to its actual usage of the network, we show that with an ideal European transmission network, a number of countries (such as Switzerland, Austria and several Balkan countries) act as transit nodes with a large number of links, although they do not themselves benefit proportionally from these connections. Other regions, such as the British Isles, the Iberian peninsula and the Baltic countries, benefit more from a strong common grid than would be expected from simply looking at their own links or sizes.

These findings may be used to develop both national and European renewable energy policies. From a national point of view, a country could for instance lower its reliance on a common grid through investments in flexible demand such as power to heat or gas. Likewise a country could choose to increase its stake in the grid by increasing the local penetration of VRES. From a common European point of view, the analysis could guide the distribution of subsidies to links or nodes that have many non-local stakeholders. It could also be used in the development of future market mechanisms where, e.g. transit countries receive fair compensation, or a smarter assessment of the ecological footprint of electricity in a region.

Table 3.1: Main trading partners for different stages of VRES penetration.

Country	2020	2035	2050
DE	DK (99%) 231 GWh SE (0%) 0 GWh LU (0%) 0 GWh	FR (16%) 8172 GWh IT (13%) 6458 GWh SE (9%) 4449 GWh	FR (17%) 12116 GWh IT (15%) 11150 GWh SE (8%) 5741 GWh
FR	ES (89%) 429 GWh PT (11%) 52 GWh DE (0%) 0 GWh	GB (19%) 10794 GWh IT (19%) 10430 GWh ES (17%) 9343 GWh	IT (21%) 15879 GWh DE (16%) 12116 GWh GB (16%) 11648 GWh
GB	IE (94%) 0 GWh NL (5%) 0 GWh FR (1%) 0 GWh	FR (32%) 10794 GWh NL (13%) 4382 GWh DE (10%) 3320 GWh	FR (30%) 11648 GWh NL (13%) 4979 GWh DE (11%) 4377 GWh
IT	GR (100%) 162 GWh SI (0%) 0 GWh CH (0%) 0 GWh	FR (26%) 10430 GWh DE (16%) 6458 GWh GR (9%) 3535 GWh	FR (27%) 15879 GWh DE (19%) 11150 GWh GR (6%) 3781 GWh
ES	FR (80%) 429 GWh PT (20%) 106 GWh LT (0%) 0 GWh	FR (38%) 9343 GWh GB (13%) 3230 GWh DE (12%) 2983 GWh	FR (38%) 11613 GWh DE (13%) 4132 GWh GB (12%) 3755 GWh
SE	DK (100%) 231 GWh DE (0%) 0 GWh NO (0%) 0 GWh	DE (22%) 4449 GWh NO (14%) 2827 GWh FI (13%) 2566 GWh	DE (21%) 5741 GWh FI (14%) 3750 GWh NO (11%) 3012 GWh
PL	DE (99%) 0 GWh DK (1%) 0 GWh SK (0%) 0 GWh	DE (18%) 3477 GWh SE (9%) 1768 GWh FI (8%) 1614 GWh	DE (16%) 4093 GWh SE (9%) 2304 GWh FI (9%) 2297 GWh
NO	DK (100%) 231 GWh DE (0%) 0 GWh NL (0%) 0 GWh	NL (25%) 5202 GWh SE (13%) 2827 GWh DE (12%) 2612 GWh	NL (24%) 5684 GWh SE (13%) 3012 GWh DE (13%) 2991 GWh
NL	DE (99%) 0 GWh DK (1%) 0 GWh BE (0%) 0 GWh	NO (29%) 5202 GWh GB (25%) 4382 GWh DE (9%) 1513 GWh	NO (28%) 5684 GWh GB (24%) 4979 GWh FR (8%) 1665 GWh
BE	NL (86%) 0 GWh FR (14%) 0 GWh LT (0%) 0 GWh	FR (21%) 2079 GWh ES (15%) 1455 GWh NO (12%) 1226 GWh	FR (20%) 2791 GWh ES (14%) 1982 GWh NO (12%) 1602 GWh

3.6. Conclusion

Table 3.2: Main trading partners for different stages of VRES penetration.

Country	2020	2035	2050
FI	EE (100%)	DE (23%)	DE (24%)
	0 GWh	2822 GWh	4373 GWh
	SE (0%)	SE (21%)	SE (21%)
	0 GWh	2566 GWh	3750 GWh
	LT (0%)	PL (13%)	PL (13%)
	0 GWh	1614 GWh	2297 GWh
CZ	DE (99%)	DE (18%)	DE (18%)
	0 GWh	1665 GWh	2457 GWh
	DK (1%)	PL (14%)	IT (16%)
	0 GWh	1308 GWh	2194 GWh
	SK (0%)	IT (14%)	PL (13%)
	0 GWh	1301 GWh	1748 GWh
AT	DE (99%)	DE (21%)	IT (25%)
	0 GWh	2253 GWh	3630 GWh
	DK (1%)	IT (21%)	DE (23%)
	0 GWh	2216 GWh	3319 GWh
	SI (0%)	FR (10%)	FR (10%)
	0 GWh	1018 GWh	1473 GWh
GR	BG (50%)	IT (31%)	IT (30%)
	162 GWh	3535 GWh	3781 GWh
	IT (50%)	FR (16%)	FR (18%)
	162 GWh	1789 GWh	2196 GWh
	LT (0%)	BG (13%)	BG (13%)
	0 GWh	1523 GWh	1574 GWh
RO	RS (56%)	HU (16%)	HU (14%)
	0 GWh	1604 GWh	1687 GWh
	HU (26%)	PL (11%)	DE (13%)
	0 GWh	1105 GWh	1482 GWh
	BG (18%)	RS (11%)	PL (11%)
	0 GWh	1092 GWh	1308 GWh
BG	GR (100%)	GR (16%)	IT (16%)
	162 GWh	1523 GWh	1926 GWh
	RS (0%)	IT (14%)	GR (13%)
	0 GWh	1275 GWh	1574 GWh
	RO (0%)	RS (13%)	RS (12%)
	0 GWh	1261 GWh	1525 GWh
PT	ES (67%)	ES (36%)	ES (35%)
	106 GWh	2296 GWh	2784 GWh
	FR (33%)	FR (30%)	FR (30%)
	52 GWh	1896 GWh	2367 GWh
	LT (0%)	DE (8%)	DE (10%)
	0 GWh	536 GWh	773 GWh
CH	DE (99%)	IT (24%)	IT (26%)
	0 GWh	2377 GWh	3554 GWh
	DK (1%)	DE (20%)	DE (22%)
	0 GWh	1933 GWh	2948 GWh
	FR (0%)	FR (12%)	FR (13%)
	0 GWh	1215 GWh	1757 GWh
HU	HR (61%)	RO (21%)	RO (16%)
	0 GWh	1604 GWh	1687 GWh
	RO (19%)	PL (13%)	DE (14%)
	0 GWh	988 GWh	1546 GWh
	SK (14%)	DE (12%)	PL (13%)
	0 GWh	915 GWh	1447 GWh
DK	DE (33%)	NO (33%)	NO (31%)
	231 GWh	2166 GWh	2223 GWh
	SE (33%)	DE (13%)	FI (12%)
	231 GWh	822 GWh	878 GWh
	NO (33%)	SE (12%)	SE (10%)
	231 GWh	800 GWh	743 GWh

Table 3.3: Main trading partners for different stages of VRES penetration.

Country	2020	2035	2050
RS	HR (50%)	BG (17%)	BG (17%)
	0 GWh	1261 GWh	1525 GWh
	RO (27%)	RO (15%)	RO (12%)
	0 GWh	1092 GWh	1112 GWh
	BG (19%)	DE (9%)	DE (11%)
	0 GWh	665 GWh	1032 GWh
IE	GB (100%)	GB (48%)	GB (38%)
	0 GWh	1404 GWh	1494 GWh
	LT (0%)	FR (17%)	FR (20%)
	0 GWh	502 GWh	771 GWh
	LV (0%)	NL (10%)	NL (13%)
	0 GWh	283 GWh	507 GWh
BA	HR (95%)	DE (12%)	DE (15%)
	0 GWh	613 GWh	945 GWh
	RS (5%)	RS (12%)	RS (10%)
	0 GWh	588 GWh	654 GWh
	LT (0%)	RO (9%)	PL (9%)
	0 GWh	449 GWh	584 GWh
SK	CZ (46%)	PL (27%)	PL (26%)
	0 GWh	1365 GWh	1786 GWh
	PL (45%)	DE (12%)	DE (14%)
	0 GWh	599 GWh	985 GWh
	HU (9%)	RO (10%)	SE (9%)
	0 GWh	525 GWh	661 GWh
HR	BA (27%)	RS (11%)	DE (14%)
	0 GWh	343 GWh	623 GWh
	SI (27%)	DE (10%)	RS (9%)
	0 GWh	334 GWh	422 GWh
	RS (25%)	BA (9%)	PL (9%)
	0 GWh	299 GWh	420 GWh
LT	LV (100%)	FI (33%)	FI (32%)
	0 GWh	380 GWh	554 GWh
	LT (0%)	EE (22%)	EE (19%)
	0 GWh	251 GWh	330 GWh
	FI (0%)	DE (10%)	DE (11%)
	0 GWh	120 GWh	197 GWh
EE	LV (50%)	DE (21%)	DE (22%)
	0 GWh	259 GWh	394 GWh
	FI (50%)	LT (21%)	LT (18%)
	0 GWh	251 GWh	330 GWh
	LT (0%)	SE (8%)	SE (7%)
	0 GWh	98 GWh	132 GWh
SI	HR (37%)	IT (25%)	IT (27%)
	0 GWh	679 GWh	1021 GWh
	AT (35%)	DE (16%)	DE (19%)
	0 GWh	427 GWh	707 GWh
	IT (28%)	AT (7%)	FR (7%)
	0 GWh	193 GWh	274 GWh
LV	EE (50%)	FI (26%)	FI (24%)
	0 GWh	132 GWh	180 GWh
	LT (50%)	DE (16%)	DE (18%)
	0 GWh	81 GWh	131 GWh
	HR (0%)	LT (9%)	LT (8%)
	0 GWh	48 GWh	62 GWh
LU	DE (99%)	DE (43%)	DE (42%)
	0 GWh	337 GWh	485 GWh
	DK (1%)	SE (7%)	SE (9%)
	0 GWh	59 GWh	106 GWh
	LT (0%)	PL (7%)	PL (7%)
	0 GWh	52 GWh	84 GWh

3.6. Conclusion

Table 3.4: Main trading pathways for different stages of VRES penetration.

Country	2020	2035	2050
DE	DE – DK (99%) 231 GWh DE – LU (0%) 0 GWh CH – DE (0%) 0 GWh	FR – DE (11%) 10968 GWh AT – DE (8%) 8079 GWh CH – DE (8%) 7662 GWh	FR – DE (11%) 16102 GWh AT – DE (9%) 12604 GWh CH – DE (8%) 11998 GWh
FR	FR – ES (90%) 481 GWh PT – ES (10%) 52 GWh FR – DE (0%) 0 GWh	FR – IT (14%) 11433 GWh FR – GB (14%) 11336 GWh FR – ES (13%) 11239 GWh	FR – IT (15%) 16882 GWh FR – DE (13%) 14880 GWh FR – ES (12%) 13981 GWh
GB	GB – IE (96%) 0 GWh NL – GB (4%) 0 GWh FR – GB (0%) 0 GWh	FR – GB (32%) 18744 GWh NL – GB (23%) 13250 GWh NL – DE (7%) 3923 GWh	FR – GB (31%) 21652 GWh NL – GB (22%) 15825 GWh NL – DE (7%) 4944 GWh
IT	GR – IT (100%) 162 GWh IT – SI (0%) 0 GWh CH – IT (0%) 0 GWh	FR – IT (19%) 14186 GWh CH – IT (12%) 9026 GWh AT – IT (10%) 7646 GWh	FR – IT (18%) 20682 GWh CH – IT (12%) 14009 GWh AT – IT (11%) 12378 GWh
ES	FR – ES (80%) 429 GWh PT – ES (20%) 106 GWh FR – DE (0%) 0 GWh	FR – ES (50%) 22474 GWh FR – GB (8%) 3437 GWh FR – DE (8%) 3359 GWh	FR – ES (51%) 27812 GWh FR – DE (8%) 4342 GWh FR – GB (7%) 4058 GWh
SE	SE – DK (100%) 231 GWh DE – SE (0%) 0 GWh DE – DK (0%) 0 GWh	DE – SE (17%) 6250 GWh PL – SE (11%) 4128 GWh NO – SE (11%) 3914 GWh	DE – SE (16%) 8491 GWh PL – SE (12%) 6256 GWh NO – SE (9%) 4785 GWh
PL	PL – DE (99%) 0 GWh DE – DK (1%) 0 GWh PL – SK (0%) 0 GWh	PL – DE (13%) 5422 GWh PL – SK (12%) 5061 GWh PL – SE (11%) 4589 GWh	PL – DE (12%) 6787 GWh PL – SK (12%) 6753 GWh PL – SE (11%) 6197 GWh
NO	NO – DK (100%) 231 GWh DE – DK (0%) 0 GWh NL – NO (0%) 0 GWh	NL – NO (28%) 10488 GWh NO – DK (14%) 5356 GWh NO – SE (14%) 5070 GWh	NL – NO (28%) 12158 GWh NO – DK (14%) 5931 GWh NO – SE (13%) 5663 GWh
NL	NL – DE (99%) 0 GWh DE – DK (1%) 0 GWh NL – GB (0%) 0 GWh	NL – NO (23%) 6357 GWh NL – GB (19%) 5023 GWh NL – DE (13%) 3655 GWh	NL – NO (23%) 7407 GWh NL – GB (19%) 6033 GWh NL – DE (12%) 3724 GWh
BE	NL – BE (62%) 0 GWh NL – DE (13%) 0 GWh NL – GB (12%) 0 GWh	FR – BE (28%) 5412 GWh NL – BE (24%) 4491 GWh FR – ES (9%) 1686 GWh	FR – BE (28%) 7514 GWh NL – BE (23%) 6158 GWh NL – NO (9%) 2310 GWh

Table 3.5: Main trading pathways for different stages of VRES penetration.

Country	2020	2035	2050
FI	FI – EE (65%) 0 GWh EE – LV (35%) 0 GWh DE – SE (0%) 0 GWh	FI – SE (40%) 11396 GWh DE – SE (11%) 3230 GWh PL – SE (9%) 2645 GWh	FI – SE (39%) 16836 GWh DE – SE (11%) 4856 GWh PL – SE (9%) 4011 GWh
CZ	CZ – DE (99%) 0 GWh DE – DK (1%) 0 GWh CZ – SK (0%) 0 GWh	AT – CZ (15%) 3018 GWh CZ – DE (15%) 2943 GWh PL – CZ (9%) 1907 GWh	AT – CZ (16%) 4556 GWh CZ – DE (14%) 4030 GWh PL – CZ (10%) 2745 GWh
AT	AT – DE (99%) 0 GWh DE – DK (1%) 0 GWh AT – SI (0%) 0 GWh	AT – DE (15%) 2991 GWh AT – IT (11%) 2203 GWh AT – CH (10%) 2005 GWh	AT – DE (16%) 4077 GWh AT – IT (13%) 3321 GWh AT – CH (11%) 2754 GWh
GR	GR – IT (50%) 162 GWh BG – GR (50%) 162 GWh BG – RS (0%) 0 GWh	GR – IT (34%) 7638 GWh BG – GR (16%) 3507 GWh FR – IT (8%) 1879 GWh	GR – IT (34%) 8630 GWh BG – GR (15%) 3682 GWh FR – IT (9%) 2352 GWh
RO	BG – RO (30%) 0 GWh BG – GR (26%) 0 GWh RO – RS (17%) 0 GWh	RO – HU (22%) 5746 GWh RO – RS (11%) 2865 GWh HU – SK (10%) 2577 GWh	RO – HU (22%) 6946 GWh HU – SK (10%) 3229 GWh RO – RS (10%) 3096 GWh
BG	BG – GR (100%) 162 GWh BG – RS (0%) 0 GWh BG – RO (0%) 0 GWh	BG – RS (16%) 3793 GWh BG – GR (15%) 3573 GWh GR – IT (9%) 2050 GWh	BG – RS (15%) 4835 GWh BG – GR (14%) 4712 GWh GR – IT (10%) 3138 GWh
PT	PT – ES (75%) 158 GWh FR – ES (25%) 52 GWh FR – DE (0%) 0 GWh	PT – ES (47%) 6346 GWh FR – ES (30%) 4049 GWh FR – DE (4%) 561 GWh	PT – ES (47%) 7917 GWh FR – ES (30%) 5133 GWh FR – DE (4%) 752 GWh
CH	CH – DE (99%) 0 GWh DE – DK (1%) 0 GWh FR – CH (0%) 0 GWh	CH – DE (18%) 2859 GWh CH – IT (18%) 2840 GWh FR – CH (15%) 2397 GWh	CH – DE (19%) 4105 GWh CH – IT (18%) 3956 GWh FR – CH (15%) 3115 GWh
HU	HR – HU (74%) 0 GWh HR – SI (17%) 0 GWh HU – SK (6%) 0 GWh	HU – SK (12%) 1965 GWh AT – HU (12%) 1951 GWh RO – HU (11%) 1847 GWh	AT – HU (13%) 3136 GWh HU – SK (13%) 3123 GWh RO – HU (9%) 2075 GWh
DK	DE – DK (33%) 231 GWh SE – DK (33%) 231 GWh NO – DK (33%) 231 GWh	NO – DK (23%) 2545 GWh DE – DK (20%) 2273 GWh SE – DK (15%) 1720 GWh	NO – DK (21%) 2833 GWh DE – DK (18%) 2463 GWh SE – DK (14%) 1938 GWh

3.6. Conclusion

Table 3.6: Main trading pathways for different stages of VRES penetration.

Country	2020	2035	2050
RS	HR – RS (74%) 0 GWh HR – SI (17%) 0 GWh BG – RS (2%) 0 GWh	HU – RS (13%) 2237 GWh BG – RS (11%) 1820 GWh HR – RS (9%) 1466 GWh	HU – RS (14%) 3044 GWh BG – RS (10%) 2143 GWh HR – RS (9%) 1934 GWh
IE	GB – IE (100%) 0 GWh FR – GB (0%) 0 GWh LV – LT (0%) 0 GWh	GB – IE (54%) 2891 GWh FR – GB (16%) 835 GWh NL – GB (12%) 652 GWh	GB – IE (49%) 3906 GWh FR – GB (16%) 1243 GWh NL – GB (15%) 1170 GWh
BA	BA – HR (81%) 0 GWh HR – SI (19%) 0 GWh RO – RS (0%) 0 GWh	BA – HR (19%) 2829 GWh BA – RS (14%) 2124 GWh HR – SI (9%) 1415 GWh	BA – HR (18%) 3700 GWh BA – RS (13%) 2532 GWh HR – SI (9%) 1895 GWh
SK	PL – SK (26%) 0 GWh CZ – SK (21%) 0 GWh HU – SK (17%) 0 GWh	PL – SK (21%) 2257 GWh HU – SK (16%) 1684 GWh CZ – SK (10%) 1111 GWh	PL – SK (22%) 3215 GWh HU – SK (14%) 2123 GWh CZ – SK (11%) 1709 GWh
HR	HR – HU (25%) 0 GWh HR – RS (25%) 0 GWh BA – HR (24%) 0 GWh	HR – HU (15%) 1102 GWh HR – SI (14%) 1042 GWh HR – RS (9%) 695 GWh	HR – HU (15%) 1722 GWh HR – SI (14%) 1637 GWh AT – SI (8%) 887 GWh
LT	EE – LV (80%) 0 GWh LV – LT (20%) 0 GWh BA – HR (0%) 0 GWh	LV – LT (25%) 1148 GWh EE – LV (24%) 1100 GWh FI – EE (19%) 849 GWh	LV – LT (24%) 1734 GWh EE – LV (23%) 1672 GWh FI – EE (19%) 1342 GWh
EE	EE – LV (83%) 0 GWh LV – LT (15%) 0 GWh FI – SE (3%) 0 GWh	FI – EE (24%) 942 GWh FI – SE (23%) 894 GWh DE – SE (8%) 316 GWh	FI – EE (24%) 1416 GWh FI – SE (23%) 1325 GWh DE – SE (8%) 466 GWh
SI	IT – SI (28%) 0 GWh AT – SI (27%) 0 GWh HR – SI (14%) 0 GWh	AT – SI (21%) 1164 GWh IT – SI (17%) 956 GWh HR – SI (11%) 604 GWh	AT – SI (22%) 1743 GWh IT – SI (18%) 1385 GWh AT – DE (10%) 763 GWh
LV	EE – LV (49%) 0 GWh FI – EE (32%) 0 GWh LV – LT (20%) 0 GWh	EE – LV (25%) 457 GWh FI – EE (24%) 438 GWh FI – SE (17%) 306 GWh	EE – LV (24%) 671 GWh FI – EE (23%) 653 GWh FI – SE (17%) 472 GWh
LU	DE – LU (99%) 0 GWh DE – DK (1%) 0 GWh FR – DE (0%) 0 GWh	DE – LU (49%) 781 GWh DE – SE (5%) 79 GWh DE – DK (4%) 64 GWh	DE – LU (48%) 1129 GWh DE – SE (5%) 127 GWh PL – DE (4%) 94 GWh

Chapter 4

Cost sensitivity

Motivation

The strength of the results obtained in [1–3] stems from their independence on changes to technical or economical assumptions. However, this also means that they have limited applications, as optimal systems defined in terms of γ_n and α_n can hardly be translated into policies without a proper economic analysis. Furthermore, results from [2] point at a set of competing optimisation goals: backup capacities and energy ($\mathcal{K}^B, E^B$) against the size of a transmission system ($\mathcal{K}^T$). The relative importance of these goals is ultimately decided by the cost and benefit that they bring to the system.

Gathering data on technologies, policies, and costs is an important part of ESA, allowing these studies to draw conclusions that are valid for that specific set of assumptions. The more concrete and specific a claim is (the choice of a specific technology, a specific location, a specific cost of electricity), the more vulnerable it is to changes in the assumptions. Uncertainties in the assumptions can be mapped as uncertainties in the results.

In this chapter, we explore the weights, or costs, that can be applied to the targets in our system, the backup, transmission, and VRES capacities, to find cost-optimal systems under a set of assumptions. In order to maintain the strength that weather-driven analysis gives to our claims, we make a sensitivity analysis on the results, to see how the optima we find respond to changes in our technological, political and economical assumptions.

Methods

Levelised cost of electricity

The levelised cost of electricity (LCOE) is the golden standard for comparing costs in ESA. The strict definition is "[the] cost that, if assigned to every unit of energy

produced (or saved) by the system over the analysis period, will equal the [present value of the investment] when discounted back to the base year" [68], or

$$\sum_{t=1}^{\mathcal{T}} \frac{\mathcal{E}_t \cdot \mathsf{LCOE}}{(1+r)^t} = \mathsf{V}_{\mathsf{sys}}\,, \tag{57}$$

though it is more often expressed as

$$\mathsf{LCOE} \;=\; \frac{\mathsf{V}_{\mathsf{sys}}}{\sum_{t=1}^{\mathcal{T}} \frac{\mathcal{E}_t}{(1+r)^t}}\,, \tag{58}$$

where $\mathsf{V}_{\mathsf{sys}}$ is the present value of the investment required by the system, $\mathcal{E}_t$ is the energy produced or saved by the system during the period t, and $\mathcal{T}$ is the study lifetime. Both the value of the energy and the present value of the investment are expressed in present value by the discount rate r. The present value of any investment is

$$\mathsf{V} = \mathsf{CapEx} + \sum_{t=1}^{\mathcal{T}} \frac{\mathsf{OpEx}_t}{(1+r)^t}\,. \tag{59}$$

Here we assume that the Capital Expenses (CapEx) happen only at the beginning of the investment. Capital expenses include all initial investments required, such as the actual energy system (wind turbines, solar panels, gas turbines), installation costs, and permits. Operational Expenses (OpEx) include all fixed and variable costs that must be covered during the lifetime of the project, such as maintenance, operational costs, and fuel, if applicable.

The expression in (58) has become so pervasive in the literature that some sources incorrectly state that the energy produced is itself being discounted, as might be apparent from the denominator. This is only a result of the rearranging the terms from the actual definition in (57).

The advantage of the LCOE is that it allows for a direct comparison of projects of differing scale and behaviour. Since it accounts for energy produced, it will result in different value for the same wind turbine, depending on the capacity factor of the location in which it is placed. In a single number, you can compare the cost of energy produced by vastly different systems.

This strength also means that LCOE values cannot be directly comparable without knowing all the details involved in the calculation. Different studies will assume different discount rates, capacity factors, lifetimes, and operational and capital expenditures. Therefore, we need to calculate the present value $\mathsf{V}_{\mathsf{sys}}$ based on CapEx and OpEx assumptions per (59). In a weather-driven approach, where the capacity factor of technologies varies significantly, this is a major disadvantage. Furthermore, the denominator in (58) cannot be always directly interpreted as just the energy generation, especially when dealing with high VRES penetrations, when not all energy generated is actually consumed. In a fully renewable system, where we assume that all of the load is being covered by either VRES of conventional backup, we can replace this by the total load of the system. See section 4.2 for more details.

Data gathering

Private companies will rarely publish data regarding the capital or operational expenditures attached to their projects. Instead, we must rely on government-funded studies, which compile this information based on historical installations. Since the CapEx and OpEx reported are inferred from the total cost of publicly funded projects, the more projects that are available, the higher the certainty on the validity of the assumptions. This complicates things for newer technologies, such as large photovoltaic installations and offshore wind parks, where few large installations have had their costs analysed in this way.

We look at studies funded by the UK, the US and Germany, [13, 21, 69–78], to get an idea of commonly used CapEx and OpEx values. These costs vary so much in the literature that many of these studies include upper and lower ranges on their assumptions, and some have even found it necessary to include a statistical distribution of costs for VRES technologies. The case of conventional sources is not better, where a variation of $\pm 25\%$ in the CapEx of a mature technology such as Combined Cycle Gas Turbine (CCGT) is classified as "low" [78].

We start the analysis with some initial assumptions; see Table 4.1. Later, we allow each of these assumptions to vary upwards and downwards, and recalculate the optimal system at every change. This allows us to make claims without losing the strength that the weather-driven approach provides us.

Main findings

Using our initial assumptions, we can find the contributions that the installed capacity of wind, solar, backup and transmission make to the total system cost, as well as the fuel usage from backup. Figure 4.3 shows these costs for a variety of penetrations $\gamma_n = 0.5, 1.0, 1.5$ and $0.0 \leq \alpha_n \leq 1.0$ for all n. At this level, it seems that the presence of transmission reduces the total system cost when compared to the zero exports scheme, for values of $\gamma > 0.5$. It is hard to see if the synchronised export scheme from [2] outperforms the simple localised scheme from [1].

Figure 4.4 shows the minimum system cost for $0.0 \leq \gamma \leq 2.0$. Here we see that, between $\gamma = 0.5$ and $\gamma = 1.5$, the added cost of transmission is worth the reduction in backup capacity that the synchronised export scheme brings (see Chapter 2). Figure 4.5(a) shows how this export scheme performs for the whole space $0 \leq \gamma \leq 2$ and $0 \leq \alpha \leq 1$. We find an optimal value at $\gamma^* = 0.5$ and $\alpha^* = 0.94$.

Given the variations in our assumptions that can be found in the literature, it is important to evaluate the strength of our results. Figure 4.6 shows the reaction of the system-optimal LCOE, γ^*, and α^* to variations in each of the assumed costs. The optimal mix α^* seems to be quite resistant to variations in assumptions other than wind and solar costs. This means that, wind and solar costs constant, variations in the other conditions do not move the optimal mix below $\alpha^* > 0.8$.

The optimal system penetration and the optimal system LCOE, on the other hand, are very sensitive to changes in the cost of wind capacity and fuel cost. The response

of the LCOE to changes in these assumptions is non-linear since a change in them will cause the system to change its characteristics, finding a different minimum. This can be seen in, for example, the case of a difference in the assumed cost of balancing in Figure 4.6(b). If this cost drops to below 75% of the assumed initial cost, then the cost-optimal penetration quickly drops to $\gamma^* = 0$. At lower prices, the response of the LCOE to reductions in fuel cost is linear, as the system consists of 0% VRES.

Increases in fuel cost, in the other hand, will lead to an increased renewable penetration, reducing the dependency of the LCOE on the increase of these costs. The optimal penetration, however, does not exceed $\gamma^* = 0.9$, save for cases when the CapEx of wind power capacity is significantly reduced.

We can also use this sensitivity analysis to explore how the system would react to technical or political changes. This could be, for example, the inclusion of a CO_2 tax or the electrification of other networks, allowing the interaction of the electricity system with other infrastructures where excess energy could be sold. Figure 4.7 shows the reaction of the system to an increasingly large CO_2 tax, allowing us to see that, for the assumed prices, carbon capture and sequestration (CCS) is not economically viable for CO_2 prices below 100 €/ton. Figures 4.8 and 4.9 show how the utilisation of excess energy could reduce the cost of the system up to the point where excess generation becomes profitable. This is, of course, only possible if the market does not reach saturation before this point, but only further studies into the electrification of other infrastructures can say if this is realistic.

Cost-optimal design of a simplified, highly renewable pan-European electricity system

Rolando A. Rodriguez[a], Sarah Becker[b], Martin Greiner[a,c]

a Department of Mathematics, Aarhus University, Denmark

b Frankfurt Institute for Advanced Studies (FIAS), Johann Wolfgang Goethe Universität, Germany

c Department of Engineering, Aarhus University, Denmark

Abstract

Based on a data-intensive weather-driven modelling approach, technically and economically optimal designs are derived for a simplified, highly renewable pan-European electricity system, which minimise the need for backup energy, backup capacity, transmission capacity and the levelised system cost of delivered electricity. The overall cost-optimal design, based on standard cost assumptions, relies on synchronised backup across the transmission grid and comes with a renewable penetration of 50% with a rather high wind fraction of 94%. Given the current European electricity consumption, this corresponds to 600 GW rated wind power capacities, 60 GW installed solar power capacities, 320 GW conventional backup power capacity, and about five times today's installed transmission capacities. A sensitivity analysis reveals that the design and cost of the optimal system depend mostly on the assumed cost of wind capacity and fuel for backup energy. Lower costs for wind capacity, higher costs for backup energy and usage of otherwise curtailed excess electricity generation lead to a strong increase of the optimal renewable penetration. The sensitivity analysis is also used to find that a CO_2 tax of over 100 €/ton would be needed for the economic viability of carbon capture and sequestration.

keywords: renewable energy system, wind power generation, solar power generation, power transmission, cost of energy , cost sensitivity

4.1 Introduction

The amount of variable renewable energy sources (VRES) continues to grow in current electricity systems of all scales. In two to three decades from now, the VRES penetration level might exceed 50%. This transition away from dispatchable conventional resources is driven by the political and societal will towards security of energy supply, sustainability, and reductions of CO_2 emissions. At very high penetration levels, a completely new backup infrastructure will be needed to cope with the strong spatio-temporal fluctuations of renewable power generation.

Technical studies have established the availability and feasibility of VRES, both globally [12, 79] and in Europe [10, 11]. These modelling approaches also include cost estimates [13, 18, 27, 80, 81]. However, with evolving policies and technologies, these estimates are subject to continuous revision, and the available elementary cost assumptions have a large margin of error and scatter by factors of 3-4 across the literature [13, 69–77].

In this study, we use the weather-driven modeling approach from [1, 6, 23–25] and cost assumptions from the literature [13, 21, 69–77] to find technically and economically optimal designs for a highly renewable pan-European electricity system. The technical optimum system designs are characterised by an optimal VRES penetration, an optimal VRES mix, and an optimal transmission paradigm. The latter describes the interaction between the backup and the transmission system. Three different transmission paradigms are discussed, which result in different reductions in backup energy, backup power capacity and transmission capacity. The economical optimum is determined from an examination of the levelised system cost of electricity (LCOE). The LCOE depends on the energy delivered to the system and on the assumed capital and operational expenditures. A sensitivity analysis examines the changes in both the design and the cost of the optimal system with respect to variations in the cost assumptions, as well as other scenarios, such as the inclusion of a tax on CO_2 emissions and the economic benefit from a usage of otherwise curtailed excess electricity. By observing the response of the properties of the optimal system to changes in the assumptions, the elements to which the system is most sensitive are identified.

Section 4.2 covers the methodology and deals with the physical and economical modelling based on the weather-driven approach. Section 4.3 compares the various technically optimal system solutions with the economically optimal solution. Section 4.4 explores the sensitivity of the cost-optimal system found in Section 4.3 to variations in the assumed component costs and to the inclusion of other variations, such as electrification of other infrastructures and CO_2 pricing. Section 4.5 concludes the paper with a summary and an outlook.

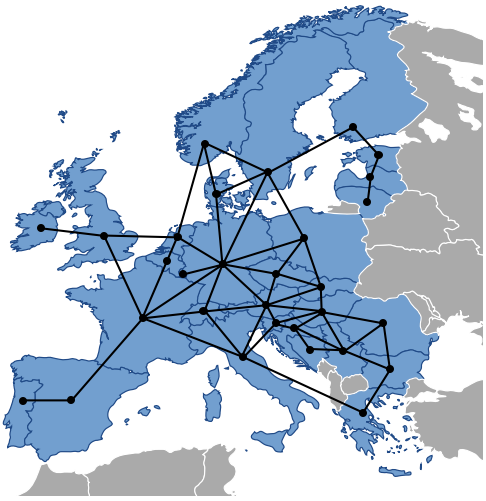

Figure 4.1: Simplified pan-European transmission network. Countries are represented by nodes linked by interconnectors.

4.2 Methodology

Energy system modelling

We model a European electricity system where $N = 30$ countries are networked together; see Figure 4.1. Each country n has a high degree of renewable generation from wind and solar resources:

$$G_n(t) = W_n(t) + S_n(t). \tag{4.1}$$

Other forms of renewable generation are either ignored due to their small magnitude (such as geothermal or run-of-river hydropower) or are considered to be part of the dispatchable backup system (such as hydroelectric storage lakes and biomass). The wind and solar time series have been derived from high-resolution historical weather data and aggregated over each country; see [23] for a more detailed description. The hourly time series are eight years long. The magnitude of these generations is described by the renewable penetration γ_n and the wind fraction α_n of renewable power generation:

$$\begin{aligned} \langle W_n \rangle &= \gamma_n \alpha_n \langle L_n \rangle, \\ \langle S_n \rangle &= \gamma_n (1 - \alpha_n) \langle L_n \rangle, \end{aligned} \tag{4.2}$$

where time-average is denoted by $\langle \cdot \rangle$. For $\gamma_n = 1$, the mean renewable power generation $\langle G_n \rangle$ is equal to the mean load $\langle L_n \rangle$. Due to the variability of wind and solar power generation, the instantaneous mismatch

$$\Delta_n(t) = G_n(t) - L_n(t) \tag{4.3}$$

is almost always non-zero. Load time series $L_n(t)$ are taken from historical data; for more details see again [23].

In order to maintain an exact match between available electric power and demand, each country must produce additional backup electricity from dispatchable sources (B_n), curtail some of the excess generation (C_n), or import/export electricity from/to its neighbours (I_n, E_n). This leads to the nodal energy balance

$$G_n(t) + B_n(t) + I_n(t) = L_n(t) + C_n(t) + E_n(t) \ , \tag{4.4}$$

which is enforced at all times. The net exports

$$E_n - I_n = \sum_{l=1}^{L} K_{n,l} F_l \tag{4.5}$$

describe the injection pattern and relate to the flows F_l along all links. The injection pattern defines how much each node is contributing and withdrawing energy from the grid. The network structure is provided by the incidence matrix

$$K_{n,l} = \begin{cases} 1 & \text{if link } l \text{ starts at node } n, \\ -1 & \text{if link } l \text{ ends at node } n, \\ 0 & \text{otherwise .} \end{cases} \tag{4.6}$$

We assume the transmission between interconnected countries to be unconstrained and lossless. Furthermore, the link impedances are assumed to be constant and not to depend on the link lengths.

Transmission modelling

The nodal energy balance (4.4) describes the interactions within and between the nodes. The renewable power generation $G_n(t)$ and the load $L_n(t)$ are a stimulus to the networked system, while the backup $B_n(t)$, the curtailment $C_n(t)$, the import $I_n(t)$, and the export $E_n(t)$ describe the reaction of the system. The interplay between backup, curtailment, import, and export define the injection pattern (4.5). Different interplays can be defined, which lead to different injection patterns and different transmission flows. In the following we sketch three different transmission paradigms.

I. Zero transmission

No flows between countries are allowed so that $F_l = 0$ for all links l and $I_n = E_n = 0$ for all nodes. This requires all nodes to fully provide their own backup and curtailment.

II. Localised transmission

As in [1], we allow countries to export only their excess renewables,

$$\begin{array}{rcll} 0 \leq E_n & \leq & G_n - L_n & \text{if } G_n \geq L_n, \\ E_n & = & 0 & \text{otherwise} \quad . \end{array} \tag{4.7}$$

This constraint is enforced implicitly by solving the following two-step optimisation problem,

$$\begin{aligned} \text{step 1:} \quad & \min_F \quad \sum_{n=1}^{N} B_n(t) \\ \text{step 2:} \quad & \min_F \quad \sum_{l=1}^{L} F_l^2(t), \end{aligned} \tag{4.8}$$

while subject to (4.4) and (4.5). The first step determines the total imports and exports that minimise backup energy needs in the system, but does not uniquely define the injection pattern. This is done in the second step, which then determines the most localised power flow within the linearised DC power flow approximation [32].

III. Synchronised backup & curtailment

For every hour, we find the total European backup needs by aggregating the mismatch of all nodes:

$$\Delta_{\mathsf{EU}}(t) = \sum_n \Delta_n(t). \tag{4.9}$$

We then force all countries to provide backup power or curtail synchronously the same amount relative to their mean loads, providing power not only for themselves but also to their neighbours, so that

$$B_{\mathsf{n}}(t) = -\min\left\{\Delta_{\mathsf{EU}}(t), 0\right\} \cdot \frac{\langle L_n \rangle}{\langle L_{\mathsf{EU}} \rangle}, \tag{4.10}$$

$$C_{\mathsf{n}}(t) = \max\left\{\Delta_{\mathsf{EU}}(t), 0\right\} \cdot \frac{\langle L_n \rangle}{\langle L_{\mathsf{EU}} \rangle}. \tag{4.11}$$

Subsequently, we solve the problem in (4.8) constrained by (4.4), (4.5) and enforcing (4.10) and (4.11) for all time steps.

Technical objectives

An energy system can be designed according to different principles. One objective is to minimise the overall annual backup energy

$$E^B_{\mathsf{EU}} = N_t \sum_n \langle B_n \rangle \ , \tag{4.12}$$

where $N_t = 8760$ counts the hours per year. The backup energy is a measure for the required usage of conventional fuels. The minimisation of the backup energy is equivalent to the maximisation of the usage of renewables and is related to the minimisation of the overall annual excess energy

$$E^C_{\mathsf{EU}} = N_t \sum_n \langle C_n \rangle \ . \tag{4.13}$$

The backup energy and the excess energy depend on the chosen sets of penetrations γ_n and mixes α_n, and on the selected transmission paradigm.

Another objective is to minimise the overall backup capacities

$$\mathcal{K}^B_{\mathsf{EU}} = \sum_n \mathcal{K}^B_n \ . \tag{4.14}$$

We define the backup capacities $\mathcal{K}^B_n$ of a country as a high quantile

$$q_n = \int_0^{\mathcal{K}^B_n} p_n(B_n) dB_n \tag{4.15}$$

of the time-sampled backup distribution $p_n(B_n)$. We choose $q_n = 0.99$ in order to ignore the effects of extreme events. The backup capacities also depend on the chosen sets of penetrations γ_n and mixes α_n, and on the selected transmission paradigm.

A fourth objective is to minimise the required transmission capacities. Those are derived as in [1] from the flows F_l between the countries. The flow quantile

$$q_l = \int_{-\infty}^{Q_l} p_l(F_l) dF_l \tag{4.16}$$

follows from the time-sampled distribution $p_l(F_l)$ of flows over link l. The resulting transmission capacity

$$\mathcal{K}^T_l = \max\left(-Q_l\left(\frac{1-q_l}{2}\right), Q_l\left(\frac{1+q_l}{2}\right)\right) \tag{4.17}$$

is then the bigger of a low and a high flow quantile, which represent the flows in different directions. Again, we choose $q_l = 0.99$, ensuring unimpeded flow for at least 99% of the time across each link. The overall transmission capacity becomes

$$\mathcal{K}^T_{\mathsf{EU}} = \sum_l \mathcal{K}^T_l d_l \ , \tag{4.18}$$

which sums over all links and takes also the length d_l of the links into account.

Table 4.1: CapEx and OpEx assumptions of different technology assets leading to the present value with an assumed 30-year lifetime and a 4% return rate. Inspired by [13, 21, 69–77].

	CapEx	OpEx	
Asset	Fixed [€/W]	Fixed [€/kW/year]	Variable [€/MWh$_{el}$]
Wind – onshore	1.00	15	0.0
Wind – offshore	2.00	55	0.0
Wind – 50/50 mix	1.50	35	0.0
Solar photovoltaic	1.50	8.5	0.0
CCGT	0.90	4.5	56.0
CCGT with CCS	2.70	13	56.0

Cost modelling

For the electricity systems described in the previous subsections, the system cost can be expressed as the sum of the costs of the different technology assets. In our analysis, we include backup energy, backup capacities, wind and solar power generation capacities, and transmission capacities. A standard economic analysis considers levelised costs of energy (LCOE) based on capital (CapEx) and operational (OpEx) expenditures.

Capital expenditures include investments in fixed assets. These can be seen as acquiring and installing a generating capacity. Operational expenditures are running costs during the lifetime of the system. These are the operation and maintenance costs (O&M) and the fuel costs, if applicable. Table 4.1 lists the CapEx and OpEx values for the different technologies.

Our assumption for solar CapEx are taken from the bottom range in the literature, assuming that increased maturity in the technology and price reductions from learning curves can reduce the cost of cells towards the year 2050 [21]. Combined cycle gas turbines (CCGT) are considered as the only form of conventional backup. We distinguish between CCGT with and without carbon capture and sequestration (CCS). Plants with CCS reduce CO_2 emissions from around 440 kg/MWh to 65 kg/MWh. While these plants have a high installation cost, natural gas fuel costs are not expected to increase in the next 50 years, as supply seems to be relatively certain [75]. Transmission cost calculations have an added complexity. We consider the distance between country capitals as a metric for the amount of upgrades which must take place for the strengthening of the grid between two interconnected countries. AC and DC lines have to be distinguished. For HVAC lines, we assume a price of 400 €/MWkm. For HVDC cables, we assume a cost of 1,500 €/MWkm plus 150,000 €/MW for the converter stations [27, 28, 64]. Placement of HVAC lines and HVDC cables is based on the existing European net-

work reported by ENTSO-E for the year 2011 [36] and new predicted lines until 2014 [37, 38]; see [1] for more details.

The present value of an initial CapEx and OpEx investment during the lifetime T of the technology asset is determined as

$$\mathsf{V} = \mathsf{CapEx} + \sum_{t=1}^{T} \frac{\mathsf{OpEx}_t}{(1+r)^t}. \tag{4.19}$$

The parameter r describes the rate of return. The "greenfield" present value of a highly renewable energy system, for which no previous infrastructure is considered and all assets must be acquired anew, is then

$$\mathsf{V}_{\mathsf{sys}} \;=\; \mathsf{V}_W \;+\; \mathsf{V}_S \;+\; \mathsf{V}_B \;+\; \mathsf{V}_T \;, \tag{4.20}$$

where W is wind generation, S is solar generation, B is dispatchable backup, and T represents the transmission system. The present values for wind, solar, and transmission depend only on the installed capacity and the fixed operational costs. V_B also includes fuel costs of backup sources (see again Table 4.1), which are proportional to the annual backup energy (4.12).

The levelised cost of electricity (LCOE) relates CapEx and OpEx with the present value V of energy costs by discounting the value of future usage of energy production [68]:

$$\mathsf{LCOE} \;=\; \frac{\mathsf{V}_{sys}}{\sum_{t=1}^{T} \frac{L_{\mathsf{EU},}}{(1+r)^t}}. \tag{4.21}$$

The energy in the denominator is, for different sources, often defined as the generated energy. In the case of VRES, when some of the generation comes at a time when it is not needed, one would have to define the denominator as the actual usage of generated energy. In this case, since we look at both conventional backup and VRES, we take generated electric energy simply as the sum of the demand, discarding excess generation.

We use the values in Table 4.1 for our discussions in section 4.3. Due to the uncertainties caused by the large discrepancies of the assumed costs in the literature, a sensitivity analysis follows in Section 4.4, where the dependence of the results on the cost uncertainties will be discussed.

4.3 Technically vs. economically optimal electricity systems

This section first focuses on the dependence of the four technical objectives (4.12 – 4.14) and (4.18) on the penetration parameters $\gamma_n = \gamma$, the mixing parameters $\alpha_n = \alpha$, and the three transmission paradigms. The penetration and mixing parameters are chosen to be the same for

each country. In the second subsection, the γ and α dependence of the economic objective (4.21) is discussed, again for all three transmission paradigms.

Technically optimal systems

The three columns of Figure 4.2 are for different penetrations. We start by looking at the middle column, which is for $\gamma = 1$. The required overall annual backup energy (4.12) shows a strong dependence on the mixing parameter α, with pronounced minima $E^B_{\mathsf{EU}} = 0.24 N_t \langle L_{\mathsf{EU}} \rangle$ at $\alpha = 0.7$ for the zero transmission paradigm and $E^B_{\mathsf{EU}} = 0.15 N_t \langle L_{\mathsf{EU}} \rangle$ at $\alpha = 0.8$ for the other two transmission paradigms. These values have been previously reported in [1]. The backup energy resulting from the localised and the synchronised transmission paradigm are identical. This equivalence not only holds for $\gamma = 1$, but for all other penetrations too. By construction, both paradigms make as much use of the renewable power generation as possible, providing the same amount of backup energy, though from different injection paterns.

The overall annual excess energy (4.13) is shown in the subfigure below. It turns out to be identical to the backup energy, as should be the case when $\gamma = 1$. For different penetrations backup energy and excess energy are related by $E^B_{\mathsf{EU}} = E^C_{\mathsf{EU}} - (\gamma - 1)$.

The required amount of overall backup capacity (4.14) is shown in third place in the middle column. It also reveals a strong dependence on the mixing parameter, resulting in a minimum at $\alpha = 0.9$. There, the minimum value is $\mathcal{K}^B_{\mathsf{EU}} / \langle L_{\mathsf{EU}} \rangle = 1.02$, 0.97 and 0.67 for the zero, localised and synchronised transmission paradigm, respectively. Compared to the 99% quantile of the load, which is $1.40 \langle L_{\mathsf{EU}} \rangle$, this is a significant reduction. The maximum reduction obtained with the synchronised transmission paradigm is easily explained as, by construction, this paradigm forces all the nodes to share their backup capacities. The last subfigure in the middle column illustrates the overall transmission capacities (4.18), which is of course zero for the zero transmission paradigm. As expected, the synchronised paradigm leads to larger transmission capacities than the localised paradigm. In both cases the minimum is around $\alpha \approx 0.4$. The first and third column of Figure 4.2 represent a smaller ($\gamma = 0.5$) and a larger ($\gamma = 1.5$) penetration.

In view of the four technical objectives, the three transmission paradigms can be rated as follows: The zero transmission paradigm leads to the largest backup and excess energy, the largest backup capacities, but no transmission capacities at all. The localised and synchronised transmission paradigms lead to identical smaller amounts of backup and excess energy. The synchronised paradigm causes larger reductions in backup capacity at the expense of requiring a larger transmission capacity than

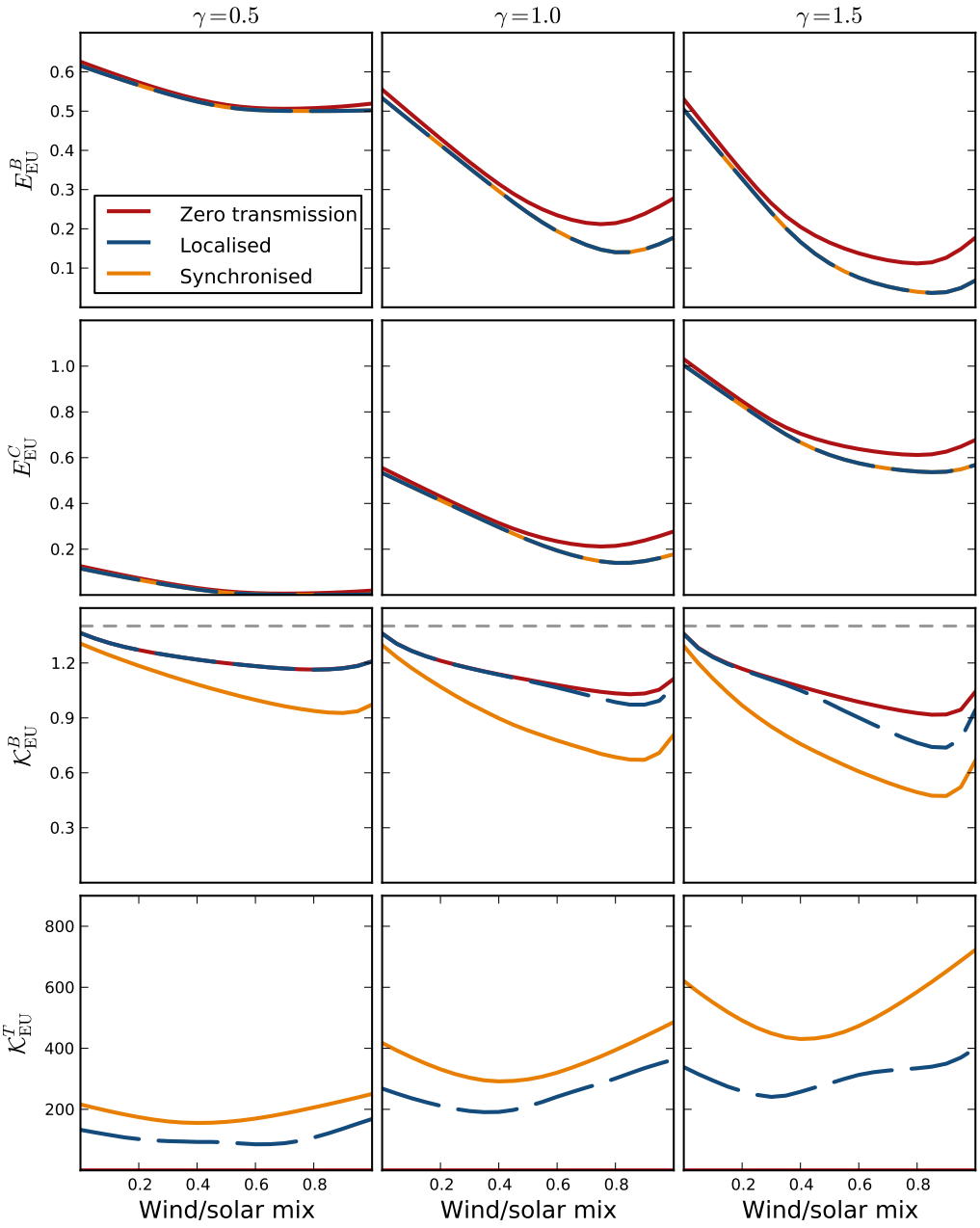

Figure 4.2: Energy deficit E^B_{EU} (4.12), energy excess E^C_{EU} (4.13), backup power capacity K^C_{EU} (4.14), and transmission capacity K^T_{EU}(4.18), as a function of a uniform wind mixing parameter $\alpha_n = \alpha$ for $\gamma_n = \gamma = 0.5$ (first column), 1.0 (central column), and 1.5 (last column). The gray dashed line in the third row shows the 99% quantile of the load. All results are normalised to the average annual European load, except for K^T_{EU}, which is expressed in GW $\times$ 1000 km $\cdot\langle L_{\mathrm{EU}}\rangle$. Three different transmission paradigms *zero transmission* (red), *localised transmission* (dashed blue) and *synchronised operation* (orange) are shown.

the localised paradigm. In the following subsection, the economical objective (4.21) will help discriminate among the transmission paradigms and find out whether the cost reductions from backup energy and power are offset by the increased cost of a larger transmission system.

Cost-optimal systems

As described in Section 4.4, the results from Figure 4.2 can be directly translated into LCOE. In the case of wind and solar capacities, the CapEx costs from Table 4.1 are multiplied with the installed capacity determined by α and γ. As to wind capacities, we assume a total European 50/50 mix between onshore and offshore turbines. Transmission costs are determined by the individual links' CapEx per km, the transmission capacities and the link lengths. The CapEx and the fixed OpEx of backup capacity are determined by each country's backup capacities. The fuel cost reported in Table 4.1 already considers conversion efficiencies, so the energy deficit in MWh can be directly related to variable OpEx.

Figure 4.3 shows a comparison between the zero, the localised and the synchronised transmission paradigms. For low penetrations of γ, the cost difference between the three paradigms is negligible. There is no clear advantage to a large transmission system in terms of reductions of backup energy. As penetrations increase, the cost of transmission becomes noticeable, but is still an order of magnitude smaller than the total system cost. From the middle and bottom panels of Figure 4.3, we observe that a sufficiently large transmission system is worth more than it costs for higher penetrations of renewables, as they reduce the total system cost due to reduced backup capacity and energy.

The effects of a larger VRES penetration on the LCOE is better appreciated in Figure 4.4. This figure shows the γ-dependent minimum cost resulting from a γ-dependent optimal VRES mix α. For values $\gamma \leq 1.3$ the larger transmission costs resulting from the synchronised paradigm are offset by the cost reductions in backup capacities. For penetrations $\gamma > 1.3$, the localised paradigm offers a lower cost, as backup capacity costs become smaller than transmission costs (see third row of Figure 4.3). For all paradigms, the cost-optimal system relies far more on wind than on solar, with $\alpha > 0.8$ for the disconnected system and $\alpha > 0.9$ for the connected one.

Figure 4.4 also shows the optimal system with the minimum overall cost at $\gamma^* = 0.5$ and $\alpha^* = 0.94$, resulting from the synchronised transmission paradigm. An exploration of the space $0 < \alpha < 1$ and $0 < \gamma < 2$ for a system with synchronised operation is illustrated in Figure 4.5a. The optimal value lies in a shallow minimum, in the area defined by $0.8 < \alpha < 1.0$ and $0.3 < \gamma < 0.7$. At the optimal values $\gamma = 0.5$, $\alpha = 0.94$, a wind capacity of 600 GW and a solar capacity of

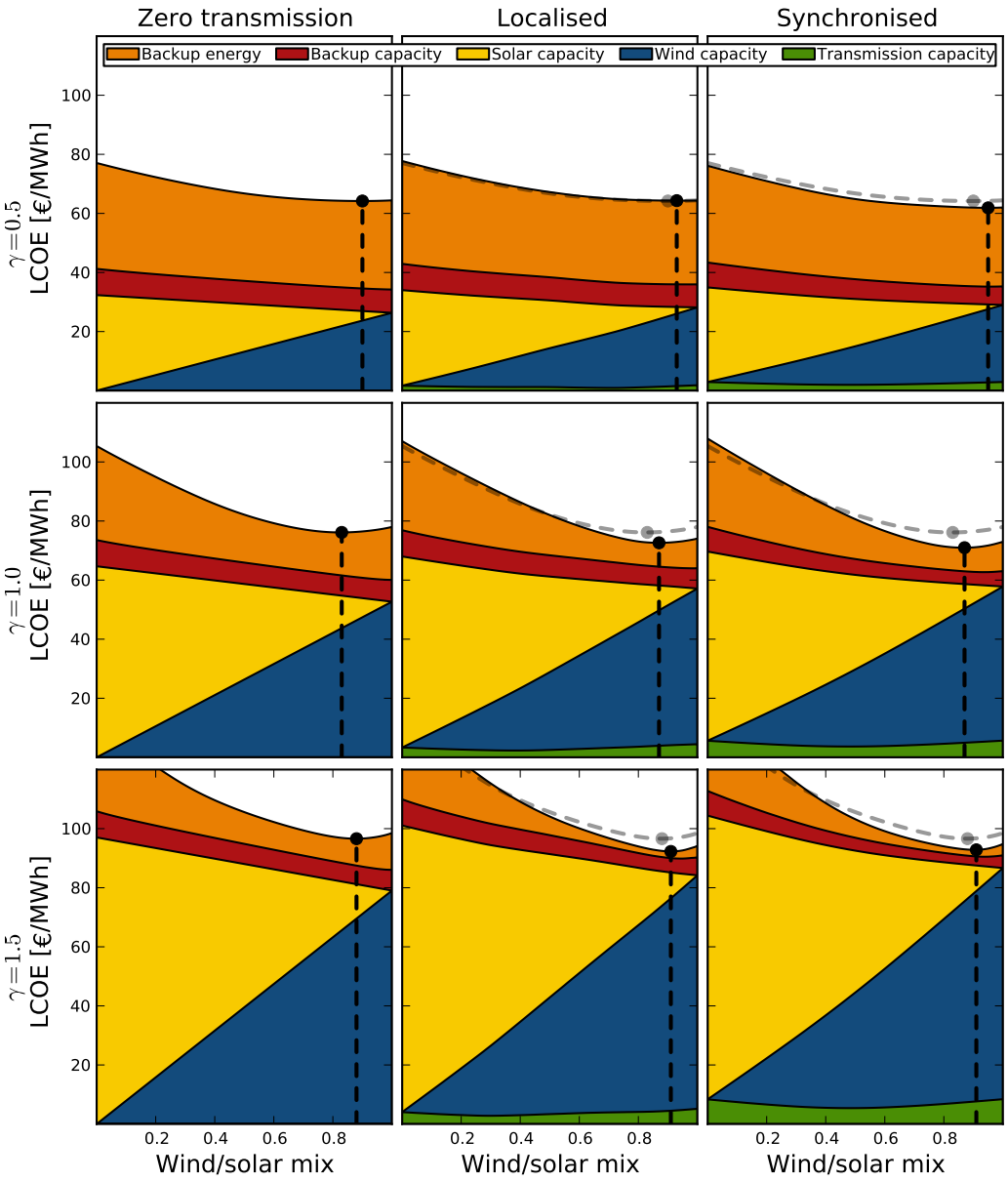

Figure 4.3: LCOE (in €/MWh) for energy delivered by the system as a function of the wind mix ($\alpha_n = \alpha$) for different penetrations of renewables ($\gamma_n = \gamma$): $\gamma = 0.5$ (top row), $\gamma = 1.0$ (middle row), and $\gamma = 1.5$ (bottom row). Contributions from transmission costs are shown in green, wind power in blue, solar power in yellow, backup capacity in red and backup energy in orange. The zero transmission paradigm is shown in the left column, and its LCOE is reproduced as a dashed line in the middle and right columns, which represent the localised and synchronised transmission paradigms. Dots and vertical dashed lines show the cost minimum.

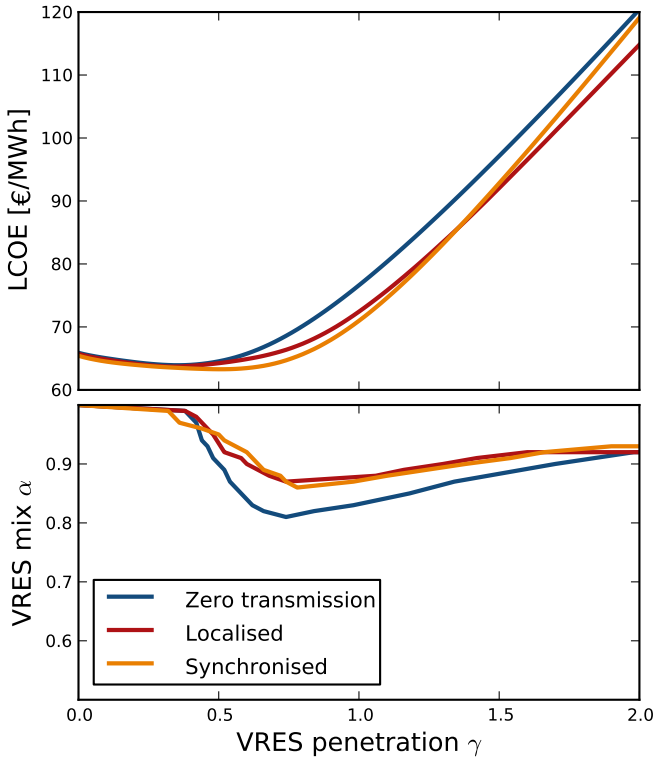

Figure 4.4: Minimal LCOE (top) for different transmission paradigms, and the optimal VRES mixes (bottom) which produce them, at different VRES penetration levels.

60 GW are required. At this level, over 320 GW of conventional backup power capacity are still needed, and the total international transmission capacity adds up to around 210 GW $\times$ 1000 km (roughly five times today's installed capacity). Interestingly enough, a system that is already plausible today, that of around 20% penetration of renewables, has the same total cost as one with a penetration closer to 60%.

4.4 Sensitivity analysis

Variation in cost assumptions

Economic analyses of energy systems are based on cost assumptions for renewable and conventional sources. The effect of the variation of these costs on the results are not often examined. Low- and high-cost scenarios are used instead to avoid this problem [13, 21, 69–78]. However, even when considering the spectrum of high and low costs, there are large variations between the assumptions, and uncertainties of $\pm 25\%$ in CapEx estimates are qualified as "low" [78]. For example, the CapEx estimate for onshore wind used in [13] for the year 2030, 1.14 €/W, falls well below

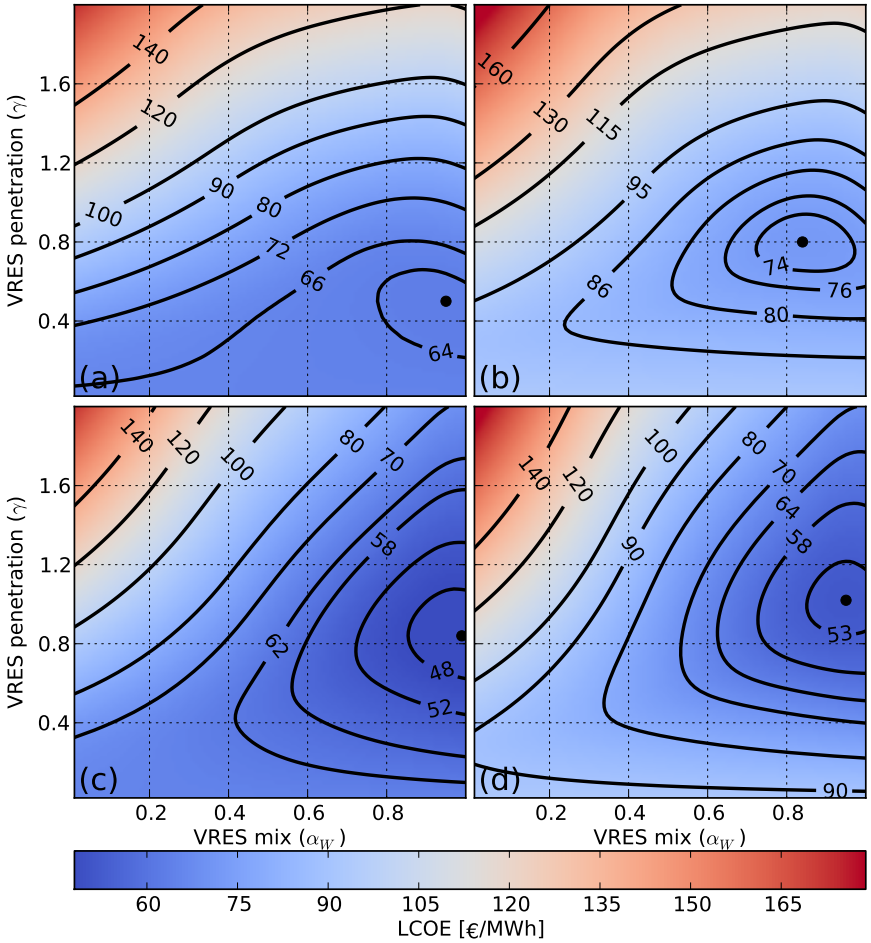

Figure 4.5: LCOE (in €/MWh) for energy delivered by the system as a function of the penetration γ and the wind mix α: (a) based on initial cost assumptions and the synchronised transmission paradigm, (b) based on a 50% cost increase of backup energy, (c) based on a 50% cost decrease of wind energy, and (d) based on a 50% increase in fuel costs and a 50% decrease in the cost of wind energy. Dark dots show the minimum cost.

the CapEx assumptions used in [76]: 1.43 – 2.20 €/W (with current exchange rates). Operational expenditures are similarly not immediately comparable, as the 7,250 €/MW/year for solar photovoltaics suggested in [72] is less than a fifth of the 41,000 €/MW/year used in [73]. These variations in CapEx and OpEx cannot be explained by variations in the quality of the resource, as they are calculated independently of energy production. Comparing LCOEs does not offer a better solution. The levelised cost for onshore wind farms used in [76] of 82 – 120 €/MWh assumes a capacity factor of 29%, whereas the 40 €/MWh reported by [13] uses a capacity factor of 46%.

The cost estimates also depend on the lifetime. Whereas most of the components have a lifetime around 30 years [64, 72], the transmission infrastructure is usually estimated with lifetimes of 40 years and higher [28]. This means that, with the given rate of return, transmission lines still possess around 10% of their value at the end of the 30-year study period. Thus, variations in the assumed lifetimes can also be studied as variations in cost assumptions.

We examine the sensitivity of the cost optimum system by allowing each cost element to vary individually. For each variation of the cost of an element, a new optimal α and γ are calculated, resulting in a new optimal cost. The new system cost is reflected in Figure 4.6. Figure 4.6(a) shows that a doubling or halving of the assumed cost for transmission or backup capacities does not affect the optimum as much as variations of the wind and fuel costs. The driving costs of a future, highly renewable electricity system are the costs of installing wind energy capacity and the fuel costs of providing backup energy. Efforts to reduce the future cost of electricity should mainly be focused on these directions. The non-linear response of the optimal system cost to variations in wind and fuel costs are due to the shifting of the optimal values of α and γ when these costs change, as seen in Figures 4.6(b) and 4.6(c).

The optimal VRES penetration γ is highly dependent on the fuel and wind cost assumptions (Figure 4.6(b)). It is far more sensitive to changes in the cost of wind power than solar power. For sufficiently low fuel costs, the optimal penetration drops to zero, as was to be expected, whereas even if fuel costs are twice as high as assumed, the optimal penetration of renewables increases, but does not reach $\gamma = 1.0$. Changes in the cost of backup capacity do not affect the optimal penetration as much, as the amount required is only marginally reduced by increased penetration of renewables. For the case of transmission capacity, we see a slight increase in the penetration of renewables with a decrease in the cost of transmission, as expected.

Figure 4.6(c) shows the sensitivity of the cost-optimal α to changes in the cost assumptions of different system elements. Increases in the CapEx of solar energy pushes the optimal mix towards more wind, and

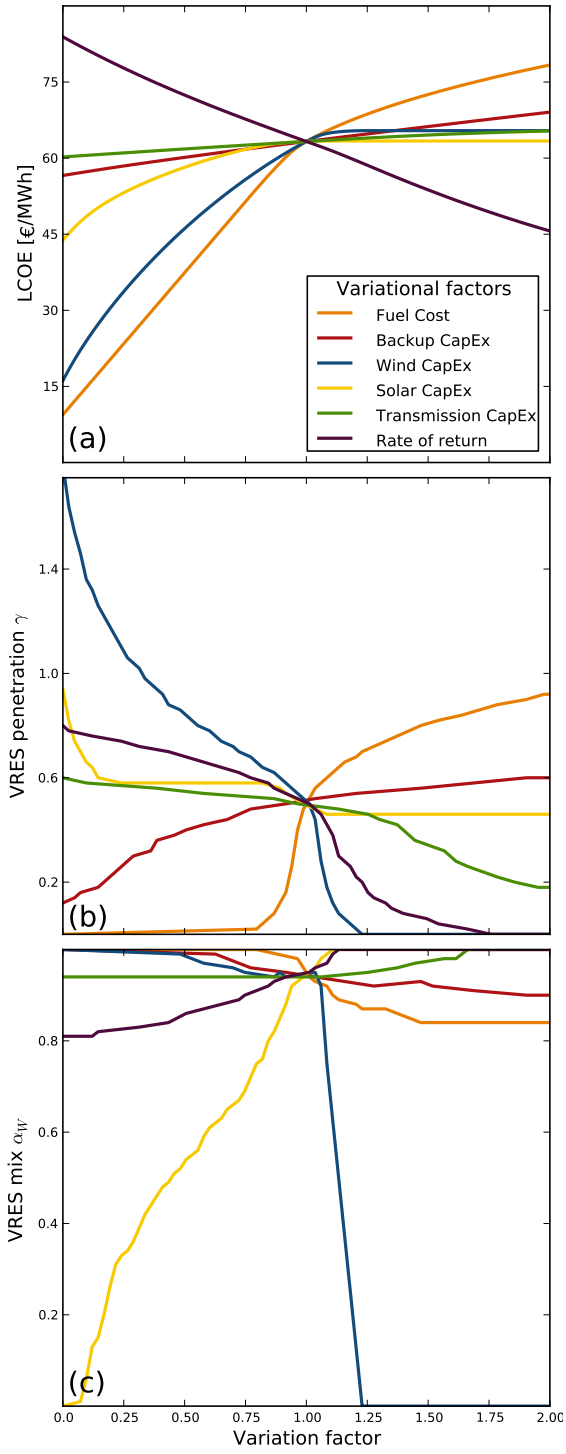

Figure 4.6: Sensitivity with respect to cost changes of different elements for (a) LCOE, (b) cost optimal VRES penetration γ^*, and (c) cost optimal VRES mix α^*. Values reflect the properties of the cost optimal system layout defined by α and γ with the synchronised transmission paradigm.

vice versa. Interestingly, increases in the cost of fuel have a limited effect on the optimal mix, arriving at around $\alpha = 0.82$, which is close to the value obtained from the technical objective (4.12) minimising the energy deficit (see again row 1 of Figure 4.2). Barring changes in the assumed costs of wind and solar power, Figure 4.6(c) shows that the cost-optimal mix α always lies above 80%.

We can quantify the sensitivity of the results from Section 4.3 by combining information from 4.6. For instance, from the top panel we can see that an overestimation of the costs of fuel by 50% (84 €/MWh instead of 56 €/MWh) translates into a 15% increase of the LCOE (73 €/MWh, instead of 63 €/MWh), while an underestimation of the costs of fuel by 50% translates into an underestimation of the LCOE by 30%. The cost-optimal system that delivers this cost is different. As shown in the middle panel, a 50% increase in fuel costs brings the penetration up to 84% from 55%, while a similar reduction brings the penetration down to 0%.

Given that wind power and backup energy costs represent the most important components of the LCOE, it is interesting to see how changes in these would affect the parameters of the optimal system. Figure 4.5(c) shows the LCOE distribution if wind costs have been reduced by 50%. Starting from the already high wind mix of $\alpha = 0.94$ from the base case in Figure 4.5(a), we see a sharp increase in both the penetration and the share of wind in the system. This is accompanied by a reduction in overall costs, as expected from Figure 4.6.

Effects of CO_2 pricing

It is interesting to see the effects of an increase in fuel costs. However, as natural gas prices are not expected to significantly increase in the following years [75], a more likely source for backup energy cost increase is CO_2 pricing.

Figure 4.5(b) shows the LCOE for a spectrum of α and γ under the assumption that fuel costs include a CO_2 tax of 28 €/MWh, equal to a 50% increase in fuel cost. The optimal α and γ shift corresponding to the predictions of Figure 4.6, but system costs in general are higher. A combination of an increase in fuel costs and a decrease in wind costs can be seen in Figure 4.5(d).

For low CO_2 prices, conventional CCGT remains more cost efficient than CCGT with CCS. This will change for high enough CO_2 prices, due to the reduced emissions of CCGT with CCS. Figure 4.7 shows the transition of the cost-optimal system from being based on conventional CCGT to CCGT with CCS. This transition, however, comes at a CO_2 price of 108 €/ton, which is much larger than the 5 to 15 €/ton that CO_2 has seen in Europe since its introduction. Whether this points to

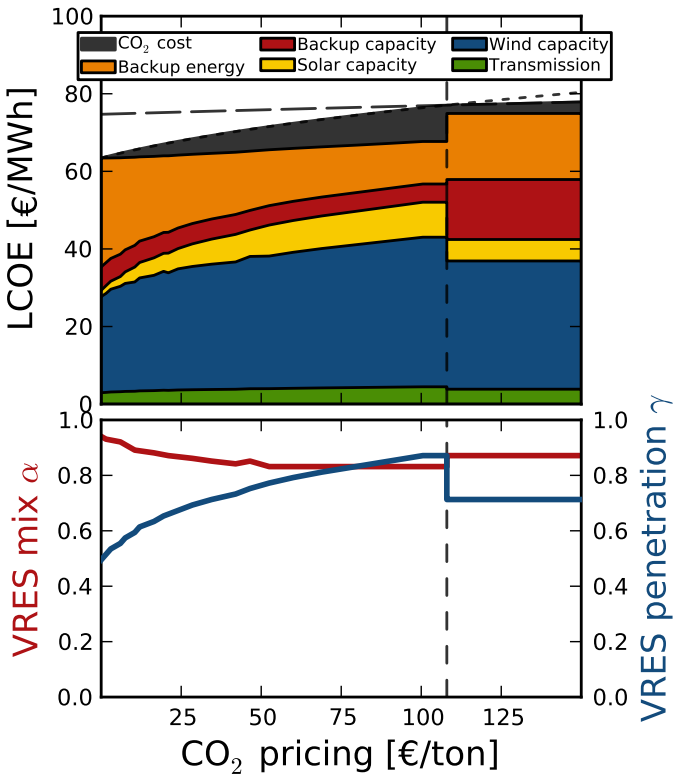

Figure 4.7: LCOE in €/MWh (top), and VRES penetration γ and mix α (bottom) of the cost-optimal system as a function of increasing CO_2 prices.

the economic unfeasibility of CCS or to the need for tighter regulation around CO_2 emissions is an important issue that lies outside the scope of this paper.

Effects of electrification

The current discourse on the future of energy systems often mentions the electrification of the other energy sectors: heating and transportation [82]. These additions to the electricity system are considered as a form of dispatchable load that would preferably use the excess generation produced by renewables. Different technologies of energy storage (from electrical storage in batteries to hydrogen storage for synthetic fuels for transportation) are also considered to increase the usage of renewable energy. Finally, a large electricity grid, such as the intercontinental super grid proposed by [10], could open new markets for electricity exports outside of Europe. Regardless of whether one considers electricity storage, outside markets, or a further electrification of the energy sector, this can be modelled as an extra usage of the excess energy, plotted in the second

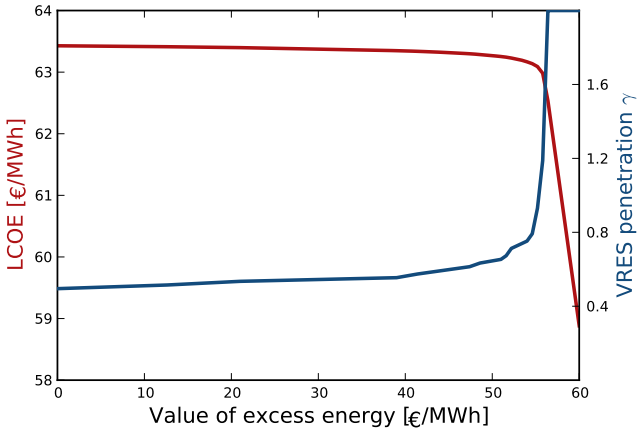

Figure 4.8: LCOE (in €/MWh) and VRES penetration γ of an optimal system where excess energy can be traded for a given value.

row of Figure 4.2.

The response of the LCOE of the cost-optimal system and the optimal VRES penetration γ to increasingly exploited excess energy is shown in Figure 4.8. The scale of these values is comparable to the 112 €/MWh reported for industrial consumers by Eurostat [83]. The low penetrations of the cost-optimal system produce only little excess electricity, so that increases in the value of this excess are not enough to produce a discernible reduction in total system cost. However, as the value of excess energy approaches 54 €/MWh, excess generation becomes profitable, causing the optimal VRES penetration to increase and the LCOE to diminish linearly. The explanation of this non-linearity can be best understood by examining Figure 4.9.

4.5 Conclusion

Summary

We have modelled a simplified pan-European electricity network with a high degree of VRES. The weather-driven approach presented in [23, 24] has been used to model the power generation from wind and solar photovoltaic. The power flow modelling of [1, 6] has been extended to include several different export schemes, like maximum flow localization and flow with synchronised backup. Each of these paradigms perform differently with respect to various technical objectives, like the minimisation of backup and excess energy, of backup capacities and of transmission capacities. Optimal VRES mixes α and penetrations γ have been found, which minimise the amount of backup energy, backup capacity, and transmission capacity.

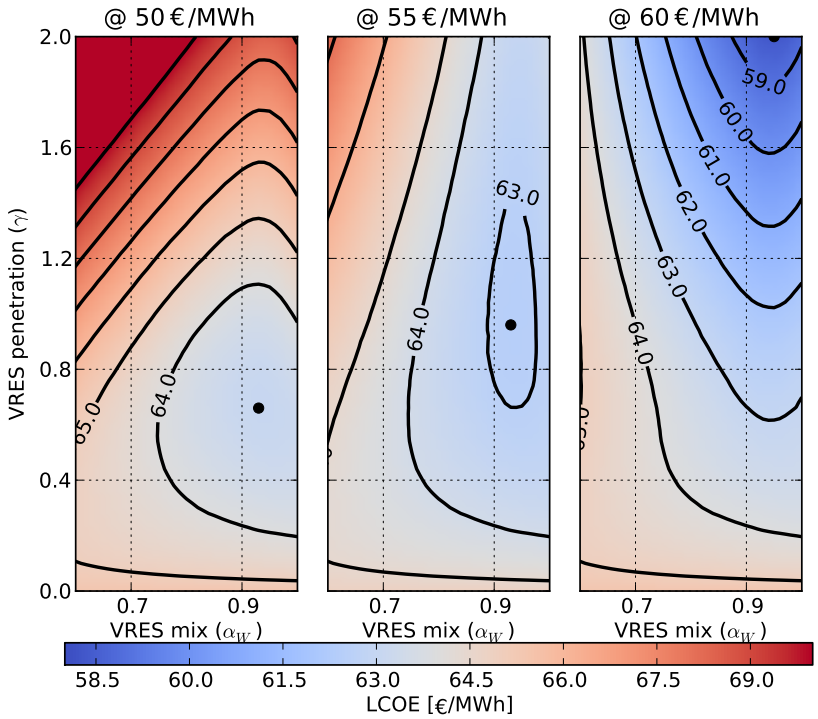

Figure 4.9: LCOE (in €/MWh) for energy delivered by the system as a function of the penetration γ and the wind mix α. From left to right, a higher value for excess energy is considered. Dark dots show the minimum cost.

The levelised cost of energy (LCOE) depends on the installed capacities of wind, solar, transmission, and backup, as well as the cost of the fuel expended in providing backup energy. It is a function of the mix and penetration parameters α and γ, and of the employed transmission paradigm. For values $0.5 < \gamma < 1.5$, a system operating with the synchronised transmission paradigm and a mix around $0.85 < \alpha < 0.9$ results in the lowest LCOE, with the absolute minimum occurring at $\gamma = 0.5, \alpha = 0.94$. A system without any transmission results in higher costs. These results are based on standard cost assumptions for the different components.

The values for the component costs vary in the literature [13, 21, 69–77]. A sensitivity analysis has been performed to quantify the stability of the cost-optimal results. In particular, variations in the assumed costs for wind power capacity and backup energy of the order of 25% can result in more than 25% changes in the cost-optimal parameters α and γ. The resulting LCOE of the optimal system is also most sensitive to the costs of wind power capacity and backup energy, pointing at these two as the defining factor in determining the cost of energy in a future, highly renewable electricity system.

The variation of cost assumptions have also been used to explore other possible changes in the design of the system. The cost of a carbon footprint, expressed through a cost of CO_2 emissions, can be reproduced by including an additional factor on backup energy from conventional sources. This allows for the modelling of different fossil fuel plants, and for a comparison between technologies with and without carbon capture and sequestration (CCS). Our analysis shows the reaction of the cost-optimal mix and penetration with respect to increases in the CO_2 costs, and points at the economic infeasibility of CCGT with CCS at the current emission costs.

Usage of excess energy through either energy storage or the electrification of other energy infrastructures can also be modelled within our approach. We find that until an average value of excess energy of 50 €/MWh the system design does not change much. Only for values larger than 54 €/MWh excess generation of electricity becomes profitable. The optimum VRES penetration then grows accordingly.

Outlook

Throughout this paper, we have assumed a homogeneous spatial distribution of renewables, where all countries have the same mix α and penetration γ of renewables. An organically evolving electricity system will likely deviate from this layout. More productive locations will likely be chosen for wind and solar developments. A heterogeneous spatial distribution could likely result in a lower overall cost.

Regarding dispatchable backup power, only CCGT, with and without CCS, has been considered. The road to $\gamma > 0.5$ will likely have to deal with several competing backup forms, such as coal and nuclear. This poses new challenges, both in the technical modelling, as other sources might have less flexibility to deal with variations, and economical modelling, as pricing mechanisms might favour the use of some technologies above others.

The potential of load shifting should also be explored, in particular when dealing with extreme events. The results presented in this study have been based on 99% quantiles of backup and transmission requirements. A more careful quantification of the extreme events might shed some light on the role of load shedding in a future, highly renewable system.

Finally, an energy system analysis, which also includes the coupling to different energy infrastructures, such as to district heating and to transportation, promises many interesting discussions. Interactions between the systems could be, for example, transforming electricity to heat via heat pumps and to fuel via electrolysers, or using a fleet of electric vehicles as energy storage. Synergies between these different energy in-

frastructures can reduce the cost of the system as a whole, and push towards a higher share of renewables across the energy sector.

Acknowledgements

S.B. gratefully acknowledges financial support from O. and H. Stöcker as well as M. and H. Puschmann. The authors also wish to thank Gorm B. Andresen for many fruitful discussions.

Chapter 5

Heterogeneity

Motivation

The results from Chapter 4 point at wind capacity costs and backup energy as the factors to which the optimal system is most sensitive. Figure 4.3 shows that, almost independently of the wind mix α_n, the capital expenses from VRES capacities make the bulk of the system cost. Thus, reducing the installed capacity while maintaining the same level of effective VRES penetration would be an effective way of reducing the LCOE from a renewable system. Wind and solar resources are not the same across Europe; by exploiting areas with a higher capacity factor for wind (ν_n^W) or solar (ν_n^S), the system-wide capacity factor ν_{EU} for renewables could be significantly increased.

The study so far has assumed homogeneous layouts, where $\gamma_n = \gamma \,\forall\, n$ and, often, $\alpha_n = \alpha \,\forall\, n$. There is no reason for this assumption other than simplicity, as homogeneous layouts would not be prefered in theory or practice. Deciding which way to distribute the capacity adds a layer of complexity, as there are a number of ways to distribute them. In this chapter, we explore an approach based on the financial theory of Optimal Portfolios, which enables the identification of the best mix of a given set of possible investments.

Methods

Optimal portfolio theory

Optimal portfolio theory was initially developed to deal with a problem in finance: Given a set of potential investments with different risks and expected returns, what is the mix of investments, or portfolio, which minimises the risk while maximising the expected returns? In the case of our VRES capacities, the risk of an investment is related to the standard deviation σ of the resulting mismatch, while the return is the capacity factor of the VRES generation ν.

We can separate a node into two investments, wind and solar. The mix and penetration of these, defined by γ_n and α_n, results in a nodal risk σ_n and a nodal return ν_n. The risk and return of given European layout, or portfolio, is then

$$\sigma_{\mathsf{EU}} = \sqrt{\langle \Delta_{\mathsf{EU}}^2 \rangle - \langle \Delta_{\mathsf{EU}} \rangle^2} \tag{60}$$

and

$$\nu_{\mathsf{EU}} = \sum_n \nu_n^W \frac{\gamma_n^W \langle L_n \rangle}{\langle L_{\mathsf{EU}} \rangle} + \sum_n \nu_n^S \frac{\gamma_n^S \langle L_n \rangle}{\langle L_{\mathsf{EU}} \rangle} \,, \tag{61}$$

where γ_n^S and γ_n^W are the solar- and wind-specific penetrations (see section 5.2 for more details).

A clear option for a layout would be a ν-proportional layout, that is, allocating more wind power to locations that have a high ν_n^W and high solar power to places with high ν_n^S. This option, however, does not account for possible correlations in the weather patterns over Europe, leading to little or no reduction in risk (standard deviation σ_{EU}).

Genetic algorithm

Another way of finding optimal portfolios is by having a genetic algorithm produce a set of low-risk, high-return layouts. Genetic algorithms are an obvious choice for multivariable, multiobjective optimisation problems. They can be seen as a sort of iterative directed Monte Carlo method, related to the natural process of evolution, in the sense that attractive traits are more likely to be repeated in the next iteration.

Starting from a population of many random layouts defined by a set of $\boldsymbol{\gamma}, \boldsymbol{\alpha}$ with entries γ_n, α_n, we select the layouts that result in the lowest system cost. The selected layouts $\boldsymbol{\gamma}$ and $\boldsymbol{\alpha}$ are then the basis for the random generation of a new population of layouts. After several generations of layouts, the lowest cost achieved become smaller and smaller, as successful traits become more abundant and inefficient layouts are discarded (see Figure 5.5).

A genetic algorithm has no guarantee for optimality, since it has no 'sense' of the analytical nature of the optimising function. Instead, we are promised a large set of suboptimal solutions. For more details on the implemented algorithm, see section 5.4.

Main findings

The portfolio analysis of the homogeneous layout shows that even randomly distributed layouts can have a lower risk and a greater return (see Figure 5.2). The ν-proportional layouts, with increasing factors on the weights of the wind and solar capacities ν_n^W, ν_n^S, provide greater capacity factors, but not much reduction in the risk, as expected from the fact that no consideration is given to potential correlations in the weather patterns at the selected locations.

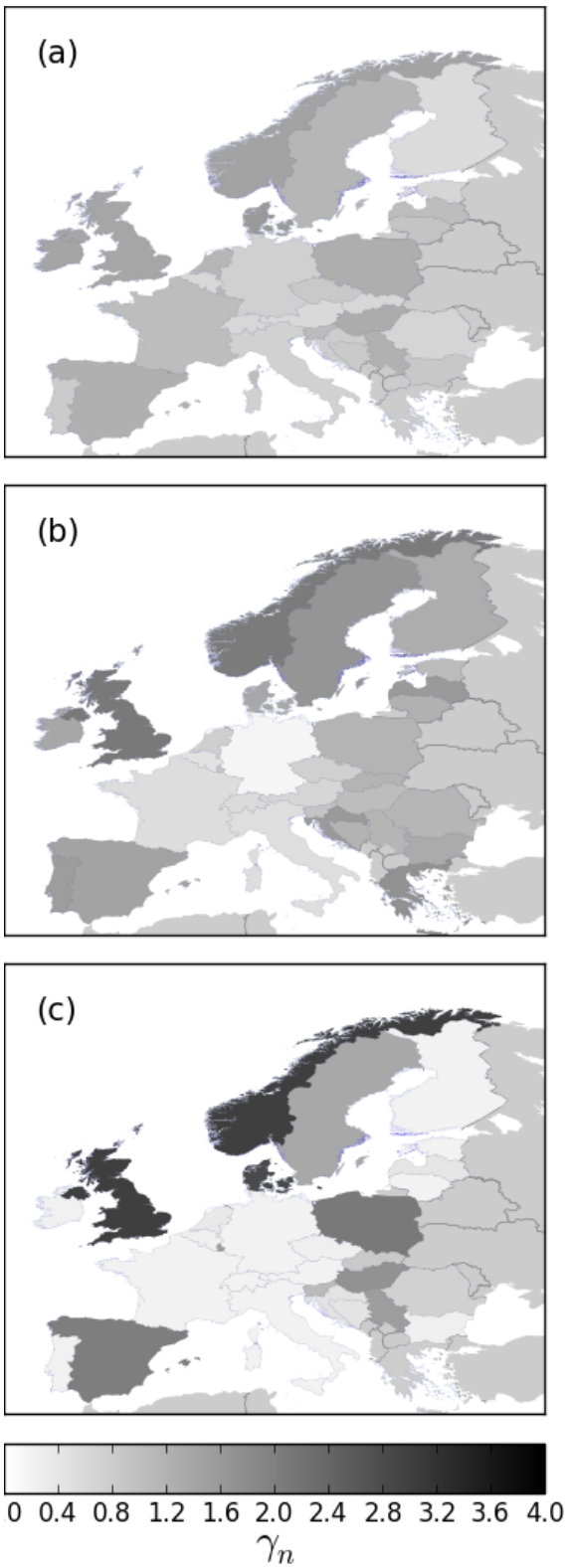

Figure 9: Distribution of VRES capacities around Europe for the (a) ν-proportional layout, (b) Pareto-optimal layout, and (c) cost-optimal layout resulting from the genetic algorithm.

Figure 5.2 also shows a Pareto front – a line at which no gain in return can happen without an increase in risk. By connecting points along this Pareto line for wind- and solar-only layouts we can find a Pareto-optimal layout (see Figure 5.3), offering a reduction in the risk of the portfolio.

Comparing the costs resulting from these layouts, using the initial assumptions from [4], we find that the ν-proportional layouts are best at minimising costs. This is presumably due to the increased heterogeneity in the Pareto-optimal layout, which can be seen in Figure 9. The variance in the distributions of capacities that this layout proposes is such that much larger transmission lines would be needed, without a clear reduction in the backup or VRES capacities (see Figure 5.1).

A genetic algorithm engineered specifically for reducing the cost of the system offers much better results. By maximising the efficiency of the capacities it places, it achieves a much higher system-wide capacity factor – above $\nu_{\mathsf{EU}} = 0.32$. This reduces the installed capacity of renewables, so that even the much larger transmission capacity it requires (see, again, Figure 5.1) is not enough to make it more expensive.

Optimal heterogeneity of a highly renewable pan-European electricity system

Rolando A. Rodriguez[a], Benjamin Sairanen[b], Martin Greiner[a,c]

a Department of Mathematics, Aarhus University, Denmark

b Department of Physics and Astronomy, Aarhus University, Denmark

c Department of Engineering, Aarhus University, Denmark

Abstract

A large weather database allows the estimation of the capacity factor and standard deviation of wind and solar resources throughout Europe. A homogeneous distribution of wind and solar capacities makes inefficient use of the resources, resulting in the need of large amounts of backup power and energy, as well as high system costs. A distribution of resources that is weighed by the regional capacity factors achieves much smaller needs for backup and a lower cost of electricity. Optimal Portfolio Theory is used to explore the space of heterogeneous distributions of renewable capacities. The standard deviation and capacity factor resulting from these distributions are analogous to the risk and return of an investment. The Pareto front defined by a set of randomly assigned capacities is used to define a Pareto-optimal distribution, but the large heterogeneity implies a much higher costs of transmission. A genetic algorithm is then used to find the heterogeneous distribution of capacities that results in the lowest cost of electricity.

keywords: renewable energy systems, portfolio theory, genetic algorithm, wind power generation,

5.1 Introduction

Of new power capacities installed in Europe over the past two years, over 20% consisted of new wind turbines and more than 50% came from solar panels [11]. As penetration from these variable renewable energy sources (VRES) increases, the problems related to the variability and availability of electricity become more apparent. The average capacity factor of renewable resources in European countries, which is determined exclusively by the weather patterns in the country, becomes of vital importance. See Table 5.1 for a summary of these values.

Analyses on the weather patterns over Europe have shown that there is an optimal mix between wind and solar power which minimises the need for backup from conventional sources [23, 24]. However, these analyses assume a homogeneous distribution of renewables throughout all countries.

In this paper, we explore very heterogeneous distributions of VRES capacities in a fully renewable Europe. Optimal Portfolio Theory (OPT), typically used to manage the risk and return of financial investments, is used to optimise VRES standard deviation and capacity factors. A genetic algorithm, together with some cost assumptions, is then used to discover even more heterogeneous mixes in an attempt to minimise the total system cost. Two previous papers [84, 85] have applied Optimal Portfolio Theory to renewable energy generation, though only to the case of wind energy. They have found that there is a significant decrease in the overall risk, or standard deviation, when increasing the aggregated region, suggesting that there are benefits in establishing a transmission network, as also shown by [1].

An out-of-the-box genetic algorithm was used in [18] in a renewable electricity system with wind turbines, solar photovoltaics, and conventional sources. Their objective was to minimise the total cost of this fully renewable system for the Australian National Electricity Market (NEM) in 2030. They found that the least cost scenario was that with a penetration of around 60% renewables, consisting of around 70% wind energy.

The paper is organised as follows: Section 2 discusses the general modelling of the electric system and presents the key metrics that will be evaluated. A homogeneous and a heterogeneous reference layout are defined and evaluated. Section 3 presents OPT and derives a new optimal layout based on an evaluation of the risk and return offered by mixes of wind- and solar-only layouts. A simple cost modelling is also introduced. Section 4 presents a genetic algorithm that finds cost-optimal layouts for Europe. Finally, the Conclusion summarises the results and presents an outlook for heterogeneous distributions of VRES capacities.

Table 5.1: Capacity factors for wind ν_n^W and solar photovoltaics ν_n^S for European countries

	ν_n^w	ν_n^s		ν_n^w	ν_n^s		ν_n^w	ν_n^s
Germany	0.19	0.15	Finland	0.14	0.13	Serbia	0.33	0.19
France	0.27	0.20	Czech Republic	0.22	0.16	Ireland	0.41	0.13
Great Britain	0.40	0.15	Austria	0.14	0.17	Bosnia & Herz.	0.20	0.21
Italy	0.16	0.23	Greece	0.18	0.24	Slovakia	0.15	0.17
Spain	0.32	0.25	Romania	0.15	0.20	Croatia	0.19	0.20
Sweden	0.32	0.14	Bulgaria	0.21	0.22	Lithuania	0.25	0.14
Poland	0.36	0.15	Portugal	0.19	0.23	Estonia	0.17	0.13
Norway	0.42	0.13	Switzerland	0.15	0.17	Slovenia	0.28	0.18
Netherlands	0.32	0.15	Hungary	0.36	0.18	Latvia	0.29	0.13
Belgium	0.15	0.14	Denmark	0.46	0.15	Luxembourg	0.30	0.14

5.2 Modelling

We are concerned with European layouts of renewables, represented by a 30-node interconnected network. Wind and solar energy generation in a country are determined by high resolution weather data and physical models, as in [23]. Every country is assumed to have generation from wind, solar, or a combination of both determined by the mixing factor $0 \leq \alpha_n \leq 1$:

$$G_n(t) = \gamma_n(\alpha_n W_n(t) + (1-\alpha_n)S_n(t))\langle L_n \rangle \ . \tag{5.1}$$

Both wind and solar time series are normalised to their mean value, so that $\langle W \rangle = \langle S \rangle = 1$. The magnitude of the generation is described by the renewable penetration γ_n while the shape is determined by the wind fraction α_n and the country's weather pattern. The instantaneous mismatch – the difference between generation and demand – is then

$$\Delta_n(t) = G_n(t) - L_n(t) \ . \tag{5.2}$$

Balance between generation and demand must be maintained at all times, so countries must either curtail generation ($C_n(t)$) or provide backup power ($B_n(t)$) for the times when $\Delta_n < 0$,

$$C_n(t) = \begin{cases} |\Delta_n(t)| & \text{if } \Delta_n(t) \geq 0, \\ 0 & \text{otherwise} \end{cases} \ , \tag{5.3}$$

$$B_n(t) = \begin{cases} |\Delta_n(t)| & \text{if } \Delta_n(t) \leq 0, \\ 0 & \text{otherwise} \end{cases} \ . \tag{5.4}$$

In backup power, we include all forms of conventional power plants, as well as dispatchable renewables, such as biomass and hydropower lakes. Alternatively, countries can use the transmission network to trade excesses generation with their neighbours, importing ($I_n(t)$) or exporting ($E_n(t)$) as needed. This leads to the node balance equation

$$G_n(t) - L_n(t) = C_n(t) - B_n(t) + E_n(t) - I_n(t) \ . \tag{5.5}$$

Many exports schemes can be devised to regulate which countries use backup and which countries trade. For simplicity, we assume that all countries use backup and curtailment synchronously,

$$C_n(t) - B_n(t) = \frac{\langle L_n \rangle}{\langle L_{\mathsf{EU}} \rangle} \cdot \left(\sum_n \Delta_n(t) \right) \ , \tag{5.6}$$

so that all countries provide the same amount of backup relative to their mean loads. Each country's initial mismatch $\Delta_n(t)$ combined with this global backup and curtailment define an injection pattern into the network. The actual flow pattern which defines $I_n(t)$ and $E_n(t)$ is determined by a calculation of the physical Kirchhoff flows resulting from this injection pattern. From the flow time series along the link connecting two countries $F_{n,m}(t)$, we can determine the capacity required by the interconnector between these two countries.

Key metrics

We can now define the quantities which can help us establish the performance of a given layout defined by the vectors $\boldsymbol{\gamma}$ and $\boldsymbol{\alpha}$ with entries γ_n and α_n. We want to minimise the amount of energy from dispatchable backup E^B, defined by

$$E^B = \frac{\sum_n \sum_t B_n(t)}{\sum_n \sum_t L_n(t)} = \frac{\sum_n \langle B_n \rangle}{\sum_n \langle L_n \rangle} \ . \tag{5.7}$$

This expresses yearly backup energy as a percentage of the total yearly demand. We also wish to minimise the presence of extreme values, which point towards an inefficient layout of renewables and high backup powers. The standard deviation σ_Δ shows both of these,

$$\sigma_\Delta = \sqrt{\langle \Delta_{\mathsf{EU}}^2 \rangle - \langle \Delta_{\mathsf{EU}} \rangle^2} \ . \tag{5.8}$$

Finally, we are interested in determining the total power capacity required from backup $\mathcal{K}^B$ across all nodes and transmission $\mathcal{K}^T$ across all links. In order to avoid anomalies stemming from extreme values, we take the 99% quantile of both amounts, so that we end up with capacities large enough to cover their needs 99% of the time:

$$q_n = \int_0^{\mathcal{K}_n^B} p_n(B_n) \, \mathrm{d}B_n \ , \tag{5.9}$$

where $q_n = 0.99$ and $p_n(B_n)$ is the time-sampled distribution of backup power. In the case of transmission, we take the larger of the 0.1% and the 99.5% quantile, to ensure at least 99% security:

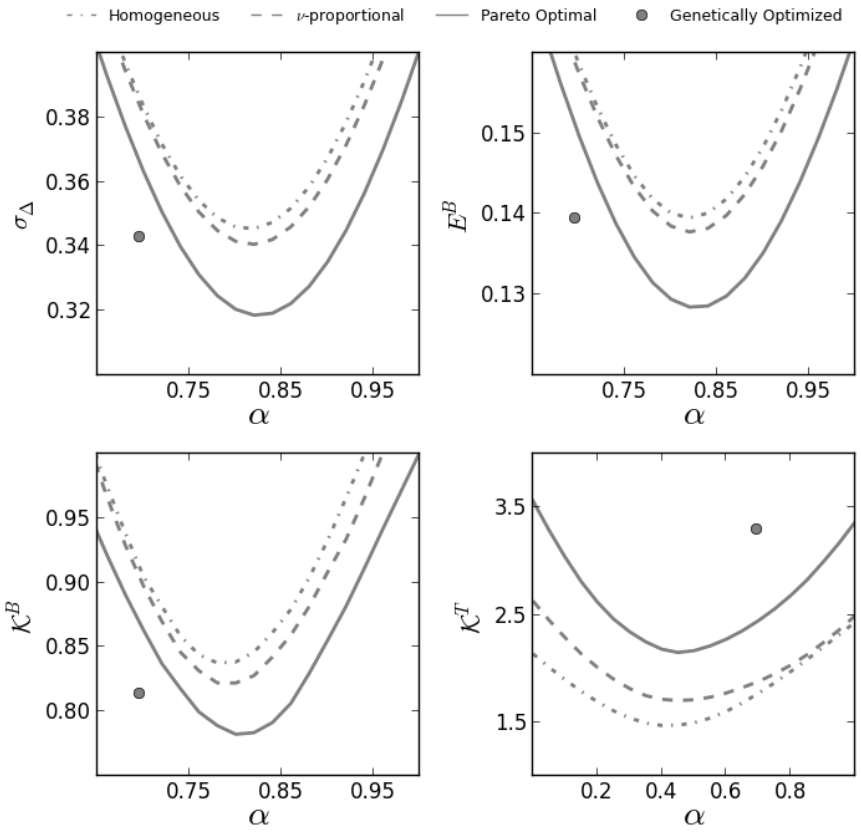

Figure 5.1: Standard deviation of the mismatch σ_Δ, total backup energy E^B, backup capacity $\mathcal{K}^B$, and transmission capacity $\mathcal{K}^T$ as a function of the mixing parameter α. Results are shown for the homogeneous, ν-proportional, and Pareto-optimal scenarios, as well as a genetically optimised layout.

$$\mathcal{K}^T = \sum_l^L \mathcal{K}_l^T \,, \tag{5.10}$$

with

$$\mathcal{K}_l^T = \max\left\{-Q_{0.5\%}, Q_{99.5\%}\right\} \,, \tag{5.11}$$

where

$$x = \int_{-\infty}^{Q_x} p_n(F_l)\,\mathrm{d}F_l \,. \tag{5.12}$$

Reference layouts

As a reference, we define a **homogeneous layout**, where $\gamma_n = 1$ for all countries, and α_n varies homogeneously. This immediately leads to the

following constraint, which is kept for the duration of this paper:

$$\sum_n \gamma_n \langle L_n \rangle = \langle L_{\mathsf{EU}} \rangle \,. \tag{5.13}$$

A smarter layout would favour the placing of wind turbines and solar panels in places where these resources were more abundant. Table 5.1 shows the capacity factors for wind ν_n^W and solar photovoltaics ν_n^S for the European countries in the analysis. A **ν–proportional layout** can be constructed by combining a wind-specific and a solar-specific layout via the mixing parameter α, so that

$$\gamma_n = \alpha \gamma_n^W + (1-\alpha)\gamma_n^S \,. \tag{5.14}$$

Here, γ_n^W and γ_n^S are determined by the country's capacity factor of the relevant resource with a weighting factor β,

$$\gamma_n^W = (\nu_n^W)^\beta \frac{\langle L_{\mathsf{EU}} \rangle}{\sum_n (\nu_n^W)^\beta \langle L_n \rangle} \tag{5.15}$$

and

$$\gamma_n^S = (\nu_n^S)^\beta \frac{\langle L_{\mathsf{EU}} \rangle}{\sum_n (\nu_n^S)^\beta \langle L_n \rangle} \,. \tag{5.16}$$

The higher the factor β, the more importance is given to the capacity factor. When $\beta = 0$, the proportional layout is equal to the homogeneous layout. The fractional terms are to ensure that the global constraint in (5.13) are maintained, whatever the value of α in (5.14) might be. Figure 5.1 shows the key metrics introduced above for both the homogeneous and the proportional layout, for a $0 \leq \alpha \leq 1$.

The proportional layout performs only slightly better than the homogeneous layout. The only significant difference comes in the transmission capacity $\mathcal{K}^T$ required. While very similar for $\alpha \leq 0.4$, the layouts diverge above that value, with the proportional layout causing less flows than the homogeneous one. While this might seem counterintuitive at first, a glance at the capacity factors (Table 5.1) helps explain the phenomenon. Solar capacity factors are more similar to each other across Europe, with rich and poor areas separated by a factor of 2, while wind capacity factors are much more heterogeneous. By placing wind turbines in the more abundant places, we ensure a better presence of renewables at the times when it is needed. The reduced need for sharing of balancing causes a higher reduction in flows that the heterogeneity causes.

5.3 Optimal portfolio theory

In building a layout where locations with high capacity factors were preferred to locations with low ones, one could have expected a larger reduction in the need for backup energy and power $(E^B, \mathcal{K}^B)$. However,

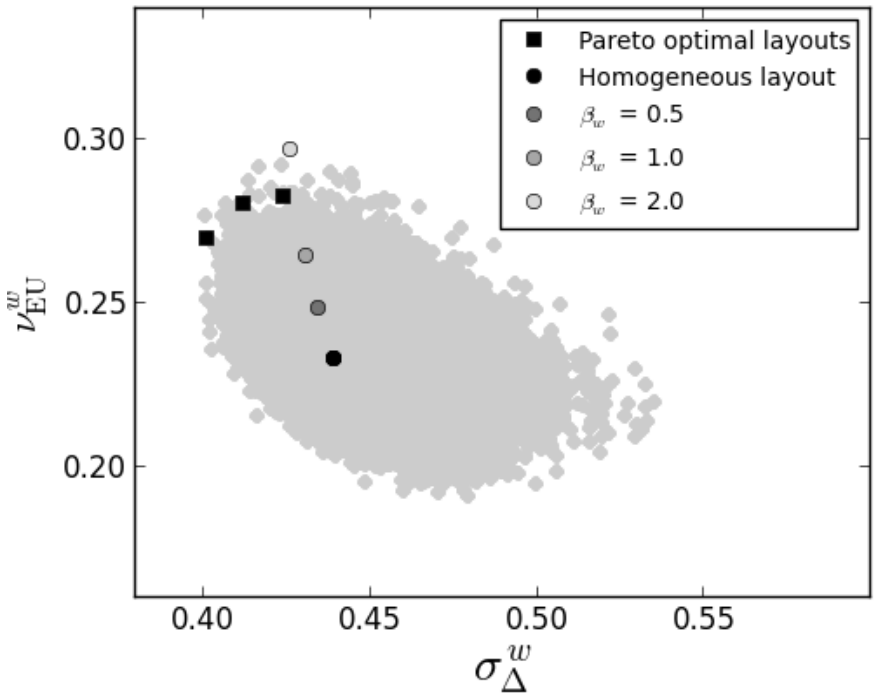

Figure 5.2: Scatter plot of risk (σ^W_Δ) against return ($\nu^W_E U$) for the wind-only case $\alpha = 1$. Random layouts or portfolios are shown in light gray dots. The homogeneous and ν–proportional scenarios are shown, as well as three example layouts along the pareto front.

correlations between resources can either contribute or detract to the overall performance of a layout. A single place can have a high capacity factor, but carry a large risk in the form of standard deviation. This is a well known problem in finance, where a portfolio of investments must be chosen so as to maximise the returns while minimising risk. In this case, returns can be seen as a layout-wide capacity factor, ν_{EU}

$$\nu_{\mathsf{EU}} = \sum_n \nu_n^W \frac{\gamma_n^W \langle L_n \rangle}{\langle L_{\mathsf{EU}} \rangle} + \sum_n \nu_n^S \frac{\gamma_n^S \langle L_n \rangle}{\langle L_{\mathsf{EU}} \rangle} \tag{5.17}$$

while the risk can be related to the layout-wide standard deviation, as defined in (5.8). A geographical dispersion of VRES capacities can help reduce the total standard deviation, as wind is generally uncorrelated beyond 500 km. Figure 5.2 is a representation of the portfolio of wind capacities in Europe. Each of the gray dots represents a randomly assigned set of wind capacities $\boldsymbol{\gamma}^W$. The homogeneous layout can be seen near the centre of the cloud, with a low risk but a low return (capacity factor). As the layout begins to favour locations with a higher ν_n^W via the factor β, the return of the system increases, without a large decrease in the risk of the investment. Portfolio theory allows us to define a Pareto

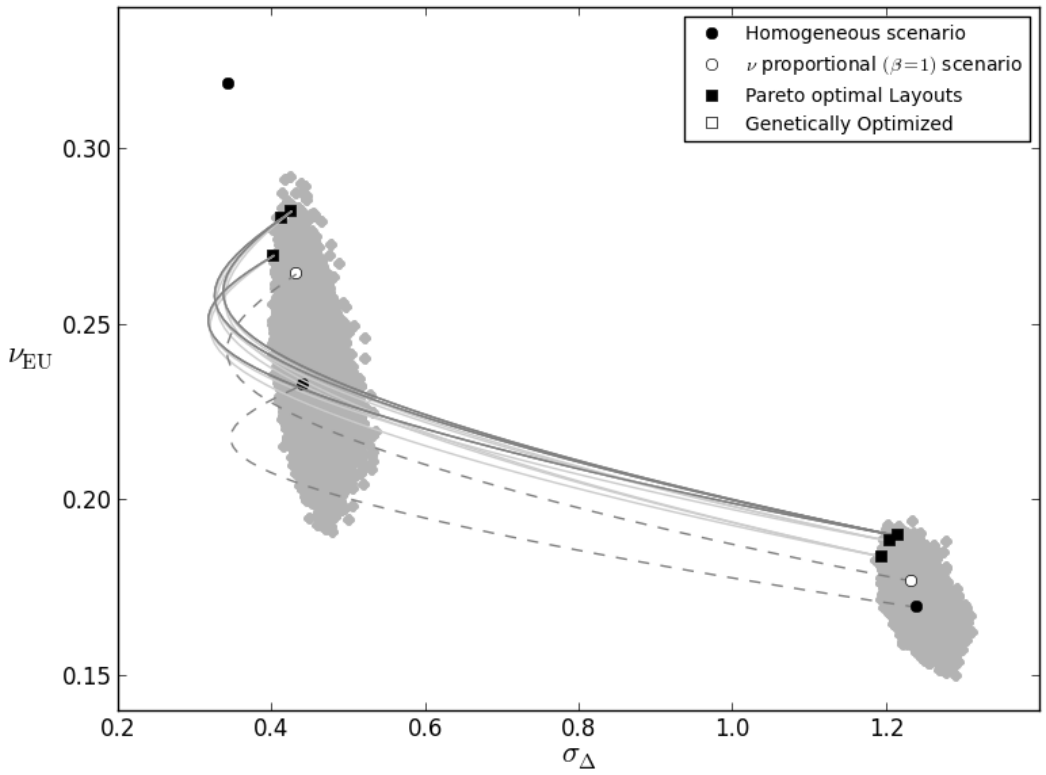

Figure 5.3: Scatter plot of risk (σ_Δ) against return ($\nu_E U$) showing both the wind- and solar-only clouds. Random layouts or portfolios are shown in light gray dots. The reference scenarios for each cloud are connected by lines, showing the path that the combination of the two end-point layouts take as the mixing parameter α goes from 0 to 1. A genetically optimised layout is also shown.

front of optimal portfolios, where we must choose between a lower risk and a higher return. This front is sketched via the squares in Figure 5.2.

A similar set of Pareto-optimal layouts can be found for the solar resources. The optimal wind capacities $\boldsymbol{\gamma}^W$ coming from Figure 5.2 can be combined with the optimal solar capacities $\boldsymbol{\gamma}^S$ via the mixing parameter α. Figure 5.3 shows these interpolations, redrawing the homogeneous and proportional layouts we have previously discussed and adding several interpolations of new layouts coming from portfolio theory. We choose one of these interpolations as a **Pareto-optimal layout**. The lines connecting these points run from $\alpha = 0$ in the solar-only portfolio (bottom right) to $\alpha = 1$ in the wind-only portfolio (top right). It is clear that moving from a pure-solar to pure-wind only increases the capacity factor, but there seems to be a minimum risk point close to $\alpha = 1$. This hints at a synergy between wind and solar resources, reinforcing the results in Figure 5.1 of an optimal value of α.

Economic optimisation

Figure 5.1 also shows the performance of the portfolio layout in our key metrics, performing slightly better than our two reference layouts in terms of σ_Δ, E^B, $\mathcal{K}^B$, though requiring a much higher transmission capacity. In the case of the portfolio layouts, the increase heterogeneity of the system is large enough to cause much larger flows. As can be seen in Figure 5.6(c), some of the countries under this layout have virtually no installed capacity, and so must rely on imports from their neighbours. This implies a high transmission capacity $\mathcal{K}^T$. It is only by weighing the costs that we can determine wether or not the added transmission capacity is worth the reduction in backup energy and capacity.

Cost assumptions for the elements of a renewable system vary greatly across the literature [4]. For this study, we assume costs on the low end for wind and solar, as it is expected that these costs will decrease as we move towards a higher penetration of VRES [21]. Table 5.2 summarises the costs.

Table 5.2: Initial assumptions for the present values for different assets, assuming a 30-year lifetime and a return rate of 4%. From [4]

	CapEx	OpEx	
Asset	Fixed [€/W]	Fixed [€/kW/year]	Variable [€/MWh$_{el}$]
CCGT	0.90	4	56.0
CCGT with CCS	2.70	13	56.0
Wind – onshore	1.00	15	0.0
Wind – offshore	2.00	55	0.0
Wind – 50/50 mix	1.50	35	0.0
Solar photovoltaic	1.50	8	0.0

Translating $\mathcal{K}^B$ and E^B into costs is straightforward, as the capacities found correspond directly to those required. From each country's VRES penetration (defined by γ_n, α, n) and capacity factors ν_n^W, ν_n^S, we can derive the cost for wind and solar capacities. Transmission is slightly more complicated, as one must distinguish between AC and DC lines, and the cost of lines is a function of the length. For AC lines, we assume a cost of 400 €/MWkm, with a higher cost of 1,500 €/MWkm for HVDC. Direct current cables also require converter substations, estimated at 150,000 €/MW [27, 28, 64]. The layout of AC and DC lines was determined according to the existing European network reported by ENTSO-E for the year 2011 [36] and new predicted lines until 2014 [37, 38].

A common expression for the cost of electricity is the levelised cost of electricity (LCOE), which is the cost that every unit of energy produced during the lifetime of the project must have to match the present value

of the investment [68]:

$$\mathsf{LCOE} \;=\; \frac{\mathsf{V}_{sys}}{\sum_{t=1}^{T} \frac{L_{\mathsf{EU},t}}{(1+r)^t}}\,, \tag{5.18}$$

where

$$\mathsf{V}_{\mathsf{sys}} = \mathsf{CapEx} + \sum_{t=1}^{T} \frac{\mathsf{OpEx}_t}{(1+r)^t}. \tag{5.19}$$

See [4] for more details.

Figure 5.4 shows the resulting costs at different mixes for the homogeneous, the proportional, and the Pareto-optimal layouts. The lines are equivalent to those in Figure 5.3, but mapped to the cost instead of the standard deviation σ_{EU}. We find that the homogeneous layout performs the worst. The lower transmission capacity $\mathcal{K}^T$ required by this layout (see Figure 5.1, bottom right) does not make up for the added cost from wind and solar capacities due to inefficiently placed wind turbines and solar panels. The lowest cost of our three layouts is achieved by the ν-proportional layout. It combines the smarter distribution of capacities (which lower total cost from VRES) while having a lower need for transmission than the Pareto-optimal layout. It seems that the additional $\mathcal{K}^T$ caused by the flows in a very heterogeneous system (see Figure 5.6) can offset the benefits of a reduced risk (σ_{EU}) and an increased return (ν_{EU}). In the following section, an optimisation is attempted in order to further reduce the total system cost required.

5.4 Genetic Algorithm

Genetic algorithms are especially suited for multi-variable, multi-objective optimisations, and although there is no guarantee for optimality, we can find a large population of sub-optimal solutions. Genetic algorithms can be seen as a directed Monte-Carlo method, where desirable traits are made more likely in future iterations.

A European VRES layout E is determined by the vectors $\boldsymbol{\gamma}$ and $\boldsymbol{\alpha}$. The entries in these vectors must fulfil the constraints

$$\begin{aligned} &0 \leq \gamma_n\,, \\ &0 \leq \alpha_n \leq 1\,, \\ &\textstyle\sum_n \gamma_n \langle L_n \rangle = \langle L_{\mathsf{EU}} \rangle\,. \end{aligned} \tag{5.20}$$

We can think of the combination of the vectors $\boldsymbol{\gamma}$ and $\boldsymbol{\alpha}$ as the chromosome of E. A pair of (γ_n, α_n) is then a gene in the chromosome, with the understanding that it is not only γ_n or α_n which define the VRES pattern coming from a specific country, rather the combination of the two. The 30 genes in the chromosome of E determine which traits

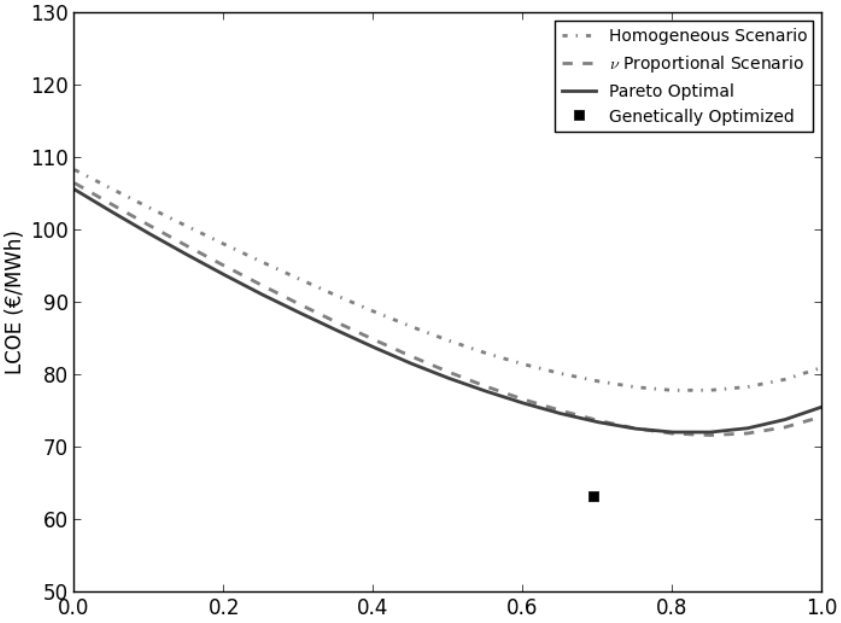

Figure 5.4: LCOE for a range of α for each of the reference scenarios. Also shown is the LCOE and α of a genetically optimised layout.

are exhibited. These traits can be summed up in the five elements of the LCOE defined in the previous section, namely E^B,$\mathcal{K}^B$,W_C,S_C, and $\mathcal{K}^T$. We can weigh these values by the assumed cost of each element, resulting in the cost function

$$\min_{\boldsymbol{\gamma},\alpha} \mathsf{P}_{E^B} + \mathsf{P}_{\mathcal{K}^B} + \mathsf{P}_{W_C} + \mathsf{P}_{S_C} + \mathsf{P}_{\mathcal{K}^T} \,. \tag{5.21}$$

The desirability of E is the value of (5.21) that its chromosome produces, with lower values being more desirable. A genetic optimisation would improve the desirability of subsequent generations by mixing the chromosomes of the most desirable layouts, using the following algorithm:

Populate: We take an initial population G_0 of p layouts

$$G_0 = \{E_1(\boldsymbol{\gamma},\alpha), \ldots, E_p(\boldsymbol{\gamma},\alpha)\} \,. \tag{5.22}$$

In the first generation, all the chromosomes $(\boldsymbol{\gamma},\alpha)$ are randomly selected from the space defined by (5.20), and the resulting layouts are ordered according to their desirability, so that E_1 is the most desirable. In the designed algorithm, $p = 100$, and an extra constraint of $\gamma_n \leq 2$ was included for G_0, serving as a sort of initial guess.

Select: We want to populate future generations with variations of the most desirable layouts' chromosomes. For this purpose, we select the 12 layouts which result in the lowest cost function and discard the rest of the

population. The selected layouts are then assigned different probabilities for being chosen for mating, based on their desirability.

Mate: As in traditional sexual reproduction from biology, we select two layouts for mating, though a combination of three or more is also possible. During mating, individual genes from each parent's chromosome are mixed together to form a new layout. The individual genes in the chromosome of a child c of parents a and b are defined by

$$(\alpha_n^c, \gamma_n^c) = \begin{cases} (\alpha_n^a, \gamma_n^a) & \text{if } X < 0.5 \\ (\alpha_n^b, \gamma_n^b) & \text{otherwise} \end{cases} . \tag{5.23}$$

where X is a random variable in $\{0, 1\}$, generated for every n.

Mutate: To avoid stagnation around local minima, we introduce the possibility of mutations during mating. The chromosome of the child can be altered slightly or radically depending on a random variable Y selected from $\{0, 1\}$ for every n.

$$(\widetilde{\alpha}_n^c, \widetilde{\gamma}_n^c) = \begin{cases} (Z_0, Z_1) & \text{if } Y < 0.05 \\ (\alpha_n^a * W_0, \gamma_n^a * W_1) & \text{if } 0.05 \leq Y < 0.25 \\ (\alpha_n^b, \gamma_n^b) & \text{otherwise} \end{cases} . \tag{5.24}$$

In rare occasions (5% of genes), a gene will be 're-seeded' from scratch with the independent random variables Z_0, Z_1, which still obey the constraints in (5.20). More commonly (20% of genes), the parent's gene will be slightly modified by independent random variables W_0, W_1, with values in $\{0, 0.25\}$

Since both Mating and Mutation can affect the layout wide VRES penetration γ_{EU}, a linear rescaling is performed to ensure that the values remain within the constraints of (5.20). Mating and Mutation are repeated until a new generation is populated with $p = 100$ different layouts. We have chosen to include the selected members of the first generation in the new one, to ensure that the value of the objective function at each generation only improves. Then, we select again from the second generation and repeat the process. After some 30 generations, a stable point is obtained, and not many improvements can be made in subsequent generations (see Figure 5.5)

We have additionally constrained the penetrations of renewables within a country to $0.2 \leq \gamma_n \leq 3.0$ for realism, as values of γ_n much larger than one will eventually encounter problems related to the energy density of VRES technologies. When optimising for cost, we obtain a much lower cost than any of the other scenarios (see Figure 5.4). This is due both to lower balancing capacities in power and energy and a more clever distribution of capacities, which results in a very heterogeneous distribution (see Figure 5.6). We also find a much larger capacity factor ν_{EU}, as seen in Figure 5.3.

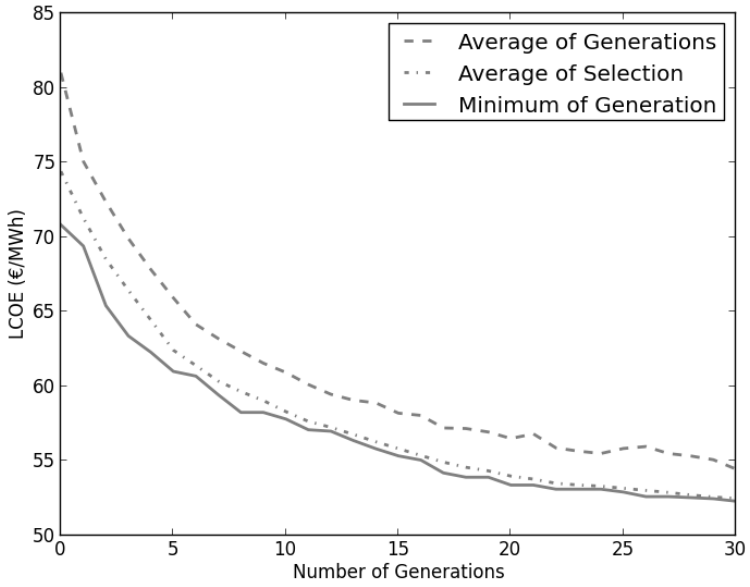

Figure 5.5: Convergence of the genetic algorithm. the x-axis shows the number of generations (iterations), while the lines show the average cost of, respectively, the whole population, the selected population, and the lowest layout. Not much improvement can be made after some 30 generations

An important caveat must be mentioned, the cost shown in (see Figure 5.5) does not include costs associated with transmission capacities, and therefore does not correspond exactly to that in Figure 5.4. Including transmission in the optimisation would considerably complicate the algorithm. As hinted in [4], however, transmission costs represent only around 10% of the total cost of the system, so it is to be expected that the optimal layout lies not far from the one found through the genetic algorithm. The additional cost of transmission is therefore performed only on the member with the lowest cost resulting from the genetic algorithm. This is the cost shown in Figure 5.4.

Looking back at Figure 5.1, it might seem surprising that the optimum resulting from the genetic algorithm results in a lower cost, given that the transmission it requires (bottom right) is far higher than that required by the other layouts. Figure 5.3 explains the reduced cost, as it is clear that the genetic algorithm reaches much higher capacity factors. In electrical systems with 100% penetration, upwards of 50% of the cost stems from the installed capacity of wind and solar [4], thus an effective usage of available capacities is seems to be the best way of reducing the cost of the system.

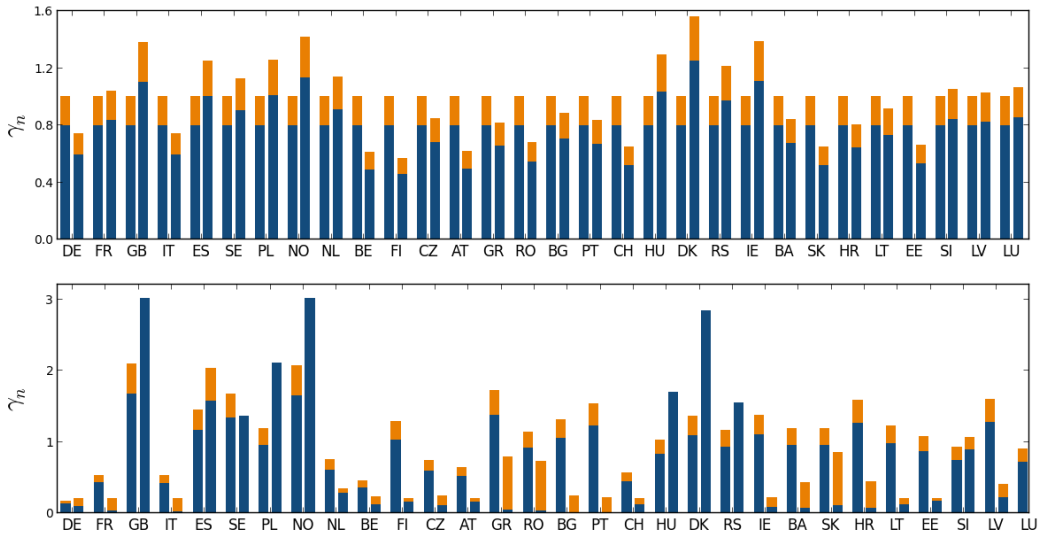

Figure 5.6: VRES penetration γ_n and wind/solar mix α (blue/yellow) for the 30 EU countries. The top bars show the homogeneous layout (left) and the ν–proportional layout (right). The bars on the bottom show the Pareto-optimal layout (left) and the genetically optimised layout (right). The distributions become highly heterogeneous in the latter cases.

5.5 Conclusion

An exploration of layouts of VRES capacities over Europe shows that heterogeneous layouts are capable of significantly increasing the overall capacity factor ν_{EU} of renewables, while reducing the standard deviation σ_{EU} of their generation. By scaling the regional penetration of renewables according to countries' capacity factors, we produce a heterogeneous mixture that favours installation primarily in countries around the North Sea, since wind is preferable to solar to increase ν_{EU} and reduce σ_{EU}. These improvements lead to an overall reduction in the cost of electricity generated by the system.

Optimal portfolio theory helps analyse the space of heterogeneous layouts. By mixing wind- and solar-only layouts that lie along the Pareto front, we find configurations that further reduce the risk (σ_{EU}) while increasing the return (ν_{EU}). However, the increased heterogeneity that these systems propose imply such an increase in transmission that the total system cost is greater than a system scaling by regional capacity factors. A genetic algorithm is the used to further explore heterogeneous layouts. With the explicit aim of reducing system costs, the genetic algorithm finds a very heterogeneous system that is nonetheless able to significantly reduce system costs, mainly through a marked increase in the European capacity factor ν_{EU}.

Conclusion

We set out to describe a fully renewable European electricity system, based only on the natural variations of weather patterns and simple, transparent mathematical models. In letting the weather decide the characteristics of our systems, we can describe strong, natural limits on what a fully renewable system can and cannot achieve, independent of changes in policies or technologies. The simplicity of our mathematical models allows us to focus on more complicated interactions, and to approach more complex networks than would be computationally possible with a more intricate modelling.

The field of ESA makes predictions about the future of energy systems, globally and in Europe. Instead of offering specific solutions, we find here the hull of all possible solutions, set by the variations and correlations in global weather patterns. Whatever improvements are made for data-collection, or even the accuracy of models, the weather-driven approach used in this study is key in the study of the energy systems of the future.

At the beginning of our study, we showed in what degree and to what extent a transmission system can help countries share their resources. Correlations between countries, combined with a physical flow model, allowed us to quantify the benefit that a constrained transmission grid brings to the system, and identify key links and upgrades required for the efficient trade of electricity. A system with 100% renewables in which countries do not interact with one another would require an average of 24% additional backup energy. We find that a doubling of the total capacity of the grid could bring this down to 18%, but an expansion by a factor five would be needed to reach the limit of 15% [1].

A simple sharing of excess generation is not enough to reduce the backup capacities needed to maintain the electricity system in balance. Cooperation between countries is required in order to significantly reduce the number of dispatchable plants. In order to bring about this cooperation, we designed a simple market-based export scheme, which makes countries provide backup synchronously [2]. While this operation makes a larger use of the transmission system, it brings down the total backup capacity required, as neighbours help each other in times of need.

The additional flows required in a sharing of electricity – whether from renewables or backup capacity – opens up many interesting questions regarding the network participation of countries. We refined and applied a flow-tracing algorithm to follow

energy exported from source to sink [3]. This in turn permits the study of the relationship between network topology, weather correlations, and trade partners and pathways. We are able to identify the parties responsible for a specific flow, leading to a quantification of the stakes that a country has on a particular link and the whole network.

While part of the strength of the weather-driven approach lies in its independence of economic factors, an economic analysis is what is needed to determine wether the increased transmission required by the synchronised export scheme defined in [2] is worth the investment. However, the variation of cost assumptions for the building blocks for the system – VRES, transmission, and backup capacities and energy – are too large to provide any meaningful answers without consideration for the effects they have on the optimal system. In order to circumvent this problem, we implement a sensitivity analysis to monitor the strength of our results when confronted with variations in the assumed costs. We find that the optimal wind mix is almost impervious to changes in assumptions other than wind and solar costs, while other system parameters – the levelised cost of electricity and the optimal VRES penetration – are especially vulnerable to changes in the assumed price of backup energy and wind capacity [4]. Under a range of VRES penetration of 50% to 130%, the synchronised export scheme provides a lower cost than the alternatives, given some initial cost assumptions.

During this economic analysis, we find (unsurprisingly) that the largest part of the total cost of a fully renewable system is the cost of VRES capacities. This high price stems, in part, from the assumption of homogeneous systems throughout Europe, as wind and solar capacities will be placed in inefficient locations. We explore a range of heterogeneous layouts, where locations with high wind and solar capacity factors are prioritised. Aided by optimal portfolio theory and a genetic algorithm, we find that highly heterogeneous layouts can significantly reduce the cost of electricity by increasing the capacity factor of the aggregated European power system (and thus requiring smaller installed capacities)[5].

Outlook

Tangential to the thread followed in this thesis, and as an extension to some of the conclusions we arrived at, there are interesting questions that can be addressed with our modelling approach. Here, we talk about three main areas: increasing the range of and improving our modelling, applications of and improvements to the flow tracing, and the coupling of infrastructures with our modelling approach.

Modelling

The first and easiest question we can answer is: How do the dynamics found in this study change as we increase the spatial scope of the study? In [7], we present a world-wide weather atlas, which allows us to model potential wind and solar generation worldwide. This new global atlas has a slightly higher spatial resolution, and a

much larger historical database, spanning 32 years – and growing. We have already made some initial efforts in exploring how intercontinental links can help Europe and neighbouring regions integrate renewables. Our undocumented preliminary results show, for example, how connecting the European network into Turkey and the Middle East could prove more beneficial than simply into Northern Africa, political and economical issues aside. With this new dataset, we could in fact study a world wide grid, where the sun is always shining or the wind always blowing.

We can also increase the scope by refining the grids we study. So far, we have treated the transmission system inside a county as a copper plate, assuming that flows within it are unconstrained. In reality, the internal network in a country has pathways and bottlenecks, as well as heterogeneous distributions of resources. Going below the country scale would show interesting dynamics inside countries, from offshore locations to cities and industrial areas, revealing pathways along specific lines. As mentioned in Chapter 5, we could also explore highly heterogenous layouts, and discover with a high spatial accuracy the correlations that can be found throughout Europe. This could lead to even more efficient VRES layouts, with lower costs and needs for backup power and energy.

We can also explore different export schemes. The market interpretation given to the synchronised export scheme presented in Chapter 2 can be used to more accurately model the merit-order effect. The linear fitting, as shown in Figure 7, does not exactly correspond to the distribution in capacities that we find in reality. We could model very intricate, and country-dependent merit-order distributions via an agent-based game theory simulation, so as to replicate an actual market. Alternatively, we can come to an analytical expression by looking closer at equation (52):

$$\mathcal{C}_n = \int_0^{B_n} f \frac{B_n}{\langle L_n \rangle} \, \mathrm{d}B_n = \frac{f}{2} \cdot \frac{B_n^2}{\langle L_n \rangle} \, .$$

We can identify the factors that make up the cost of balancing in a node:

$$\mathcal{C}_n = B_n \cdot \left(\frac{B_n}{\langle L_n \rangle} + b \right)^a \, . \tag{62}$$

When $a = 0$, we return to the localised export scheme introduced in [1], where every MWh of backup power has the same cost in all nodes, regardless of how much that node is already providing to the system. When $b = 0$ and $a = 1$, we have the synchronised export scheme, corresponding to the linear approximation to the supply and demand curves in Figure 7. The factors b could be used to designate a node with higher or lower costs of balancing, while the factor a could be used to designate the shape of the supply curve for different nodes.

Flow tracing

The flow tracing algorithm developed in [3] offers a wealth of possible applications and refinements. Firstly, the algorithm could be improved to distinguish between power coming from different sources. Each country would have, instead of a single 'colour', a

vector of colours designating power coming from wind, solar, or conventional sources. The power mix in a node, as expressed in equation (3.14), would not be

$$\vec{p}_n = [\, p_{n,1} \;\cdots\; p_{n,j} \;\cdots\; p_{n,N} \,]^{\mathsf{T}} \;,$$

but instead

$$\boldsymbol{p}_n = [\, \vec{p}_{n,1} \;\cdots\; \vec{p}_{n,j} \;\cdots\; \vec{p}_{n,N} \,] \;, \tag{63}$$

where the elements $\vec{p}_{n,j}$ signal the presence of power of all sources of j in n:

$$\vec{p}_{n,j} = \left[\, \mathsf{wind}_{n,j} \;,\; \mathsf{solar}_{n,j} \;,\; \mathsf{backup}_{n,j} \;\cdots \,\right]^{\mathsf{T}} \;. \tag{64}$$

Combining this with a higher grid resolution, as suggested above, could help identify the flow and destination of renewables within a country. Knowing where in a country renewables are being used could also help produce new pricing mechanisms for end consumers, so that CO_2 taxes would be higher where renewables are not used, hopefully reversing the "not-in-my-backyard" attitude that plagues the wind industry. Flow tracing might also provide aid in discussions of the fate of renewables within a country.

A higher resolution grid in which flows are traced could also offer benefits to grid stability. Full knowledge of where flows are originating and of which parties are responsible for flows along a given link could help TSOs make decisions regarding congestion management. Bottlenecks could be resolved not only by rerouting power flows or curtailing generation or consumption at the ends of the links, but also by curtailing generation or consumption at the responsible parties.

Determining which are the responsible parties is not yet a settled issue. In [3], we have assumed that the responsibility of a node in a link is proportional to the average flow through the link caused by that node. It could be argued that a fairer assessment comes from looking at the use that pushes the maximum flow of the link, as it is these maximum flows which determine the total capacity. A fairer mechanism for determining the stake a node has in a link would account for these high flows. Such mechanism could add to our modelling toolkit, and, combined with a higher resolution network, offer planners and policy makers new options to assess the stakes that a participant has in the electricity network.

Coupled infrastructures

So far, we have limited our energy studies to electricity. A complete ESA should also explore the heating/cooling sectors and the transport sector, all of which are of similar magnitude. In European countries, one can approximate the relative size of these sectors as each contributing roughly $1/3^{\text{rd}}$ of the total energy consumption of a region [52]. Electricity is of special interest because it is a very convenient energy vector: it can deliver high-quality, low entropy energy, with minimum losses over long distances. Gas is another useful energy vector (as are all fossil fuels) in that it has a high energy density, making it suitable for transportation. Lastly, warm water is one of the lowest forms of energy due to its high entropy, but it is in a ready-to-use format, suitable for district heating.

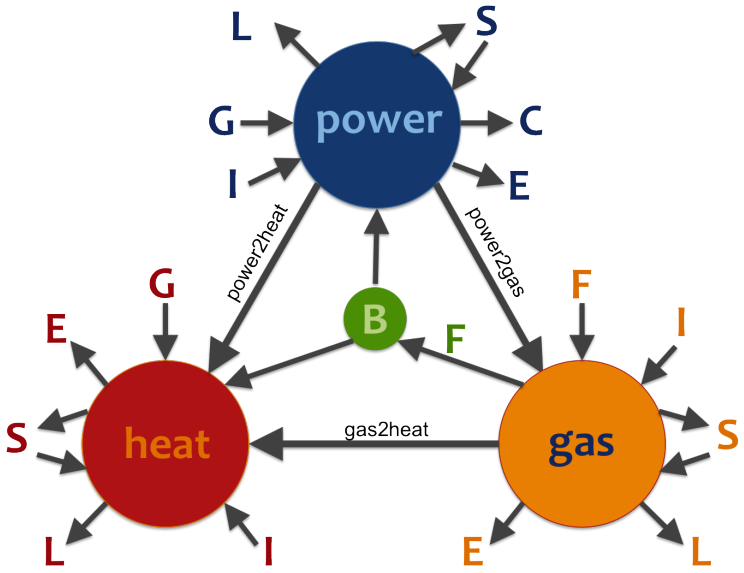

Figure 10: Expanded node representation of three energy sectors: electricity, gas, and heating. Each sector has a load (L), as well as imports and exports (I and E) to corresponding sectors in other nodes. Some processes allow transfer of energy across sectors.

Gas has an added advantage, in that it is already possible to transform electricity to gas via electrolysis and other electricity to hydrocarbon conversions (power2gas). Gas can also be burned directly for heat (gas2heat), transformed back into electricity via a gas turbine, or, more effectively, via a combined heat and power plant, or CHP, which is able to distribute both heat and electricity. It is also possible to use electricity for heating (power2heat), either by a direct electric radiator or boiler, or by driving a heat pump, which uses the thermal gradient underground to achieve higher efficiencies.

Figure 10 shows the relations between the three sectors. The top node is similar to the one used throughout this study (see Figure 2), with the added possibility of energy storage (S). This could represent any technology, from compressed air, to a fleet of electric vehicles. The links to other sectors represent the transformations power2gas, power2heat, and gas2heat. In the gas sector, we have an input additional to imports and exports (I, E) within the gas grid: input from conventional sources F (in orange). The gas incoming from F can represent either normal inputs from gas wells or biogas from renewable sources. There is also the possibility of storing gas, with much more ease than in the case of electricity. The output L represents all uses of gas that are not converted to heat or electricity, namely transportation. An extra output, F (in green) is used to represent the feeding of gas into conventional and CHP plants, which provide backup to both the electricity and heating sectors. The heating sector also receives some energy from renewables, either solar or geothermal. In small scales, it is also possible to import and export heat via an extended district

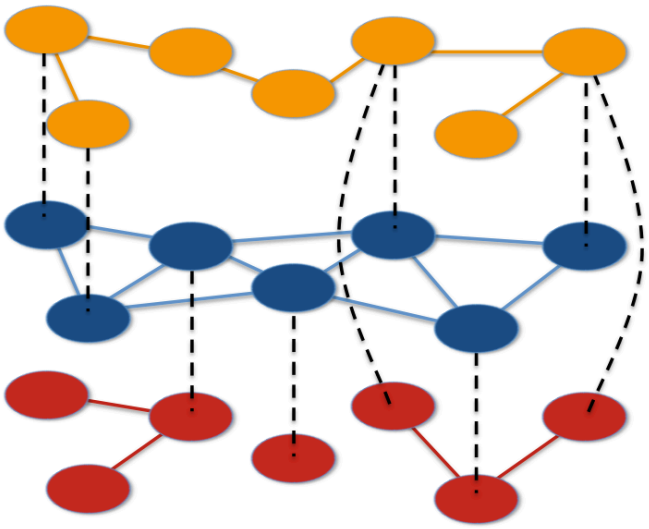

Figure 11: Representation of an energy network, comprised of three coupled infrastructures. Connections exist across the same sector in different nodes via transmission networks, as well as within different sectors in the same node, via energy conversion processes.

heating system, as well as heat storage.

There are, of course, many interactions either hidden or ignored in our model. The large hydro lakes of Scandinavia and the Alps can be modelled as part of the electricity energy storage. The process from electricity to gas can either produce pure hydrogen or use biomass to produce methanol. There are other important forms of backup, such as geothermal, tidal and run of river. Not all the loads are modelled, as it is to be expected that not all the transport system can be fed via the gas grid. We model here only the general dynamics of what we believe can represent the energy system of the future, in a way simple enough to allow for a meaningful discussion of the dynamics of the network.

Other modelling tools already approach the problem of complex energy systems [22], offering higher detail in the interactions between the sectors. The simplified nodal expression of the energy sectors in Figure 10 allows for a clearer approach to the problem of networked energy systems. Figure 11 shows how such a system might be interconnected. Each column of nodes represents a single geographical area, separated by sectors. The sectors are strongly connected within themselves (via links of the same color), while not all nodes necessarily offer the same interconnections to other sectors (via black dashed links). Some nodes might not have district heating, or be connected to the gas network, or belong to the same synchronous electrical grid.

Under this visualisation, the problem becomes indistinguishable from the networks we have solved so far. There are some additional constraints to regulate how the sectors interact with each other, and nodes from different sectors are dominated by

different node equations, but virtually no modification to our general algorithm is required. Networks of gas, electricity, or water are all potential flows, so similar rules define their flows.

In this case, the full node equations, as seen from Figure 10, would be

$$G_E + B_E + I_E + S_E = L_E + C_E + E_E + \mathsf{P2G} + \mathsf{P2H}\,, \tag{65}$$

for the electric sector of the node, where S_E is positive when discharging, negative when charging. For the gas sector, the equation would be

$$\mathsf{P2G} \cdot \eta_{\mathsf{P2G}} + I_G + F_F + S_G = L_G + E_G + F_G + \mathsf{G2H}\,, \tag{66}$$

where η_{P2G} is the conversion efficiency of the power to gas process, F_F are external fuel inputs, and F_G are the exports into the backup subsector. The heating sector would be described by

$$\mathsf{P2H} \cdot \eta_{\mathsf{P2H}} + \mathsf{G2H} \cdot \eta_{\mathsf{G2H}} + G_H + B_H + I_H + S_H = E_H + L_H\,. \tag{67}$$

Finally, the dynamics of the backup subsector can be described by

$$B_E = \epsilon \cdot (F_G \cdot \eta_{\mathsf{CHP}}) + (1 - \epsilon)(F_G \cdot \eta_{\mathsf{el}}) \tag{68}$$

and

$$B_H = \epsilon \cdot (1 - \eta_{\mathsf{CHP}}) \cdot F_F\,, \tag{69}$$

where ϵ is the instantaneous (and variable) share of CHP plants in use the backup subsector.

When operating the system in Figure 11, we are constrained by the above equations (65 - 69). The signals from renewables (G_E, G_H) and the demands (L_E, L_G, L_H) are assumed to be the inalterable stimulus to the system (save for the possibility of some degree of flexibility in the demands). The abilities that the system operators have in order to decide how to best cover the loads are intra-sector trading (I_E, I_H, I_G and E_E, E_H, E_G), inter-sector exchanges (P2G, P2H, G2H), and storage (S_E, S_G, S_H), with the residual demand being covered by backup power (B_E, B_H) and fuel inputs (F_F). A possible objective function for our problem could be

$$\min_{T,S} \quad \sum_n F_F^n \tag{70}$$

subject to (65 - 69), where T is the vector of all inter- and intra-sector flows, S the vector of all storages, and F_F^n is the fuel input into node n. This objective function would minimise the need for additional fuel, making the energy usage within the node – and across all nodes – as effective as possible.

Other objective functions are conceivable, perhaps with an aim to minimise the need for backup capacities, electric storage volumes, or to simply minimise to operational cost of the system. Any of these would give us the ability to study the dynamics within the sectors and across nodes, and help us assess the need for transmission (either of gas or electricity), electrolysers, heat pumps, energy storage (in

any form), and CHP backup. When comparing these results with the existing network and planned expansions of renewables, we could also identify bottlenecks for the integration of renewables.

The tools we have described here could all work in this network with coupled infrastructures. The weather atlas developed in [7] could provide data for anything ranging from city to a continent, allowing national and international energy studies that include all energy sectors. The flow tracing algorithm would provide new insight into the usage of renewable sources, not only in the electricity system, but in everything from heating to the gas turbines that compete with the same renewables.

Bibliography

[1] Rodriguez RA, Becker S, Andresen G, Heide D, and Greiner M. Transmission needs across a fully renewable European power system. Renewable Energy, 63:467–476, 2014.

[2] Rodriguez RA, Dahl M, and Greiner M. Selfish vs. cooperative exports across a fully renewable pan-European transmission network. Submitted to Energy, Sustainability and Society, 2014.

[3] Rodriguez RA, Thomsen A, Andresen G, and Greiner M. Tracing the flow of energy in a highly renewable Europe. To be submitted, 2014.

[4] Rodriguez RA, Becker S, and Greiner M. Cost-optimal design of a simplified, highly renewable pan-European electricity system. Submitted to Energy, 2014.

[5] Rodriguez RA, Sairanen B, and Greiner M. Optimal heterogeneity of a highly renewable pan-European electricity system. To be submitted, 2014.

[6] Becker S, Rodriguez RA, Andresen GB, Schramm S, and Greiner M. Transmission grid extensions during the build-up of a fully renewable pan-European electricity supply. Energy, 64:404–418, 2014.

[7] Andresen GB, Rodriguez RA, Becker S, and Greiner M. The potential for arbitrage of wind and solar surplus power in denmark. Energy, 2014.

[8] MacKay D. Sustainable energy – without the hot air. UIT Cambridge, 2009.

[9] European Photovoltaic Industry Association. Connecting the Sun: Solar photovoltaics on the road to large-scale grid integration. Technical report, EPIA, September 2012.

[10] Van de Putte J and Short R. Battle of the grids. Technical report, Greenpeace International, 2011.

[11] Teske S, Tröster E, Schierhorn P, and Ackermann T. powE[R] 2030: a European grid for 3/4 renewable electricity by 2030. Technical report, Greenpeace Germany, 2014.

[12] Jacobson MZ and Delucchi MA. Providing all global energy with wind, water, and solar power, Part I: Technologies, energy resources, quantities and areas of infrastructure, and materials. Energy Policy, 39(3):1154–1169, 2011.

[13] Delucchi MA and Jacobson MZ. Providing all global energy with wind, water, and solar power, Part II: Reliability, system and transmission costs, and policies. Energy Policy, 39(3):1170–1190, 2011.

[14] Corcoran BA, Jenkins N, and Jacobson MZ. Effects of aggregating electric load in the United States. Energy Policy, 46:399 – 416, 2012.

[15] Mason IG, Page SC, and Williamson AG. A 100% renewable electricity system for New Zealand utilising hydro, wind, geothermal and biomass resources. Energy Policy, 38:3973–3984, 2010.

[16] Mason IG, Page SC, and Williamson AG. Security of supply, energy spillage control and peaking options within a 100% renewable electricity system for New Zealand. Energy Policy, 60:324–333, 2013.

[17] Elliston B, Diesendorf M, and MacGill I. Simulations of scenarios with 100% renewable electricity in the Australian National Electricity Market. Energy Policy, 45:606–613, 2012.

[18] Elliston B, MacGill I, and Diesendorf M. Least cost 100% renewable electricity scenarios in the Australian National Electricity Market. Energy Policy, 59(0):270 – 282, 2013.

[19] Elliston B, MacGill I, and Diesendorf M. Comparing least cost scenarios for 100% renewable electricity with low emission fossil fuel scenarios in the Australian National Electricity Market. Renewable Energy, 66(0):196 – 204, 2014.

[20] Energy Styrelsen. Ny analyse: Vind er billigst. Klima-, Energi og Bygningsministeriet, 2014. Accessed online July 2014, http://www.ens.dk/info/nyheder/nyhedsarkiv/ny-analyse-vind-billigst.

[21] Kost C, Schlegl T, Thomsen J, Nold S, and Mayer J. Levelized cost of electricity: renewable energies. Technical report, Fraunhofer Institute for solar energy systems ISE, 2012. Online, retrieved October 2013.

[22] Connolly D, Lund H, Mathiesen B, and Leahy M. A review of computer tools for analysing the integration of renewable energy into various energy systems. Applied Energy, 87(4):1059 – 1082, 2010.

[23] Heide D, von Bremen L, Greiner M, Hoffmann C, Speckmann M, and Bofinger S. Seasonal optimal mix of wind and solar power in a future, highly renewable Europe. Renewable Energy, 35(11):2483–2489, 2010.

[24] Heide D, Greiner M, von Bremen L, and Hoffmann C. Reduced storage and balancing needs in a fully renewable European power system with excess wind and solar power generation. Renewable Energy, 36(9):2515–2523, 2011.

[25] Rasmussen MG, Andresen GB, and Greiner M. Storage and balancing synergies in a fully or highly renewable pan-european power system. Energy Policy, 51:642 – 651, 2012.

[26] Andresen GB, Rasmussen MG, Rodriguez RA, Becker S, and Greiner M. Fundamental properties of and transition to a fully renewable pan-European power system. EPJ Web of Conferences, 33, 2012.

[27] Schaber K, Steinke F, and Hamacher T. Transmission grid extensions for the integration of variable renewable energies in Europe: Who benefits where? Energy Policy, 43:123 – 135, 2012.

[28] Schaber K, Steinke F, Mühlich P, and Hamacher T. Parametric study of variable renewable energy integration in Europe: Advantages and costs of transmission grid extensions. Energy Policy, 42:498–508, 2012.

[29] Bofinger S, von Bremen L, Knorr K, Lesch K, Rohrig K, Saint-Drenan Y, and Speckmann M. Raum-zeitliche Erzeugungsmuster von Wind- und Solarenergie in der UCTE-Region und deren Einfluss auf elektrische Transportnetze. Technical report, Institut für Solare Energieversorgungstechnik, ISET e.V., 2008. Kassel, Germany.

[30] Søndergaard A. Development of a Renewable Energy Atlas and Extreme Event Analysis in Renewable Energy Systems. Master's thesis, Aarhus University, 2013.

[31] Widen J. Correlations between large-scale solar and wind power in a future scenario for Sweden. IEEE Transactions on Sustainable Energy, 2:177–184, 2011.

[32] Wollenberg B and Wood A. Power Generation, Operation, and Control. John Wiley & Sons, 1996.

[33] Van Hertem D, Verboomen J, Purchala K, Belmans R, and Kling WL. Usefulness of DC power flow for active power flow analysis with flow controlling devices. In The 8th IEE International Conference on AC and DC Power Transmission, pages 58–62. IET, 2006.

[34] Heide D. Statistical Physics of Power Flows on Networks with a High Share of Fluctuating Renewable Generation. PhD thesis, Johann Wolfgang Goethe University, 2010.

[35] Penrose R. A generalized inverse for matrices. Mathematical Proceedings of the Cambridge Philosophical Society, 51:406–413, 7 1955.

[36] European Transmission System Operators. Indicative values for Net Transfer Capacities (NTC) in Continental Europe. Technical report, ENTSO-E, 2011.

[37] BritNed Development Limited. BritNed Construction. http://www.britned.com/. Online, retrieved July 2013.

[38] Skog JE, Koreman K, Pääjärvi B, Worzyk T, and Andersröd T. The NorNed HVDC cable link: a power transmission highway between norway and the netherlands. Technical report, ABB, 2007. Online, retrieved July 2013.

[39] Cho A. Energy's tricky tradeoffs. Science, 329(5993):786–787, 2010.

[40] Steinke F, Wolfrum P, and Hoffmann C. Grid vs. storage in a 100% renewable Europe. Renewable Energy, 50(0):826 – 832, 2013.

[41] Van Hulle F et al. Integrating wind. Developing Europe's power market for the large-scale integration of wind power: Executive Summary. Technical report, European Wind Energy Association, 2009.

[42] Buijs P, Bekaert D, Cole S, Van Hertem D, and Belmans R. Transmission investment problems in Europe: Going beyond standard solutions. Energy Policy, 39(3):1794–1801, 2011.

[43] Tröster E, Kuwahata R, and Ackermann T. European grid study 2030/2050. Technical report, Energynautics GmbH, 2011.

[44] European Transmission System Operators. Ten-Year Network Development Plan 2012. Technical report, ENTSO-E, 2012.

[45] Zugno M, Pinson P, and Madsen H. Impact of Wind Power Generation on European Cross-Border Power Flows. Submitted to IEEE Transactions of Power Systems, 2012.

[46] Lehmkoster C. Security constrained optimal power flow for an economical operation of FACTS-devices in liberalized energy markets. IEEE Transactions on Power Delivery, 17(2):603–608, 2002.

[47] Mattingley J and Boyd S. CVXGEN: a code generator for embedded convex optimization. Optimization and Engineering, pages 1–27, 2012.

[48] Zeyer T. Modeling of spatio-temporal flow patterns in a fully renewable pan-European power system. Master's thesis, Aarhus University, 2013.

[49] Sensfuss F, Ragwitz M, and Genoesse M. The merit-order effect: A detailed analysis of the price effect of renewable electricity generation on spot market prices in Germany. Technical report, Fraunhofer Institute for Systems and Innovation Research (Fraunhofer ISI), 2007. Karlsruhe, Germany.

[50] Jacobson MZ and Delucchi MA. A path to sustainable energy by 2030. Scientific American, 301:58–65, 2009.

[51] Popp M. Speicherbedarf bei einer Stromversorgung mit erneuerbaren Energien. Springer, Heidelberg, 2010.

[52] Lund H. Renewable Energy Systems – The Choice and Modeling of 100% Renewable Solutions. Elsevier, Amsterdam, 2010.

[53] Connolly D, Lund H, Mathiesen B, and Leahy M. The first step towards a 100% renewable energy system for Ireland. Applied Energy, 88:502–507, 2011.

[54] Kempton W, Pimenta FM, Veron DE, and Colle BA. Electric power from offshore wind via synoptic-scale interconnection. Proceedings of the National Academy of Sciences, 107:7240–7245, 2010.

[55] Budischak C, Sewell D, Thomson H, Mach L, Veron DE, and Kempton W. Cost-minimized combinations of wind power, solar power and electrochemical storage, powering the grid up to 99.9% of the time. Journal of Power Sources, 225:60–74, 2013.

[56] Schäfer M, Scholz J, and Greiner M. Proactive robustness control of heterogeneously loaded networks. Phys. Rev. Lett., 96:108701, 2006.

[57] Heide D, Schäfer M, and Greiner M. Robustness of networks against fluctuation-induced cascading failures. Physical Review E (Statistical, Nonlinear, and Soft Matter Physics), 77:056103, 2008.

[58] Shahidehpour M, Yamin H, and Li Z. Market operations in electric power systems. Wiley Interscience, New York, 2002.

[59] Ping W, Bin Y, Yixin N, and Wu FF. Power flow tracing for transmission open access. In Electric Utility Deregulation and Restructuring and Power Technologies, 2000. Proceedings. DRPT 2000. International Conference on, pages 476–481, 2000.

[60] Kirschen D, Allan R, and Strbac G. Contributions of individual generators to loads and flows. Power Systems, IEEE Transactions on, 12(1):52–60, Feb 1997.

[61] Bialek J. Tracing the flow of electricity. IEE Proc.-Gener. Transm. Distrib., 143(4):313–320, 1996.

[62] Hugh S and Henrik M. Wind energy: the case of Denmark. Technical report, CEPOS - Center for Politiske Studier, 2009. Copenhagen, Denmark.

[63] Lund H et al. Danish wind power: Export and Cost. Technical report, CEESA - Coherent Energy and Environmental System Analysis, 2010. Aalborg, Denmark.

[64] McKinsey. RoadMap 2050: A Practical Guide to a Prosperous, Low-Carbon Europe. Technical report, European Climate Foundation, 2010. Online, retrieved October 2013.

[65] Fürsch M, Hagspiel S, Jägemann C, Nagl S, Lindenberger D, and Glotzbach L. Roadmap 2050 – a closer look. Technical report, energynautics and Institute for Energy Economy at the University of Cologne, 2011.

[66] Sorknæs P, Mæng H, Weiss T, and Andersen AN. Overview of current status and future development scenarios of the electricity system in Denmark — allowing integration of large quantities of wind power. Technical report, www.store-project.eu, July 2013.

[67] Solem G, Wangensteen I, Sæle H, Uhlen K Bjørndalen J, Revdal T, and Årdal F. Transit in the european power market. Technical report, SINTEF, November 2007.

[68] Short W, Packey D, and Holt T. A Manual for the Economic Evaluation of Energy Efficiency and Renewable Energy Technologies. Technical report, National Renewable Energy Laboratory, 1995.

[69] Parsons Brinckerhoff. Electricity Generation Cost Model - 2011 Update Revision 1. Technical report, Department of Energy and Climate Change, 2011. Online, retrieved October 2013.

[70] Mott MacDonald Group Limited. UK Electricity Generation Costs Update. Technical report, Department of Energy and Climate Change, 2010. Online, retrieved October 2013.

[71] OpenEI. Transparent Cost Database. http://en.openei.org/apps/TCDB/. Online, retrieved October 2013.

[72] EIA. Levelized Cost of New Generation Resources in the Annual Energy Outlook 2013. Technical report, U.S. Energy Information Administration, 2013. Online, retrieved October 2013.

[73] Fürsch M, Golling C, Nicolosi M, Wissen R, and Lindenberger D. European RES-E Policy Analysis: A model-based analysis of RES-E deployment and its impact on the conventional power market. Technical report, Institute of Energy Economics at the University of Cologne, 2010.

[74] Ernst & Young LLP. Cost of and financial support for offshore wind. Technical report, Department of Energy and Climate Change, 2009. Online, retrieved October 2013.

[75] The World Bank Group. World bank commodities price forecast, october 2013. http://go.worldbank.org/4ROCCIEQ50, 2013. Online, retrieved October 2013.

[76] Ove Arup & Partners Ltd. Review of the generating costs and deployment of potential renewable electricity technologies in the UK. Technical report, Department of Energy and Climate Change, 2011. Online, retrieved October 2013.

[77] Ernst & Young LLP. Analysis of the value creation potential of wind energy policies: A comparative study of the macroeconomic benefits of wind and CCGT power generation. Technical report, Ernst & Young LLP, 2012. Online, retrieved October 2013.

[78] Black & Veatch. Cost and performance data for power generation technologies. Technical report, National Renewable Energy Laboratory, Overland Park, KS, 2011.

[79] Hand MM, Baldwin S, DeMeo E, Reilly JM, Mai T, Arent D, Porro G, Meshek M, and Sandor D. Renewable Electricity Futures Study. eds. 2 vols. NREL/TP-6A20-52409.

[80] Connolly D, Lund H, Mathiesen B, Pican E, and Leahy M. The technical and economic implications of integrating fluctuating renewable energy using energy storage. Renewable Energy, 43(0):47 – 60, 2012.

[81] Nelson J, Johnston J, Mileva A, Fripp M, Hoffmann I, Petros-Good A, Blanco C, and Kammen DM. High-resolution modeling of the western North American power system demonstrates low-cost and low-carbon futures. Energy Policy, 43(0):436 – 447, 2012.

[82] Williams JH, DeBenedictis A, Ghanadan R, Mahone A, Moore J, Morrow WR, Price S, and Torn MS. The Technology Path to Deep Greenhouse Gas Emissions Cuts by 2050: The Pivotal Role of Electricity. Science, 335:53–59, 2012.

[83] Eurostat. Half-yearly electricity and gas prices. http://www.bit.ly/1ljbhbg. Online, retrieved February 2013.

[84] Rombauts Y, Delarue E, and D'haeseleer W. Optimal portfolio-theory-based allocation of wind power: Taking into account cross-border transmission-capacity constraints. Renewable Energy, pages 2374–2387, 2011.

[85] Roques F, Hiroux C, and Saguan M. Optimal wind power deployment in europe - a portfolio approach. Energy Policy, pages 3245–3256, 2009.